Automatic positioner and control system for a motorized parabolic solar reflector

by

Gerhardus Johannes Prinsloo

Thesis presented in partial fulfilment of the requirements for the degree of Master in Engineering (Mechatronic) at Stellenbosch University

Department of Mechanical and Mechatronic Engineering,
Faculty of Engineering,
University of Stellenbosch
Supervisors: Mr. R.T. Dobson & Prof. K. Schreve

December 2014

Stellenbosch University http://scholar.sun.ac.za

Declaration

By submitting this thesis electronically, I declare that the entirety of the work contained therein is my own, original work, that I am the owner of the copyright thereof (unless to the extent explicitly otherwise stated) and that I have not previously in its entirety or in part submitted it for obtaining any qualification.

Date: 2014/04/17 .....

Copyright © 2014 Stellenbosch University
All rights reserved.

Stellenbosch University http://scholar.sun.ac.za

Abstract

Most rural African villages enjoy high levels of sunlight, but rolling out solar power generation technology to tap into this renewable energy resource at remote rural sites in Africa pose a number of design challenges. To meet these challenges, a project has been initiated to design, build and test/evaluate a knock down 3 kW peak electrical stand-alone self-tracking dual-axis concentrating solar power system.

This study focusses on the mechatronic engineering aspects in the design and development of a dynamic mechatronic platform and digital electronic control system for the stand-alone concentrating solar power system. Design specifications require an accurate automatic positioner and control system for a motorized parabolic solar reflector with an optical solar harnessing capacity of 12 kW_t at solar noon. It must be suitable for stand-alone rural power generation. This study presents a conceptual design and engineering prototype of a balanced cantilever tilt-and-swing dual-axis slew drive actuation means as mechatronic solar tracking mobility platform for a $\sim$12 m^2 lightweight parabolic solar concentrator. Digital automation of the concentrated solar platform is implemented using an industrial Siemens S7-1200 programmable logic controller (PLC) with digital remote control interfacing, pulse width modulated direct current driving, and electronic open loop/closed loop solar tracking control. The design and prototype incorporates off-the-shelf components to support local manufacturing at reduced cost and generally meets the goal of delivering a dynamic mechatronic platform for a concentrating solar power system that is easy to transport, assemble and install at remote rural sites in Africa. Real-time experiments, conducted in the summer of South Africa, validated and established the accuracy of the engineering prototype positioning system. It shows that the as-designed and -built continuous solar tracking performs to an optical accuracy of better than 1.0° on both the azimuth and elevation tracking axes; and which is also in compliance with the pre-defined design specifications.

Structural aspects of the prototype parabolic dish are evaluated and optimized by other researchers while the Stirling and power handling units are under development in parallel projects. Ultimately, these joint research projects aim to produce a locally manufactured knock down do-it-yourself concentrated solar power generation kit, suitable for deployment into Africa.

Stellenbosch University http://scholar.sun.ac.za

Opsomming

Landelike gebiede in Afrika geniet hoë vlakke van sonskyn, maar die ontwerp van betroubare sonkrag tegnologie vir die benutting van hierdie hernubare energie hulpbron by afgeleë gebiede in Afrika bied verskeie uitdagings. Om hierdie uitdagings te oorkom, is 'n projek van stapel gestuur om 'n afbreekbare 3 kW piek elektriese alleenstaande selfaangedrewe dubbel-as son-konsentreeder te ontwerp, bou en te toets.

Hierdie studies fokus op die megatroniese ingenieurs-aspekte in die ontwerp en ontwikkeling van 'n dinamiese megatroniese platform en 'n digitale elektroniese beheerstelsel vir die alleenstaande gekonsentreerde sonkrag stelsel. Ontwerp spesifikasies vereis 'n akkurate outomatiese posisionering en beheer stelsel vir 'n motor aangedrewe paraboliese son reflekteerder met 'n optiese-kollekteer-kapasiteit van 12 kW_t by maksimum sonhoogte, en veral geskik wees vir afgeleë sonkrag opwekking. Hierdie studie lewer 'n konsepsuele ontwerp en ingenieurs-prototipe van 'n gebalanseerde dubbelas swaai-en-kantel swenkrat aandrywingsmeganisme as megatroniese sonvolg platform vir 'n $\sim$12 m^2 liggewig paraboliese son konsentreerder. Digitale outomatisering van die son konsentreerder platform is geimplementeer op 'n industriële Siemens S7-1200 programmeerbare logiese beheerder (PLB) met 'n digitale afstandbeheer koppelvlak, puls-wydte-gemoduleerde gelykstroom aandrywing en elektroniese ooplus en geslote-lus sonvolg beheer. Die ontwerp en prototipe maak gebruik van beskikbare komponente om lae-koste plaaslike vervaardiging te ondersteun en slaag in die algemeen in die doel om 'n dinamiese megatroniese platform vir 'n gekonsentreerde sonkrag stelsel te lewer wat maklik vervoer, gebou en opgerig kan word op afgeleë persele in Afrika. Intydse eksperimente is gedurende die somer uitgevoer om die akkuraatheid van die prototipe posisionering sisteem te evalueer. Dit toon dat die sisteem die son deurlopend volg met 'n akkuraatheid beter as 1.0° op beide die azimut en elevasie sonvolg asse, wat voldoen aan die ontwerp spesifikasies.

Strukturele aspekte van die prototipe paraboliese skottel word deur ander navorsers geëvalueer en verbeter terwyl die Stirling-eenheid en elektriese sisteme in parallelle projekte ontwikkel word. Die uiteindelike doel met hierdie groepnavorsing is om 'n plaaslik vervaardigde doen-dit-self sonkrag eenheid te ontwikkel wat in Afrika ontplooi kan word.

Stellenbosch University http://scholar.sun.ac.za

Acknowledgements

I express my deep appreciation to my study leaders Mr. Robert Dobson and Prof. Kristiaan Schreve, for their support, advice and guidance during the many research meetings and discussions.

A special word of thanks to Mr. Robert Dobson for providing financial support for this project and for financial assistance with the implementation of the design prototype.

Sincere thanks also goes to Mr. Paul Gauche and Mr. Kevin Neaves for their valuable technical inputs during the course of the project, as well as to all the members of the Mechatronics Laboratory who created a very pleasant working and discussion environment.

Further acknowledgement is given to the Department of Science and Technology and the National Research Foundation, Eskom and the Centre for Renewable and Sustainable Energy at Stellenbosch University for financial assistance to present this research at the SolarPACES conference held in Las Vegas USA during 17-20 September 2013.

Stellenbosch University http://scholar.sun.ac.za

Nomenclature

Abbreviations and Acronyms

A	Area (m^2)
BTU	British Thermal Units
BBC	Backup Battery Capacity
CAD	Computer Aided Design
CO_2	Carbon Dioxide
CG	Centre of Gravity
CSP	Concentrating Solar Power
CMOS	Complementary Metal Oxide Semiconductor
CPV	Concentrated Photovoltaic
D	Diameter (m)
DC	Direct Current
DNI	Direct Normal Irradiation
F	Parabolic Focal Point
FC	Fuzzy Control
GPS	Global Positioning System
HMI	Human Machine Interface
IP	Internet Protocol
IR	Infra Red
IRP	Integrated Resource Plan
ISP	Image Signal Processing
I2C	Inter-Integrated Circuit
LDR	Light Dependent Resistor
MEMS	Micro Electrical Mechanical System
MSA	Maximum Solar Altitude (e.g. 12pm)
P	Power (W)
PCU	Power Conversion Unit
PLC	Programmable Logic Controller
PV	Photovoltaic

Stellenbosch University http://scholar.sun.ac.za

PWM	Pulse-Width Modulation
RE	Renewable Energy
RPM	Revolutions Per Minute
SPA	Solar Position Algorithm
Q	Observer Location (GPS)

Companies, Institutions and Countries

ASTM	American Society for Testing and Materials
DOE	Department of Energy (South Africa)
DST	Departments of Science and Technology (South Africa)
IITM	Indian Institute of Technology Madras
ESKOM	National Electricity Supplier (South Africa)
MDAC	McDonnell Douglas Astronomics
NASA	National Aeronautics and Space Administration (USA)
NREL	National Renewable Energy Laboratory (USA)
NRF	National Research Foundation (South Africa)
PSA	Plataforma Solar de Almerya
SA	South Africa
SCE	Southern California Edison Company (USA)
SES	Stirling Engine Systems (USA)
STERG	Solar Thermal Energy Research Group
SUN	Stellenbosch University
UK	United Kingdom
USA	United States of America
USAB	United Stirling AB

Greek Letters

α	Angular sun position ref earth surface (degrees)
δ	Angular sun position ref equator (degrees)
ϕ	Latitude of installation
ζ	Longitude of installation
S	Sun vector or solar vector
δ	Declination solar noon ref to equator (degrees)
β	Slope angle horizontal (degrees)
ω	Hour angle solar time
γ	Azimuth angle (degrees)
θ	Elevation angle (degrees)

Stellenbosch University http://scholar.sun.ac.za

f	Parabolic focal distance (m)
ϵ	Solar tracking deviation error (degrees)
Δ	Solar tracking angle resolution (degrees)

Subscripts

a	ambient
az	azimuth
c	concentrator
e	electrical
el	elevation
m	mean
p	predicted
q	observer
s	sun/solar
t	thermal
z	zenith

Stellenbosch University http://scholar.sun.ac.za

Contents

Stellenbosch University http://scholar.sun.ac.za

Stellenbosch University http://scholar.sun.ac.za

Stellenbosch University http://scholar.sun.ac.za

Stellenbosch University http://scholar.sun.ac.za

List of Figures

Stellenbosch University http://scholar.sun.ac.za

Stellenbosch University http://scholar.sun.ac.za

Stellenbosch University http://scholar.sun.ac.za

Stellenbosch University http://scholar.sun.ac.za

Stellenbosch University http://scholar.sun.ac.za

Stellenbosch University http://scholar.sun.ac.za

List of Tables

Stellenbosch University http://scholar.sun.ac.za

1. Introduction

The first democratic elections in South Africa (SA) took place during 1994. Today, nineteen years later, limited power grid infrastructure to sparsely populated areas still deprive many rural Africans from access to electricity. National electricity provider Eskom therefore actively supports the development of renewable energy technologies aimed at supplying electricity to sparsely populated areas. Renewable energy is seen as a solution for remote rural communities and engineers are looking at developing renewable energy power generation systems to satisfy the needs of these communities.

As such, Stellenbosch University defined a research initiative aimed at solving challenges faced by rural African villages in terms of electrical power generation and distribution. As part of this initiative, one project relates to small independent off-grid stand-alone solar energy heat and electrical power supply systems, which aims at the implementation of novel mechanical and mechatronic technology principles in moving towards the advancement of solar thermal engineering and the application of scientific principles to support the use of renewable energy technologies in rural applications.

1.1. Research Scope

Climate change is likely to have a more severe impact on communities in Africa because of adverse direct effects, like floods and droughts, and a high dependence on agricultural success for large parts of the continent (Collier *et al.*, 2008). This puts additional pressure on African governments to provide technology, incentives and economic environments to help facilitate social adjustments to change. While most rural African villages experience high levels of solar radiation, rolling out reliable solar solutions for tapping into this renewable energy resource in rural areas pose a number of challenges, for example the cost of these systems, maintenance at remote sites and the reliability and robustness of the design (Collier *et al.*, 2008).

On 6 May 2011, the South African Government published the South African Integrated Resources Plan (IRP) (Department of Energy South Africa, 2011). To help reduce the impact of fossil fuel power generation, the IRP emphasizes the development of green energy technology to utilize renewable energy

Stellenbosch University http://scholar.sun.ac.za

resources and ensure sustainable power generation. The IRP supports this global responsibility and would assist in achieving the South African Millennium Development Goals (Cleeve and Ndhlovu, 2004).

In the IRP, the South African Department of Energy ranks the renewable energy potential for South Africa in terms of capacity potential (Department of Energy South Africa, 2011). Table 1.1 emphasizes the relative importance of CSP (concentrated solar power) energy as the highest potential renewable energy source in terms of capacity to supply in the country's needs (129964 GWh). The capacity potential for CSP is ranked twice as high as the potential for wind energy, the second highest source with potential to supply the country's energy needs. In terms of cost considerations though, Table 1.1 highlights the fact that the cost for CSP is higher than that of wind technology, emphasizing the need for extended research aimed at reducing the cost of CSP technology in order to meet the implementation goals of the IRP.

Table 1.1: Renewable energy capacity potential ranking and the role of CSP in the DOE Intergrated Resource Plan (Kiszynski and Al-Hallaj, 2011).

Renewable Energy Technologies	**Capacity** (GWh)	**Cumulative quantity** (GWh)	**Weighted Cost** (Rand/kWh)
Biomass pulp/paper	110	110	0.30
Landfill gas	589	707	0.33
Biomass sugar bagasse	5 848	6 555	0.38
Solar water heating	6 941	13 496	0.57
Small scale Hydro	9 244	22 740	0.65
Wind	64 103	86 843	0.93
Solar Thermal/CSP	129 648	216 491	1.76

It is well known that Africa is a solar rich continent. The solar resource map in Figure 1.1 reveals that parts of Africa have a very high potential for solar energy harvesting and shows good potential for solar energy project development. Comparative studies have shown that places on the African continent measures annual global irradiation levels of approximately double that of a region such as southern Germany (SolarGIS, 2013), a region which invests heavily in renewable energy projects. It supports the view that solar energy is an ideal natural resource for driving economic development and that novel solar thermal power generating designs are called for to utilize the rich sunlight resource in Africa for the betterment of especially the disadvantaged community.

1.2. The Technological Challenge

In order to harvest solar energy, an apparatus is required to concentrate and convert the solar power into electrical power. Stirling engine technology pro-

Stellenbosch University http://scholar.sun.ac.za

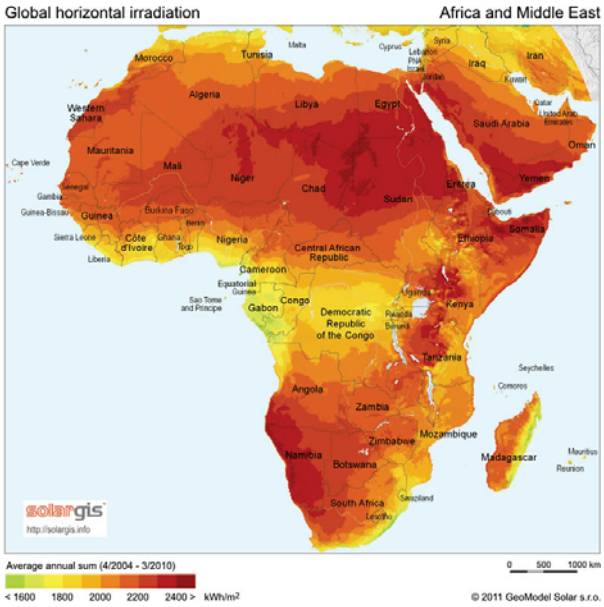

Figure 1.1: Average annual solar distribution for Africa (SolarGIS, 2013).

vides an efficient and robust solution for thermal to electrical power conversion. The United Nations Framework on Climate Change expresses the view that an autonomous off-grid low-cost Stirling or concentrating photo voltaic (CPV) solar power generating system has the potential to empower rural participation in economic development and to improve living conditions to help restore peoples' dignity within developing countries (Makundi and Rajan, 1999).

Figure 1.2 presents a comparison of the average solar-to-electrical power conversion efficiencies between four types of concentrated solar power conversion technologies (Greyvenstein, 2011). Stirling power generation technology, with an average efficiency of around 21.5%, is identified as candidate which offers the best efficiency for implementing a high-power, stand-alone rural power generating system. One type of Stirling engine, namely the *free-piston Stirling engine*, is of particular importance as it consists of only a few moving parts and does not have a direct internal mechanical linkage system. This means that the engine runs very silent and ensures optimum internal operation of a Stirling engine power supply unit. Apart from its relative mechanical simplicity, the device has no lubrication system, uses no mechanical seals and is deployed as a hermetically sealed unit. Free piston Stirling engines are thus regarded as being the most reliable and maintenance-free of all heat engines and most suitable for solar power generation in Africa (Tsoutsos *et al.*, 2003).

In terms of the climate change challenge, Stirling technology in combination with a reliable solar concentrator and automated solar tracking solution can generate high-power electrical energy with close-to-zero CO_2 or harmful greenhouse gas emissions. Such solar power systems are expected to reach energy conversions efficiencies above 30% by 2015 (Gary *et al.*, 2011) and by

Stellenbosch University http://scholar.sun.ac.za

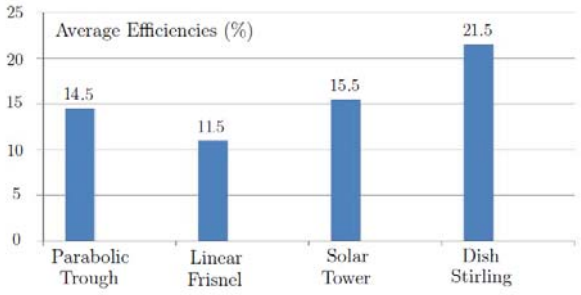

Figure 1.2: Average solar technology conversion efficiencies (Greyvenstein, 2011)

comparison, is considered to be amongst the most economic and green energy power generation technology platforms (Lopez and Stone, 1993).

This study therefore sets the goal to develop an efficient low-cost high-power parabolic dish system in order to be able to exploit the solar resource through concentrated solar Stirling technology. For a Stirling device to generate electrical power, it needs to be connected to a sun-concentrating optical device which focuses the light rays of the sun onto the *solar receiver* of the Stirling engine. A typical solar reflector system consists of a matrix of reflecting mirrors, often manufactured of reflecting polymer film, that are fixed onto a parabolic dish and arranged to concentrate the sun's energy onto a solar receiver. The solar reflector system also needs to be dynamically tilted at certain angles to continuously face the sun throughout the day. Mechanical drives and a control system are required to direct the dish structure to keep a tight focus directly on the sun as it moves across the sky.

To serve the electrical power needs of around five to ten households with a 3 kW_e electrical system at a typical site of installation in Africa, a concentrated solar power system needs to collect around 12 kW_t of energy at noon (assuming 25% conversion efficiency). This means that a mechanical platform and electronic control solution for a positioning system should have the capacity to support solar tracking for a parabolic dish with a diameter of $\sim$4 meter ($D = \sim$4 m to collect $\sim$12 kW_t). The technology challenge is thus focussed on the development of a simple and robust electro-mechanical positioning means suitable for off-grid stand-alone systems and capable of dynamically steering a 12 kW_t parabolic dish structure to follow the sun with great precision.

A solution for stand-alone off-grid Stirling power generation at remote rural villages calls for a novel design with technology features not generally available in commercial systems. This project therefore becomes not only justifiable, but also essential. In advancing towards such a stand-alone, self-tracking concentrated solar Stirling electrical power generation system for off-grid rural communities, this study has set the goal to develop an automatic positioner and control system for an off-grid stand-alone motorized parabolic solar reflector. Given the social circumstances and technological capacity of many developing communities in rural areas, simplicity and maintenance will be crucial to the

Stellenbosch University http://scholar.sun.ac.za

proposed solution.

In this study, an easy-to-assemble concentrated solar power system with PLC driven mechatronic platform will be designed and preliminary results obtained will be discussed.

1.3. Hypothesis

The aim of this project is to help solve challenges faced by rural African villages in terms of electrical power generation and distribution. The goal is to utilize Africa's rich natural sunlight resources to deliver on socio-economic objectives in terms of providing solar electric power to communities in deep rural areas.

The hypothesis of this study postulates that it is possible to develop an accurate automated positioner and control system for a stand-alone motorized parabolic solar reflector with a capacity to harness 12 kW_t of solar thermal energy at noon, which in turn is essential to provide off-grid rural communities with a stand-alone knock down 3 kW_e peak electrical power generation and supply system. This supports the objectives of the Stellenbosch University HOPE Project (Figure 1.3), which defines *energy and sustainable environment* as one of the five research focus areas in support of local communities. In general, Stellenbosch University's HOPE Project creates sustainable solutions to some of South Africa's and Africa's most pressing challenges within five development themes, namely the eradication of poverty and related conditions; the promotion of human dignity and health; democracy and human rights; peace and security; as well as energy and sustainable environment/industries.

Figure 1.3: Stellenbosch University HOPE Project identified energy and environment as key focus area for new developments (Stellenbosch University, 2013).

The STERG group (Solar Thermal Energy Research Group) focus on the implementation of novel mechanical and mechatronic technology principles in striving towards the advancement of thermal engineering and the application of scientific principles in support of the use of renewable energy technologies. Under this thrust, the goal of this thesis is to design, construct and test a

Stellenbosch University http://scholar.sun.ac.za

solar tracking positioning system for a self-tracking concentrated solar power generating system suitable for deployment into Africa.

1.4. Objectives

This thesis describes the mechatronic development of a robust concentrated solar power system parabolic dish tracking system for rural deployment and harsh environmental conditions. The project forms part of research which ultimately aims to produce a locally manufactured knock-down CSP power generation kit which is suitable for off-grid solar power applications. Since this CSP power generation kit is primarily intended for deployment in the rural market, the design calls for a simple and robust technical solution suitable for inhabitants from rural villages (the "user") who will typically assemble and install the system on site.

From a technical perspective, the main objective of this study is to design a robust mechatronic platform with automated solar tracking control for a stand-alone parabolic solar concentrator with a thermal harvesting capacity of 12 kW_t at solar noon. The mechatronic system should incorporate the design of an altitude-azimuth drive system, feedback sensing devices and a digital electronic solar tracking control system to command the various modes of operation during solar tracking and power generation. The design ventures into the conceptual phases of the structural and optical solar concentrator dish development. The parabolic dish serves as payload for the mechatronic platform, necessitating the development of the dish as load onto the dynamic tracking platform. As final product, the complete stand-alone concentrated solar power system should ideally be self-contained and is not intended to be connected to the grid but rather to serve as a power supply where there is no grid power available. The design methodology, described in Chapter 3, details the design specifications and system requirements suitable for the commercialization of the technology as a CSP power generation kit.

This thesis primarily deals with the technical design, implementation and testing of the tracking accuracy of the prototype mechatronic platform for a concentrated solar power generating system under various tracking methods. Structural aspects of the prototype parabolic dish will in future be optimized by other researchers while the Stirling and power handling units are under development in parallel projects. A cost analysis and feasibility study are also progressing in a parallel project, in preparation of the commercialisation of the technology.

Stellenbosch University http://scholar.sun.ac.za

1.5. Thesis Layout

This thesis will consist of eight chapters. Chapter 1 introduces the topic of the thesis, defines the research scope with technological focus and states the hypothesis of the study. Chapter 2 details the literature review, which includes a plethora of information on sun tracking mechanisms, altitude and azimuth actuating systems and electronic control and automation structures. The literature review provides background information for the design of the system. The design methodology, user requirements and technical design specifications are presented in Chapter 3. Chapter 4 details the mechatronic platform design and prototype implementation, as well as various design concepts and options. The design and implementation of the digital control system and the electronic control logic software are discussed in Chapter 5. In Chapter 6, experimental results of the performance of the mechatronic system and digital electronic control system for the self-tracking solar reflector and positioning system are presented. The thesis concludes with Chapters 7 and 8 in which the study is summarized and conclusions with recommendations towards future work are offered.

Stellenbosch University http://scholar.sun.ac.za

2. Literature Review

This chapter presents a literature review and introduces theoretical models for harvesting solar power by means of a concentrated solar power system. A broad overview of existing solutions from literature on commercial dish Stirling systems are presented in this review.

2.1. Solar Energy as a Natural Resource

The sun radiates energy in the form of electromagnetic energy and the amount of electromagnetic radiation that reaches the earth from the sun in referred to as solar radiation. The term "irradiance" is used to define the amount of solar energy per unit area received over a given time. As the solar electromagnetic energy passes through the atmosphere of the earth, the solar energy levels is around 1000 W/m^2 when it reaches the surface of the earth (Duffie and Beckman, 2006).

Direct radiation is usually found in the higher electromagnetic light energies, such as in the blue and ultraviolet spectrum. For CSP thermal systems, direct radiation is of more importance since this radiation energy can be optically collected and focused onto a solar concentrator to harvest mostly solar thermal energy. Solar radiation can be measured using a device called a solarimeter or a pyranometer. This device measures the total electromagnetic radiation levels from various angles of incidence by way of determining the photon levels of light within selected spectral frequency bands through different masks and sensors. The solarimeter can be configured to specifically measure the direct component of the solar radiation in which case it is referred to as a pyrheliometer (Duffie and Beckman, 2006).

The next section describes mathematical models of the sun's apparent trajectory in the sky and serves as an introduction to solar tracking mechanisms required to optically harvest solar thermal energy from the sun as it moves across the sky.

Stellenbosch University http://scholar.sun.ac.za

2.2. Solar Trajectory

Harvesting energy from the Sun, using an optical means such as a parabolic dish, requires the development of a simple yet accurate sun following mechanism, or solar tracking mechanism. The sun tracking mechanism uses information about the position of the sun to direct the dish system to continuously point towards the centroid of the sun. For this purpose, the location of the sun and its trajectory of movement as observed from a given geographical perspective needs to be carefully studied and analysed.

The *sun vector* (coordinates of the sun from any point of observation) as well as the trajectory of the sun path can be calculated at any instance of time and is of primary importance for steering the parabolic dish to face the sun (Stine and Geyer, 2001). These coordinates can be calculated as a vector $S_Q(\gamma_s,\ \theta_s)$ from mathematical astronomical frameworks. One of the most accurate algorithms for computing the location of the sun using an algebraic astronomical base was developed under contract at the National Renewable Energy Laboratory (NREL) for the Department of Energy in the United States (DOE,USA) (Reda and Andreas, 2008). This algorithm, known as the NREL solar position algorithm (SPA), calculates the position of the Sun with an accuracy of $\sim 0.0003°$ (Reda and Andreas, 2008).

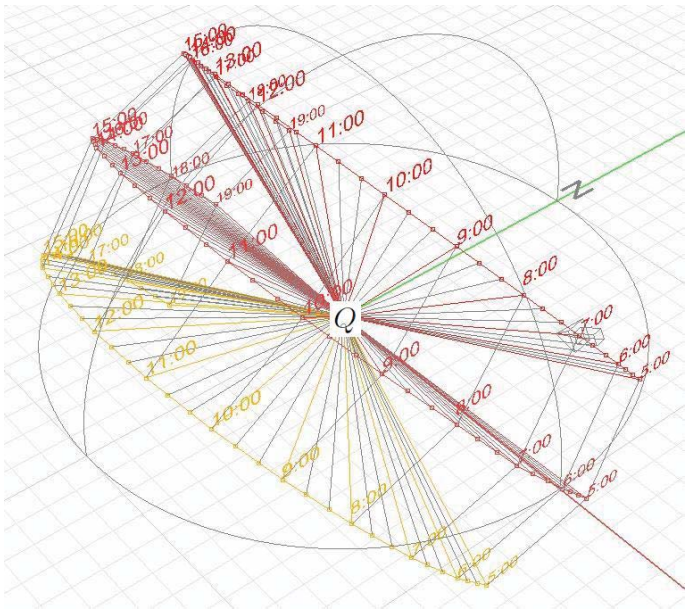

Figure 2.1: Geometric view of the sun path as seen by an observer at Q during winter solstice, equinox, and summer solstice (Wood, 2010).

Depending on the location of the observer (Q) and season of the year, the sun appears to move along the circumference of a disc which is displaced

Stellenbosch University http://scholar.sun.ac.za

from the observer at various angles. The solar path's disc-like movement pattern around the earth is illustrated in Figure 2.1. This solar path diagram is regularly used in architectural designs where the solar seasonal movement geometry is generated with the Autodesk Ecotect tools package (Wood, 2010) for the sun's movement to be considered in property and landscape models by rendering sunlight on designs to analyse shadowing.

From a solar tracking perspective, the sun needs to be tracked as it moves across the sky, while the coordinates of the sun path at the solar concentrator location site (Q) presented in Figure 2.1 can be calculated using an astronomical based solar position algorithm. From the solar tracking location perspective, the sun path geometry illustrates the geometric view of the sun's apparent path where the sun appears to be travelling about the disc circumference at an angular rate of around 15° per hour. The centre axis of the seasonal moving solar discs in Figure 2.1 appears to move along a fixed angle of inclination with respect to the observer (Stine and Geyer, 2001).

Algorithms such as the NREL SPA can be used to compute the sun-path diagram, which is a visual representation of the sun-path during various seasons and time-of-day. A sun path diagram (also sun path chart or sun path map) describes the aspect of the solar position in terms of the location, time of day, direction of movement, sun path movement lines, altitude angles as well as azimuth angles of the sun. The sun-path diagram is important visualisation tool with which to model and display the path of the sun as it moves through the sky, whilst being observed from a specific geographic location on the earth's surface. Such diagram further show the dynamics of change throughout the various solar seasons and monthly solar cycle changes. Together with irradiation data tables, sun path diagrams provide the daily irradiation levels available at a specific location for a concentrated solar power system.

Solar harvesting requires accurate solar tracking, which in turn requires precise focusing of the optic reflecting device onto the centroid of the sun. With the exact solar coordinates and the trajectory path of the apparent movement of the sun known (i.e. the SPA or sun path diagram at any given geographic location of the surface of the earth), this information can serve as input to the positioning system controller. The next section describes some of the basic principles of solar harvesting and mechanical solar tracking using the solar trajectory knowledge described in this section.

2.3. Solar Tracking Platforms

In azimuth/elevation solar tracking, the concentrated solar power system harnesses solar energy by rotating in the azimuth plane parallel with the horizon as well as in the elevation plane perpendicular to the horizon. This dual axis movement allows for the parabolic dish to be moved in an upwards or down-

Stellenbosch University http://scholar.sun.ac.za

wards direction as well as from left to right in order to follow the movement of the sun throughout the day.

By way of example, Figure 2.2 illustrates the solar path (azimuth and elevation angle contours) which typically need to be tracked by the parabolic dish drives at a solar installation site at a given geographical location. This figure shows the sun path contours for that site, as well as the estimated available solar energy at that particular location (Manfred, 2012). This information can be used to configure a solar tracking platform system for that site as well as predict and evaluate the viability of installing a solar energy system at the site on an *a-priory* basis.

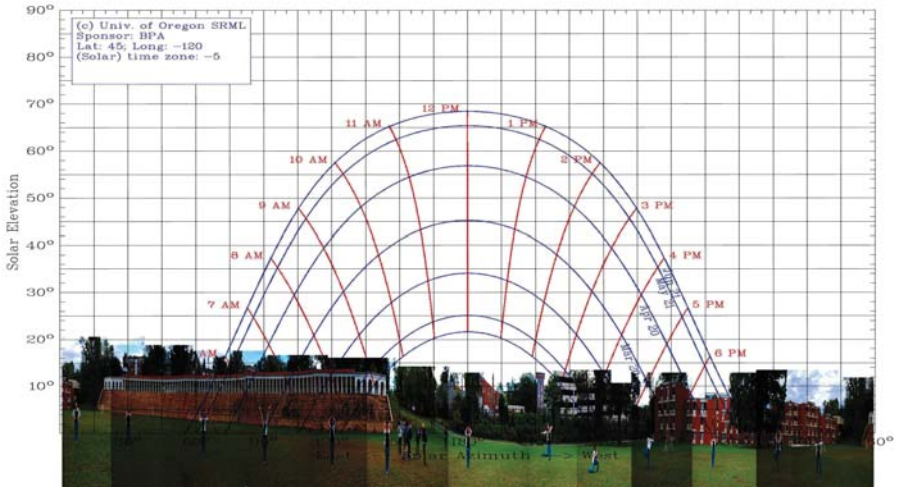

Figure 2.2: Typical sun path diagram in Cartesian coordinates, showing the azimuth/elevation of the sun daytime path at a given location (Manfred, 2012).

In this example, the solar concentrator dish needs to dynamically track the movement of the sun throughout the duration of the day on both azimuth and zenith angles. The actuator responsible for correct positioning on the azimuth angle is referred to as the azimuth drive while the actuator responsible for the correct positioning on the elevation angle is known as the altitude drive.

The azimuth/elevation tracking drive mechanism of the solar tracking system shown in Figure 2.3 was developed by Infinia Corporation and uses a dual slew drive pan-tilt control mechanism to realise dual axis solar tracking (Greyvenstein, 2011). In this tracking mechanism, the altitude and azimuth drives have been combined into one gearbox unit (see Figure 2.3). This balanced cantilever design allows for smaller and less expensive drives to be used. Unfortunately this type of design requires a triangular cut from the bottom half of optical dish to allow for mechanical movement during elevation, which in turn results in loss ($\sim$ 10% to 15%) in square meter solar reflecting area.

Stellenbosch University http://scholar.sun.ac.za

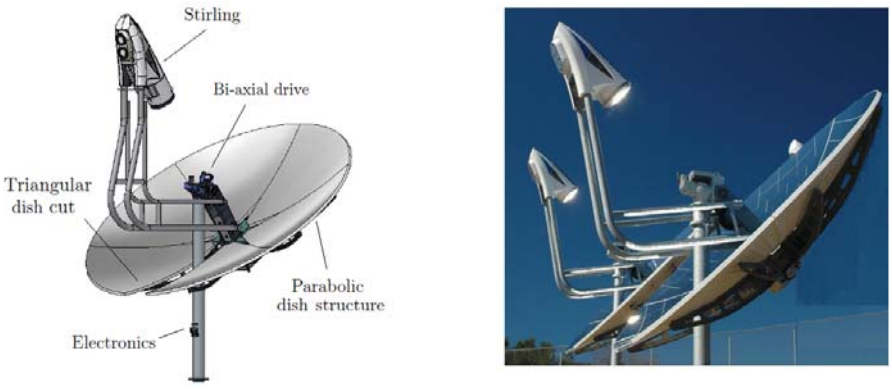

Figure 2.3: Bi-axial drive implemented by Infinia (Greyvenstein, 2011)

In other systems, dual axis solar tracking mechanisms drives the altitude and azimuth movements independent from each other. Two examples of such independent solar concentrator drive mechanisms are shown in Figure 2.4. In this figure, drawing (a) shows how the dish elevation movement pivots in front of the dish, and in drawing (b), the elevation movement pivot point is located behind the dish. One problem with solar tracking systems driven from behind the dish is that there is a large load bias on the front of the dish due to the weight leverage of the solar receiver (usually as Stirling power generator). This requires large and overly expensive tracking drives to overcome the hanging load of the power conversion unit on both the azimuth and elevation angle drives. Large counterweights are often employed to reduce the solar receiver load, but this increases the total weight of the system and increases the potential for system instability. Increased additional weight (with no physical benefit) requires larger and more expensive bearings as well as a stronger and more expensive pedestal framework.

McDonnell Douglas proposed a novel point-focusing parabolic dish solar

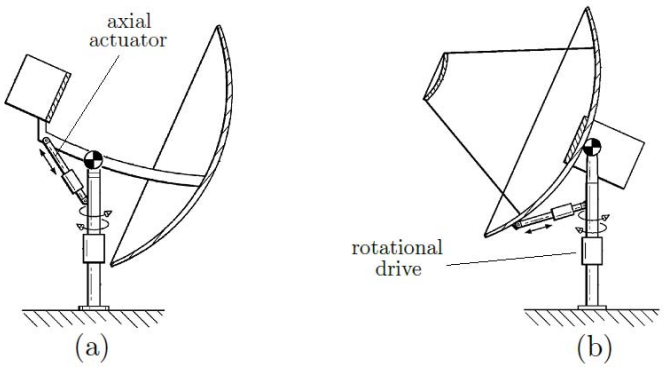

Figure 2.4: Dual axis solar tracking system using independent actuators located (a) in front of the dish and (b) at the back of dish (Esmond *et al.*, 2011)

Stellenbosch University http://scholar.sun.ac.za

tracking system with full tracking capabilities in on an elevation-over-azimuth axis. The parabolic dish reflector was developed to meet commercial requirements in both power grid connected and remote (off-grid) applications (Dietrich *et al.*, 1986). The McDonnell Douglas parabolic dish solar tracking system is presented in Figure 2.5(a) to illustrate the typical components of a mechatronic solar tracking platform design.

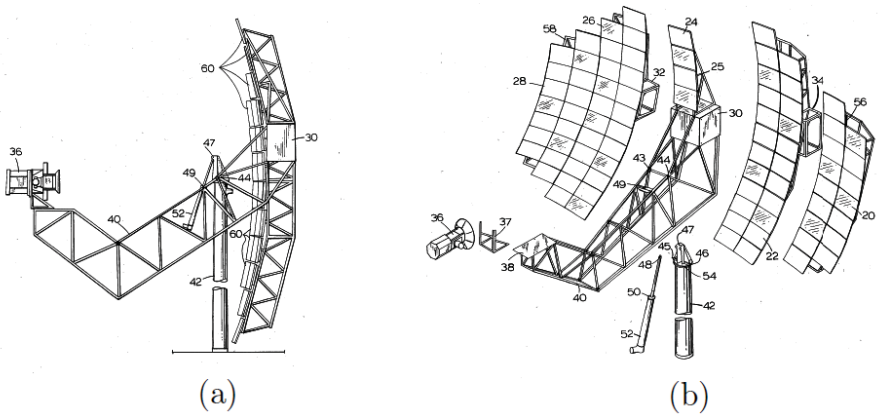

Figure 2.5: McDonnell Douglas counter-balanced tilt-and-swing concentrated solar tracking platform (a) side-view and (b) exploded view (Dietrich *et al.*, 1986).

Figure 2.5(b) shows the exploded view of this concentrated solar power system design configuration, in which five sub-assemblies can be identified, namely: the solar dish surface, the solar tracking structure, the base structure, the azimuth drive and the elevation drive. This design uses a weight balanced cross-beam design, where the weight of the parabolic dish (on one end) and the receiver/generator (on the other end) is balanced on a pivot point over the pedestal stand. This solar tracking design integrates a dual drive system for which the positioning of the altitude and the azimuth drives were placed in separate positions. These positions were chosen so that the drives can perform as close to their ideal efficiency points as possible. The azimuth drive in both the McDonnell Douglas and the ESE designs were planetary gear drives (Winsmith Planocentric drives) with a gear ratio of at least 30000 : 1. The advantage with such a large gear ratio is that very precise positioning can be achieved with relatively small permanent magnet electric motors driving the azimuth and elevation movements. In general for solar tracking solutions, large gear-ratio drives are preferred in sun path tracking, since the movement of the sun is limited to less that 1° minute. Such relatively slow moving requirements through large gear-ratios provide the added advantage that less torque is required for the initial stages of every incremental movement of the dish. With less torque required, less current is drawn by the electric motors during every incremental start-up phase.

Stellenbosch University http://scholar.sun.ac.za

Lopez and Stone (1993) investigated field problems of solar concentrator/dish stations, and reported that oil leaks on the concentrator and actuator drives caused oil to spill onto the solar optic reflector mirrors. This resulted in severe mirror soiling problems due to the oil attracting dust/soil particles. In such cases, expensive manual scrubbing had to be employed to remove the oil from the dish mirrors. This experience raised an alert against the use of oil lubricated tracking drives in solar concentrator design, suggesting that grease lubricated actuator drives for solar concentrators operating in extreme heat conditions might ensure fewer problems with field maintenance.

In the next section, some of the actuator systems or transmission drive solutions that have been used by other system developers to accomplish dual-axis solar tracking will be discussed.

2.4. Solar Tracking Control

In this particular study, the focus is on solar thermal systems, and particularly on controlling the movement of a CSP system in an energy efficient manner. For this purpose a control system needs to be designed around continuous orientation or positioning of the CSP solar concentrating tracking system with respect to the sun vector. The sun vector $S_Q(\gamma_s, \theta_s)$ describes the sun's angle and elevation from the perspective of a specific Global Positioning System (GPS) orientation on the earth (Reda and Andreas, 2008).

Since accuracy and stability are two of the primary design parameters for a CSP solar tracking system, various control strategy options have been proposed, tested and reported on in the general literature. These include open-loop control systems, closed-loop control systems and in some cases an integrated or hybrid-loop control system where open-loop and closed-loop control configurations are combined.

There are four main categories of control elements that will need to be considered in open-loop and closed-loop controllers in order to meet the design criteria for this study. These include:

1. Position of the sun: To determine the sun vector $S_Q(\gamma_s, \theta_s)$ from the location of the CSP system;

2. Effective drive system: To be able to move the structure efficiently so that it points directly towards the sun;

3. Control inputs: Type of control inputs to use, e.g. sun vector algorithm, photo-diodes or camera;

4. Control system: Control sequence and intelligence (state diagrams) to manage the electric motors and drives that move the payload or Stirling power system.

Stellenbosch University http://scholar.sun.ac.za

Since the solar tracker will be used to enable the optical components in the CSP systems, tracking accuracy and mechanical stability will be two of the main elements.

The current trend in modern industrial programmable logic controlled (PLC) solar concentrator and tracking systems is to use open-loop controllers, sometimes also referred to as passive controllers. These controllers use solar positioning algorithms, such as the one provided by NREL, to direct the motion of the solar concentrator system. Closed-loop controllers (or active controllers) reach optimal tracking precision by using light sensitive electronics to enable the controller to observe the movement of the sun and for the concentrator system to be dynamically positioned towards the sun. More complex alternatives involve camera-based solutions, but these are less popular in PLC based controller solutions due to the electronic sensitivity and the processing power requirements for image processing.

2.5. Open-loop Sun Tracking

The sequence of solar vectors $S_Q(\gamma_s,\ \theta_s)$ for a specific geographic location (Q) is determined in real-time by the control system and is required for the solar tracking system to accomplish efficient sun tracking. In this section the three astronomically based methods, or algorithms used in implementing sun-tracking on a micro-controller system, will be discussed. Artificial intelligence (AI) or fuzzy control (FC) mechanisms, in which two or even all three of these methods can work together with other controller inputs, may also be considered to accomplish accurate tracking with very low parasitic losses.

In astronomical based algorithms, the sun vector or solar position is described in terms of the sun's apparent azimuth and elevation angles with respect to an observer at a specific geographic location "Q" on the surface of the earth, as a function of local hour and season. The term sun-vector, or sun-pointing vector, stems from algebraic grounds associated with the earth surface based coordinate system in Figure 2.6 through which an observer at location Q is illuminated by a central sun ray, observed along direction vector "S_Q", where this vector points towards the sun at solar azimuth angle (γ), and the solar altitude angle (α) or solar zenith angle (θ) (Stine and Geyer, 2001).

It was noted in Section 2.2 that NREL developed one of the most accurate algorithms for computing the sun vector $S_Q(\gamma_s,\ \theta_s)$ using an astronomical approach (Reda and Andreas, 2008). This algorithm is known as the NREL solar position algorithm (SPA) and calculates the position of the sun with an uncertainty of $\sim 0.0003°$ at vertex, compensating for cosmic changes (including the leap second) from the year 2000 until the year 6000.

The notation of the earth surface based vector system used in this study is depicted in Figure 2.6. Although some conventions measure the azimuth angle from the south-pointing coordinate, this study uses the general convention

Stellenbosch University http://scholar.sun.ac.za

through which the azimuth angle is measured from the north-pointing coordinate, with a positive increase in the clockwise direction. The parameters for the sun vector $S_Q(\gamma_s, \theta_s)$ and the various angles to be considered when a solar concentrator tracks the sun using a digital electronic platform in conjunction with an astronomical algorithm are illustrated in Figure 2.6.

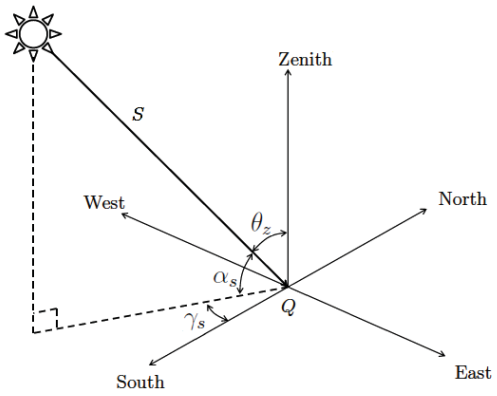

Figure 2.6: Observer at location Q illuminated by sun ray observed along sun vector S_Q, showing solar tracking azimuth and elevation/zenith angles.

Comparative algorithms are less accurate or may deviate in terms of accuracy over time, but needs to be mentioned for the processing speed benefits and integration simplicity they offer. These are the Grena algorithm (Grena, 2008), the Muriel algorithm by La Plataforma Solar de Almeria (PSA) (Blanco-muriel *et al.*, 2001), and the Duffie and Beckman algorithm which, like the Grena and PSA algorithms, can be implemented on a PLC platform (Duffie and Beckman, 2006). An algorithm proposed by Meeus in 1988 is accurate to approximately 0.0003° deviation, but it requires significant processing power and processing time (Reda and Andreas, 2008).

Feedback sensors such as signals from photodiodes, phototransistors, light dependent resistors, sun sensors or processed camera images are some solutions which may be considered to ensure that the instantaneous errors in the azimuth and elevation angles calculated from the SPA algorithm can be corrected. Such feedback mechanisms and their implementation in various solar tracking solutions will be discussed in the next section.

2.6. Closed-loop Sun Tracking

Any discrepancy between the angles calculated through an algorithm and real-time position of the solar concentrator can be detected and corrected in a closed-loop tracking control solution. With this feedback, the pointing control

Stellenbosch University http://scholar.sun.ac.za

system ensures that any tracking errors due to wind effects, mechanical backlash, installation mismatches, accumulated errors or other disturbances in the positioning of the parabolic dish can be corrected or eliminated.

Solar sensor feedback, camera images or optical encoders typically serve as input to the closed-loop controller in order to activate the drive mechanisms to augment the precise movement the solar dish so that it pin-points towards the exact solar position in the sky. Some of these solutions and their operating mechanisms will be discussed in more detail below.

2.6.1. Sun Tracking: Photodiodes and Transistors

Photo sensitive devices and the principles behind their operation are commonly used in closed-loop control for solar tracking systems. In these solutions, light sensitive sensors or infra-red detectors can be employed either to autonomously direct sun tracking or to fine-tune the positioning of the parabolic dish. In general, differential signals from these devices are used in output balancing circuits in order to compensate for differences in component characteristics or changes in light sensitivity levels.

In some solar tracking designs, dual angle tracking is accomplished with optical slot photo-diode sensor arrays which is used to detect whether a solar dish has been oriented towards the solar home position. These photodiode homing sensors are typically mounted on the parabolic dish structure to assist with feedback to the control mechanism for adjusting the dish collector to a position directly facing the sun. Phototransistors have the added benefit in that they can be connected in current circuits to drive the servo motors, thereby physically commanding the drives which directs the parabolic dish mechanism.

2.6.2. Sun Tracking: Light Sensitive Resistors

A light-dependant-resistor (LDR) or photoresistor operates on the principle of photoconductivity in which the resistance of a semiconductor decreases as its exposure to light intensity increases. The semiconductor absorbs the light energy, causing free electrons to move over the silicon band-gap, thereby lowering the resistance of the device (Kalogirou, 1996).

In solar tracking applications, the LDR is typically fixed on the outside or inside edges at the base of a square metallic, ceramic or plastic tube. The variance in resistance of the LDR matrix, as a result of the combined shadowing effect of the square housing tube, is used as feedback signals to determine the solar tracking error angles.

Stellenbosch University http://scholar.sun.ac.za

2.6.3. Sun Tracking: Sun Sensor

The use of sun sensors stems from the satellite and space industry where the position of the sun, or sun vector, is used in real-time to continuously determine the orientation of the satellite or spacecraft very precisely. In spacecraft and satellite body orientation, a precise sun sensor (Figure 2.7(a)) is spun at a constant rate to determine the spacecraft orientation with respect to the sun. Designed for use in nano-spacecraft, these sensors are claimed to achieve higher measurement accuracies compared to photodiodes (SolarMEMS, 2013). In Figure 2.7(a), incident sunlight enters the sun sensor through a small pin-hole in a mask plate (giving a $\sim$50° field of view, around four hours exposure to the sunpath), where the light is exposed to a silicon substrate which outputs four signals in relation to the horizontal and vertical incidence of light. The sun vector $S_Q(\gamma_s, \theta_s)$ is then calculated through an image detector and a calibration algorithm, providing a solar vector accuracy to $\sim$0.2° (SolarMEMS, 2013).

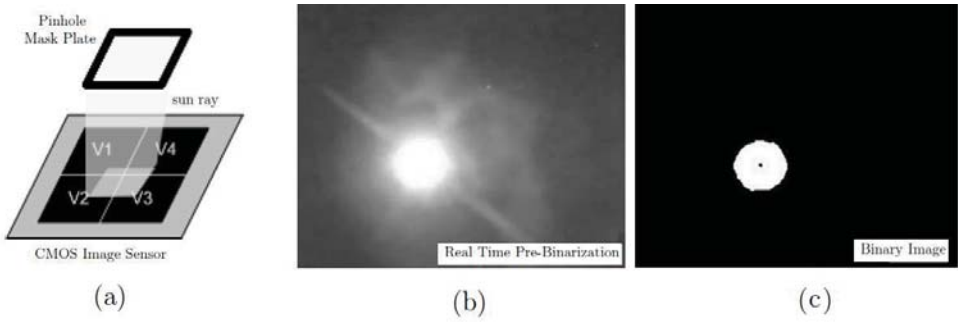

Figure 2.7: Determining the solar concentrator orientation using (a) a CMOS sun sensor to compute the incident ray angle (SolarMEMS, 2013) and (b,c) a web camera with image processing to determine the coordinates of the sun centroid on a binary image (Arturo and Alejandro, 2010).

One practical difficulty anticipated when using spacecraft type sun sensors in solar tracking applications is potential problems with dust and rain. The sensor use a very small aperture pinhole configuration to determine the angle of the sun very accurately. This pinhole mechanism may cause the sensor to be prone to dust and rain interferences in the rough rural environmental and agricultural conditions in which a concentrated solar tracking system would typically be required to operate.

2.6.4. Sun Tracking: Camera Image Processing

Camera image processing may also be used to optically control the solar tracking operation or to assist in compensating for errors in azimuth and elevation angle errors experienced in open-loop control mode. With an optical feedback means, the control system can ensure that any tracking errors due to wind

Stellenbosch University http://scholar.sun.ac.za

effects, mechanical backlash, installation mismatches, accumulated errors or other disturbances in the positioning of the parabolic dish are reduced.

The use of a web camera system to augment or fine-tune the positioning of the solar dish during continuous sun tracking was presented by Arturo (Arturo and Alejandro, 2010). Figure 2.7(b) shows a snapshot real-time pre-binarization image of the sun taken by the web camera, while Figure 2.7(c) shows the converted binary image processed to compute the centroid position of the sun on the snapshot image, determining the sun vector $S_Q(\gamma_s, \theta_s)$ according to the principles used by Arturo *et.al.* (Arturo and Alejandro, 2010).

Web camera mechanisms with image processing can be employed in closed-loop solar tracking control. It uses the image processed sun vector S_Q to align the parabolic concentrator dish towards the sun. In this control strategy, the dish may also be directed through a homing process to guide the dish closer to the true focus point of the parabolic dish.

2.7. Existing Concentrated Solar Power Systems

As part of the literature study, emphasis is placed some of the most successful field-proven designs. In this section some of the design concepts found in technical- and evaluation- reports will be studied, as these reports typically provide valuable insights into best-practice designs.

The precursor to most successful utility scale industrial solar tracking systems for solar thermal electrical power generation is considered to be the Vanguard system (Figure 2.8). This 25 kW_e system includes a 10.5 m diameter glass faceted dish and has set eight world records in 1984 (Mancini, 1997). Solar tracking is achieved by means of a novel design in which elevation lift is accomplished through rotational movement. The design incorporated a gimbal mechanism to attain lift through increased rotational torque (similar to a cam) and where on average 8% of the generated energy is used to drive solar tracking (92% nett gross energy generation efficiency). Whilst a solar flux to electrical conversion efficiency of 29% was achieved, problems were however experienced with noise, vibration, and excessive wear on non-hardened gears.

The Vanguard design was soon overshadowed by the simplicity, weight reduction and mechanical stability realised with the McDonnell Douglas tilt and swing solar tracking mechanism design (Figure 2.9; concept shown in Figure 2.5) (Mancini, 1997). In this design geometry, the weight of the reflector dish and the receiver/generator is balanced on a pivot point over the pedestal stand to achieve mechanical balance and stability.

Developed in 1984, the McDonnell Douglas Aerospace design proved to be one of the first commercially successful solar concentrator solar power generating devices (Mancini, 1997). This 25 kW_e Stirling dish solar concentrator

Stellenbosch University http://scholar.sun.ac.za

Figure 2.8: The Vanguard solar tracking system and drives (Mancini, 1997).

Figure 2.9: The McDonnell Douglas tilt-and-swing solar tracking system (Mancini, 1997).

comprises of a 11 m diameter modular dish constructed as a support structure tiled with 82 mirror facets to provide 91.4 m^2 of solar reflective area. The positioning system uses a balanced boom arm positioning system design to accomplish solar tracking on a dual-axis control mechanism. With the reflector dish on one end, and the receiver/generator on the other end, the boom balances on the pedestal stand on a pivot point at its centre of gravity. This solar tracking design integrates a dual drive system to electronically control the movement of the curved solar dish reflector in the altitude and the azimuth directions to ensure maximum heat to electrical power conversion through a Stirling engine.

In terms of a dish structure, two alternative design changes have been made and tested, as shown in Figure 2.10. The modular dish on the left use multifaceted spherically shaped mirrors in a truss support structure, while the dish on the right is padded with shaped mirror sections to focus sun flux on the

Stellenbosch University http://scholar.sun.ac.za

Figure 2.10: Modifications to balanced cantilever-type design of the McDonnell Douglas modular parabolic dish (WGAssociates, 2001).

solar receiver. These "balanced cantilever" type designs inherently guarantee near linear stability, while eliminating the need for additional counterweights to reduce the torque load on the drives. These features make this design concept ideal for solar tracking applications as it uses the structure's own weight to balance the beam, which puts less strain on the bearings and drives. The lower torque demand requires less expensive drives and smaller electric motors to drive the concentrator dual-axis tracking motions.

Slight variations to the McDonnell Douglas design were also incorporated into the Cummins Power Generation solar tracker design, namely the 25 kW_e solar concentrator model WGA-1500 (Figure 2.11(a)), and the Sandia 10 kW_e model WGA-500 (Figure 2.11(b)). The 10 kW_e system (Figure 2.11(b)) proved to be suitable for remote off-grid applications when high gear ratio and smaller electric motors were used (WGAssociates, 2001). Field-proven commercial drives (mostly planocentric 16000:1 gear ratios) and linear actuators (off-the shelf ball screw linear actuators) were used and sized to fit weight and gravity load conditions for each concentrator.

Figure 2.12 shows (a) an 11 m diameter parabolic dish concentrator system built as a test system by WG Associates for Sandia in the USA, and (b) the 25 kW_e Sandia faceted *stretched membrane concentrator*. The design configuration of Southwest Solar Technologies (2013), namely the SolarCAT system (Figure 2.13), includes struts in front of the dish (similar to an umbrella structure) to support the 20 m diameter optical dish (focusing 230 kW_t of solar energy on the solar receiver). The struts were included to bring stability to the dish structure, however, it introduces a shadowing effect onto the mirrors which impacts on the efficiency of the system.

The Fresnel dish concept (Figure 2.14) is different from most other dish designs in that flat mirrors are individually orientated on a flat platform instead of a parabolic dish structure (Stine and Geyer, 2001). This focusing system operates similarly to the solar tower heliostat concept, but only on a

Stellenbosch University http://scholar.sun.ac.za

limited-scale single dish frame. The mirrors are placed in a Fresnel configuration on a flat metal structure so that the composite shape of the mirrors approximates a parabolic shape, while the dish tracks on two axes. HelioFocus (Smith and Cohn, 2010) developed the *HelioBooster* system (Figure 2.14), which uses an array of small flat mirrors in order to reduce the complexity. This design resulted in lower manufacturing costs with dish efficiencies similar to conventional parabolic dish systems. This design geometry further allows for upscaling to accommodate larger dish configurations without the need for a larger footprint area. In comparison with a conventional parabolic dish, this flatter dish structure does not cause significant shifts in solar tracking balance if the dish size is increased (Smith and Cohn, 2010).

Figure 2.15 displays two similar solar tracking arrangements, namely (a) the Schlaigh Bergermann designed Eurodish design comprising of a 3.5 m diameter 10 kW_e dish (Mancini, 1997) and (b) the patented 3.2 m double diameter Titan Tracker dish designed in Spain (TitanTracker, 2013). These two designs are based on the same concept, namely a circular rail azimuth

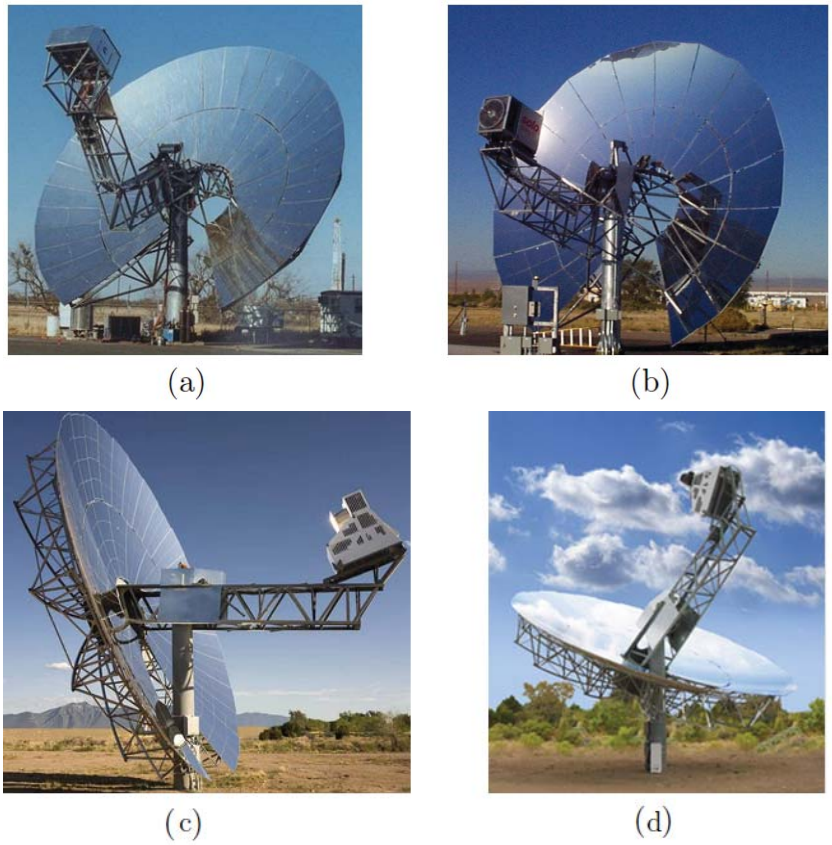

Figure 2.11: Solar tracker designs for (a) model WGA-1500 25 kW_e solar concentrator, (b) model WGA-500 10 kW_e solar collector and (c,d) the Suncatcher system (WGAssociates, 2001).

Stellenbosch University http://scholar.sun.ac.za

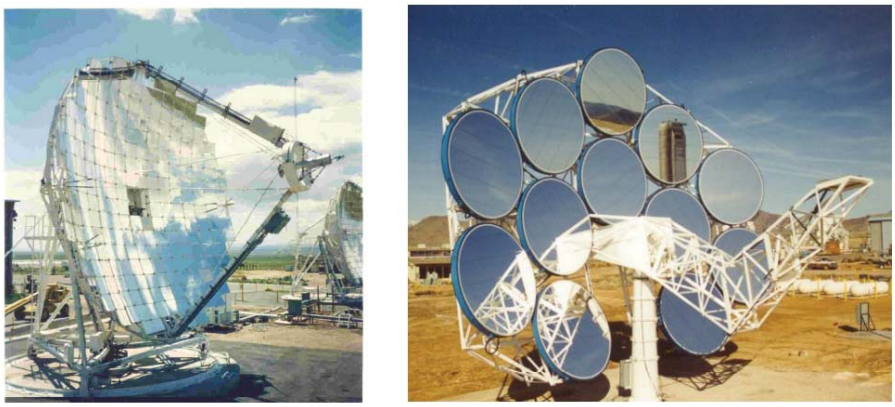

(a) (b)

Figure 2.12: Concentrated solar tracker designs for (a) a test solar Stirling system by WG Associates, and (b) the Sandia stretched-membrane concentrated solar power system (WGAssociates, 2001).

Figure 2.13: SolarCAT system of Southwest Solar, incorporating support struts for structural stability (Southwest Solar Technologies, 2013).

Figure 2.14: The HelioFocus concentrated solar dish with mirrors mounted on a flat surface (Smith and Cohn, 2010).

Stellenbosch University http://scholar.sun.ac.za

rotation path mechanism, with the Titan differing mainly in terms of the double dish system. The rail path provides some benefit in terms of azimuth stability, but problems may be experienced with accuracy due to dirt and dust on the rail-path.

(a) (b)

Figure 2.15: The (a) German Eurodish (Mancini, 1997) and (b) Spanish Titan solar tracker designs (TitanTracker, 2013).

Although the systems described thus far are suitable for stand-alone operation, they also offer the possibility of interconnecting several individual systems to create a solar farm, thus meeting an electricity demand from 10 kW to several MW. Many of these solar tracking system platforms suspend larger dish reflector systems with higher capacity.

For the purposes of the current study, however, smaller (less than <5 kW) field tested systems, with their respective design features, tracking actuators and control benefits need to be carefully evaluated. Some of these designs and their features will be considered.

Figure 2.16: Arizona University boxed telescope concentrated solar power system and solar tracking design (Angel and Davison, 2009).

Viewing concentrated solar tracking design from a precision telescope design point of view, Arizona University researchers proposed a novel solar con-

Stellenbosch University http://scholar.sun.ac.za

centrator and tracking design concept (Figure 2.16). This solar tracking design emerged from team research in the field of astronomy and low cost high precision telescope design (Angel and Davison, 2009). Their dual-axis solar tracker includes multiple dish-shaped monolithic mirror elements, made from low cost float glass. These elements are co-axially aligned in an array supported by a large moveable lightweight box-shaped steel frame. In order to minimize gravity and wind forces on the structure, the steel frame and array is able to swing about the cantilever which is balanced on the elevation axis. The tracking actuator assembly includes independent chain drives for both azimuth and elevation angle mobility. This design provides a cost-efficient solution for capturing light from the sun and provides a platform for both Stirling and concentrated photovoltaic power generation.

The Solartron system (Figure 2.17) was designed for direct heat transfer or CPV power generation and is strictly speaking not a Stirling solar concentrator power generating system (Solartron, 2013). However, the dish and actuator presents a solution aimed at simplicity and low cost. The dual-axis solar tracking actuator system for the Solartron concentrator solar system includes a slew drive mechanism for achieving azimuth axis rotational mobility. The advantage with the slew mechanism is that a large gear ratio can be realized through a planetary gear supplemented DC drive system. Very precise positioning can thus be achieved with relatively small permanent magnet electric motors to drive the azimuth movements. Elevation mobility on the Solartron solar concentrator system is accomplished independently through a linear-drive actuator system. The advantage with this design is that the linear actuator inherently guarantees large gear-ratios with little or no backlash and require smaller motors with less torque, drawing less electrical current.

Figure 2.17: Solatron hot water system produced in New Zealand showing (a) linear actuator elevation and (b) rotational azimuth drives (Solartron, 2013).

Researchers at the Department of Mechanical Engineering of the Indian

Stellenbosch University http://scholar.sun.ac.za

Institute of Technology Madras (IITM) have developed a prototype 20 m^2 parabolic solar collectors (Figure 2.18(a)) (Reddy and Veershetty, 2013). The IITM solar concentrator dish is made of highly reflective light weight plastic mirrors placed on a rigid structure mounted on a single truss support. A circular slot midway in the dish structure diameter accommodates air flow through the dish to reduce the effect of wind on the structure. The thermal receiver is placed at the focal point, using supporting rods, while a counterweight at the back of the dish supports cantilever-type balancing of the dish over a support pedestal.

(a) (b)

Figure 2.18: Concentrated solar tracking systems developed by (a) Indian Institute of Technology Madras (Reddy and Veershetty, 2013) and (b) H-Fang dual-axis slew drive solar tracking mechanism (Juhuang, 2013).

Chinese based JuHuang New Energy Company also manufacture solar energy systems for photovoltaic and heliostat applications. One of their actuator designs include a dual-axis slew drive tracking mechanism (Figure 2.18(b)) (Juhuang, 2013). This solar tracking mechanism was developed for mobility of photovoltaic and heliostat systems. From a rural power generation perspective, this dual slew mechanism provides an effective means of directing a parabolic solar concentrator. It incorporates a tracking system controller and supports astronomical dual-axis sun following. The actuator drive assembly integrates two slew gear drives fitted on a mounting in a perpendicular fashion. The slew drives ensures azimuth and elevation solar tracking motions using permanent magnet DC motors. The advantages of this assembly is that it provides a simple, easy-to-assemble and cost effective transmission solution built around two independent grease lubricated slew drives. The slew drives inherently ensures a self-locking mechanism which helps to prevent wind damage. Slew drives further require minimum motor inertia which ensures full motor movement control with high solar pointing precision and control reliability.

The *Trinum*, a 3 kW_t thermodynamic concentrated solar co-generating system (Figure 2.19) was developed in Italy by Innova (Innova, 2013). This co-

Stellenbosch University http://scholar.sun.ac.za

Figure 2.19: The *Trinum* thermodynamic solar co-generating system produced by Innova in Italy (Innova, 2013).

generating system has the capability to produce 1 kW_e grid-parity AC electric energy through a Stirling unit (without an inverter) switchable to a 3 kW_t fluid flow thermal energy output, for example to dispatch hot water. The design of the Trinum system includes a dual-axis tilt-and-swing balancing beam cantilever concept similar the McDonnell Douglas solar tracking design (Mancini, 1997). In terms of actuator design, the Trinum differs from the McDonnell Douglas design in that it incorporates a perpendicular slew drive system instead of the planetary azimuth gearbox and linear elevation gear drive. The grease-lubricated slew drive design provides advantages in terms of simplicity and increased freedom of movement, while reducing the risks of soiling due to oil leaks and maintaining gearbox oils levels.

Aiming to improve the conventional McDonnell Douglas type designs, the Infinia Corporation evaluated a number of solar concentrator designs to find a design for small scale solar power generation suitable for mass-manufacturing (Infinia, 2012). These designs focuses on smaller supply systems, utilizing Stirling systems developed for spacecraft, for which the company was able to develop a smaller solar concentrator/reflector and less complicated solar tracking systems. Figure 2.20 illustrate various Infinia design generations. The first model, Powerdish-I (a), was developed in 2006 and delivered 1 kW_e of electrical energy. Powerdish-II (b) was a 3 kW_e system completed in 2007, while the Powerdish-III (c) 3 kW_e saw the light in 2008. The latest model of Infinia, the 1 kW_e Powerdish-IV (d,e), was released early in 2012 and was built around design concepts borrowed from the automotive industry. For example, the dish frame which supports the mirrors was designed on the principle of a lightweight automotive chassis.

The Powerdish-IV solar concentrator design (Infinia, 2012) resembles the structure of a spoke-wheel design of Erez *et. al.* (Shelef and Erez, 2011). This 3.5 kW_e system concentrator dish frame includes a plurality of angularly placed

Stellenbosch University http://scholar.sun.ac.za

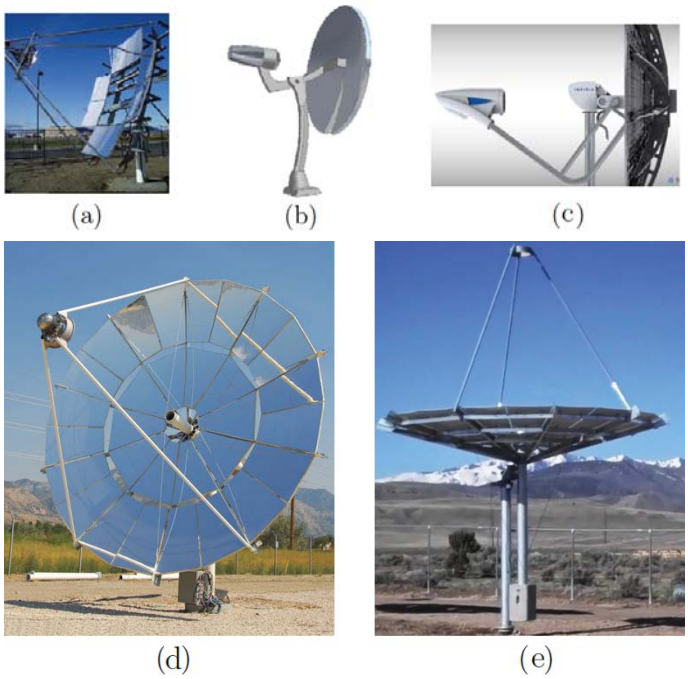

Figure 2.20: Four generations of the Powerdish I, II and III designs (a,b,c) and two photo angles of the latest Powerdish IV design (d,e) (Infinia, 2012).

elongated structural members which supports the parabolic concentrator mirror facets on a lightweight automotive steel chassis, structurally stabilised using tension cables. The slewing actuator comprises two grease lubricated slew drives fitted in a perpendicular fashion. Two slew drives allows elevation and azimuth movements. An industrial standard PLC platform ensures electronically controlled solar tracking. This type of actuator design is commonly used in photovoltaic and heliostat systems, similar to the JuHuang actuator design (Figure 2.18) (Juhuang, 2013). A modification by Infinia was to place the vertical slew drive on the side of the horizontal slew in order to ensure that an overhanging cantilever beam would allow for a greater degree of freedom.

The Powerdish-III concentrated solar power system was claimed to be the worlds first industrialised, mass-manufactured Stirling-based solar power system, said to enable broad access to inexpensive solar power (Infinia, 2012). Although the design concepts used in the Powerdish shows some promising features suitable for rural power generation in Africa, none of the Infinia solar power generation solutions is suitable for *stand-alone deployment* as it requires a grid-connection as backup power source.

Zenith Solar developed a scalable modular concentrated solar photovoltaic system fitted onto a dual axis actuator drive mechanism (Figure 2.21) (Tsadka *et al.*, 2008). The slewing actuators were designed to save on mechanical component costs for large solar farm installations and supports actuation of a dual-dish configuration driven by a compact dual-axis actuator. In terms of

Stellenbosch University http://scholar.sun.ac.za

the dual-dish configuration, the Zenith Solar optical dish configuration deploys multiple mirrors onto a plastic surface casing which acts as housing for the dish elements. The 11 m^2 moulded plastic surface is divided into quadrants that are fixed onto a rigid, high precision metal frame mounted on an azimuth and elevation solar tracking system.

Figure 2.21: Zenith solar system produced in Israel (Tsadka *et al.*, 2008).

This concludes the broad review of existing solutions from literature on commercial dish Stirling systems and serves as background in compiling quantitative design specifications for the required concentrated solar power system.

2.8. Literature Study Motivation

A parabolic dish must be tracked in two dimensions in order to allow focussing of the sunlight and to maintain the incident beams of the sun normal to the solar receiver aperture. This chapter detailed a literature study relating to various design options presented present-day and past commercial solar concentrator and positioning systems. This background serves to give insight into practical challenges with deploying concentrated solar and positioning systems in the field and demonstrate design concepts proposed by other researchers and designers. The latter part of the discussion dealt with some smaller capacity field tested designs, comparable to the capacity required in this study. Therefore, this study aimed to assist in ascertaining features needed from a rural power generation perspective. Some of these designs offer attractive features for rural deployment. This includes for example the balancing positioning mechanisms as well as the sealed and grease lubricated slew drive solutions. Other attractive features include the use of robust PLC-based electronic control, robust steel/plastic chassis structure forming the dish frame/chassis, a flatter overall dish concentrator face, and smaller curved mirror facets or stretched membrane material that are easier to transport on rural dirt road and easier to fix to the concentrator dish frame. In the next chapter, user specifications as well as design considerations for a suitable design concept, based on the information obtained from this literature study, will be discussed.

Stellenbosch University http://scholar.sun.ac.za

3. Specifications and Design Considerations

In this chapter, the design methodology, user requirements and quantitative design specifications for the concentrating solar power system, as well as mechanical and the mechatronic design considerations in developing a stand-alone solar electrical power supply system for off-grid rural communities will be discussed.

3.1. Design Methodology

This section will give a clear outline of the design problems and objectives along with a description of the mechatronic design approach.

3.1.1. Design Problem and Objectives

The research is concerned with the design, building and testing of an off-grid 3 kW peak electrical stand-alone, self-tracking and concentrating solar power system. The project emanates from a research initiative at Stellenbosch University aimed at solving challenges faced by rural African villages in terms of electrical power generation and distribution. Therefore, the concentrating solar power system must be suitable for stand-alone rural power generation.

Compared to most of the grid-connected concentrating solar power systems and technologies described in the literature study (Chapter 2), the stand-alone rural power generation requirement poses some unique design challenges. Most of the existing solar power generating systems shown in the previous chapter are not suitable for solar power generation in off-grid applications for one or more of the following reasons: existing systems require grid-connection to kick start their operation, dish structures are complex and difficult to assemble at remote rural sites without skilled personnel and most use large heavy mirror panels that are expensive and pose a damage-risk with transport over large distances along rural dirt roads.

Moreover, existing concentrating solar power generating designs discussed in Chapter 2 do not offer simplicity in terms of on-site assembly. Concentrating

Stellenbosch University http://scholar.sun.ac.za

solar housing structures are complicated to assemble at remote rural sites due to the mathematical precision required with the assembly of the structural members. Skilled expertise would be required to rig up and optically align these parabolic concentrator assemblies. In most cases an industrial crane or mechanical hoist would further be required to tension the cable trusses and optically align the system. These are not always available or transportable to remote rural or mountainous sites.

The study therefore focusses on the mechatronic engineering aspects in the design and development of a robust and dynamic mechatronic platform and digital electronic control system to help realize a stand-alone concentrating solar power system. Such a system requires an accurate automatic positioner and control system for a motorized parabolic solar reflector with an optical solar harnessing capacity of 12 kW_t at solar noon.

3.1.2. Design Steps

The design and development process for the intended mechatronic tracking mobility platform is subdivided into four phases of development. These phases are detailed below:

- The first phase of the development is concerned with the user requirements and with defining a set of technical design specifications suitable to meet the user requirements. This is detailed in Chapter 3.
- Phase 2 of the development deals with the mechanical design aspects and sub-assemblies of the solar tracking mobility platform, as discussed in Chapter 4.
- Phase 3 of the development, detailed in Chapter 5, is concerned with the electronic design and digital control automation integration aspects of the design.
- In the fourth and final phase of the development, the prototype mechatronic tracking mobility platform with assembled mechanical positioning and electronic control systems will be tested and evaluated in terms of solar tracking accuracies under various solar tracking methods.

This study eventually presents a conceptual design and engineering prototype of a balanced cantilever tilt-and-swing dual-axis slew drive actuation means as mechatronic solar tracking mobility platform for a $\sim$12 m^2 lightweight parabolic solar concentrator. Since the dynamic mobility of the parabolic dish structure as payload rests on the design of the positioning system, aspects of the dish structure design (form, shape and dimensions) are also be considered in this study (Chapter 4).

Stellenbosch University http://scholar.sun.ac.za

3.2. User Requirements

The user requires a solar concentrating mechatronic platform with automated solar tracking control, primarily for deployment in rural Africa in solar power generation applications. The intended "user" would typically be semi-skilled individuals living in a rural village environment where grid connected electricity would not be available.

The self-tracking parabolic solar concentrator system must have the capacity to accommodate a parabolic solar concentrator with a thermal harvesting capacity of 12 kW_t during maximum solar altitude (MSA). User requirements further centre around issues of simplicity and ease of installation at remote rural sites, with special consideration to ensure low cost maintenance and electronic reliability in harsh environments (i.e. highly varying daily temperatures and extreme drought and violent rainstorms).

The project requires delivery of the design as well as an engineering prototype of a mechatronic platform and electronic control system which incorporates the design of an altitude-azimuth drive system, feedback sensing devices, and an electronic pointing and solar tracking control system to command the states of control during solar tracking and solar power generation.

3.3. Design Goals

Concentrating parabolic solar systems are relatively small units compared to other point focusing solar harvesting systems. It includes a power generator system mounted at the focal plane of the reflector to convert solar thermal energy to electrical energy, while the concentrator is dynamically controlled to track the sun in order to receive radiated solar electromagnetic energy. The design goals are summarised in Table 3.1.

Parabolic dish systems require a high degree of accuracy to ensure that the sunlight is directed at the focal point of the reflector. At the same time the mechanical drive and electronic controls must ensure smooth transitions during stepwise or continuous dynamic tracking movement to allow the tracking system to lock onto the source or sun and to remain stable irrespective of changes in external environmental conditions.

The application thus requires a dynamically controlled parabolic dish solar tracker system with self-positioning capabilities for both the horizontal and vertical axes. The dual axis tracking capability is extremely important in parabolic dish applications since the system needs to track the sun in a three-dimensional space, using both an azimuth and elevation drives to dynamically focus the sunlight directly onto the focal point of the reflector where the power conversion unit (PCU) is mechanically suspended. The design needs to focus on the altitude-azimuth drive system and on an electronic tracking system

Stellenbosch University http://scholar.sun.ac.za

Table 3.1: Design goals for the concentrating solar power system.

Design Goals		
Design Goals	**Effected Components**	**Anticipated Results**
Dual axis tracking	Actuators and transmission system, dish structure weight balance	Support structure can be cantilevered space-frame beam that supports the receiver, engine and generator at the dish focal point with minimum deflections.
Good energy collection performance	Dish, power unit tracking accuracy	The tilted axis design increase in performance over single axis trackers.
Tracking accuracy	Controller software, drive tolerances, encoder-tilt angle sensors	Maximum 1% error tolerances. The transition assembly firmly interfacing with Stirling/dish support structure with the elevation axis and the azimuth drive.
Reduce deployment time	Concentrator dish design and drives	Preassembled tracker and precast foundations allow for fast installation
Minimize impact of terrain variation	Pedestal, Actuators	Articulated drive mechanisms, which allow for the system to be installed on uneven terrain with minimal site work
Minimize on site labour	Remote HMI interface, actuators, control system	Factory assembled to reduce onsite labour. Precast or preformed foundations and an adjustable mounting system
User-friendly	Control, alarms and remote feedback	A user-friendly interface
Self tracking	Control system, battery backup	Provide its own energy. Ensure low power solar tracking power consumption
High efficiency	Electric components, mechanic precision	Stirling/CPV power generation vs solar tracking consumption
Design for safety	Electrical parts, mechanical components	Adhering to modern safety and quality standards
Safety and emergency	Controller software, control strategy alarms	Power failure mode off focus, maintenance, environmental: wind, emergency defocusing, solar walk-off protection
Wind stow	Azimuth drive, elevation drive	Geometry considerations disclose wind load and inertia differences, keep to a minimum to reduce wind and inertia effects.
Lightning	Controller, comms system, drive motors	Lightning protection with proper earthing of electronics, drives and pedestal
Maintenance	Datalogger, feedback sensors	Control panel with maintenance and fault-finding procedures
Local manufacturing	All components	The ability to be reproduced and manufactured locally for deployment into Africa

which defines the states of control as well as an algorithm to achieve self-tracking in an energy efficient manner.

Stellenbosch University http://scholar.sun.ac.za

3.4. Quantitative Design Specifications

The design of the control- and mechanical- drive systems of the parabolic dish depends on elements such as the mechanical platform, mechanical system behaviour, transmission drives, the control strategy, control system inputs, sensor mechanisms and control system outputs and must be operating within the user defined specification parameters. The design of the control- and mechanical-drive systems of the parabolic dish therefore depends on elements such as the control strategy, control system inputs, sensor mechanisms, mechanical system behaviour, control system outputs and within the user defined specification parameters.

In technical terms, the primary user specification requires the design, implementation and testing of a self-tracking parabolic concentrating solar power system which has the potential to collect or generate 12 kW_t of solar electrical energy during MSA at Noon. The control system for this concentrating solar power system should control solar tracking within set accuracies. Although the sensitivity of the intercepted solar energy with respect to the solar tracking optical pointing error is strictly a function of the shape and size of the Stirling receiver, guidance in terms of setting a solar tracking accuracy specification for the present concentrating solar tracking design is taken from technical reports for existing concentrating solar dish systems (Bendt *et al.*, 1980)(Kinoshita, 1985)(Le Roux *et al.*, 2012)(Hughes, 1980). In these reports, the solar energy intercept factor remains above 90% for angular accuracies, or allowable solar tracking misalignment/errors, between 0.25° (∼4 mrad) and 1.0° (∼17 mrad). Le Roux *at. al.* (2012) determined the effects of solar tracking inaccuracies on the intercepted heat rate for a comparable capacity parabolic dish concentrating solar power system (4.8 m dish, 15 kW_t unit with 500 mm/330 mm diameter solar receiver/aperture), confirming through NREL Soltrace simulations that solar tracking errors within an error margin of ∼1.0° translated into dish intercepted heat rate losses of less than 4%. Above this tracking error rate (i.e. 22% for ∼2.0° tracking error), the study also confirmed that the heat losses increase exponentially as a function of solar tracking error. Thus, in this study, Table 3.2 calls for a system tracking accuracy specification within the ±1.0° error band, in order to limit solar receiver flux spillages to a maximum anticipated value of around 4%.

Using the above user specifications and tracking error resolution as basis, a set of quantitative design specifications for the solar tracking platform and control system has been compiled in Table 3.2.

Under these specifications, the design and prototype development should strive to produce a dynamic mechatronic platform for a concentrating solar power system that is easy to transport, assemble and install at remote rural sites in Africa, while ensuring low-cycle field maintenance preferably supported by remote monitoring/diagnostic capabilities. In support of the design specifi-

Stellenbosch University http://scholar.sun.ac.za

Table 3.2: Concentrating solar power system design specifications.

Quantitative Design Specifications		
Design Guidelines	**Spec Dimensions**	**Design Implications**
CSP parabolic dish	12 kW_t	Dish size focal length to diameter(f/D) ratio ~ 0.6
Azimuth tracking	$-190° < \gamma < 190°$	Azimuth actuator freedom of movement
Elevation tracking	$0° < \alpha < 100°$	Elevation actuator freedom of movement
Tracking accuracy	$-1.0° < \epsilon_{az} < 1.0°$ $-1.0° < \epsilon_{el} < 1.0°$	On both azimuth and elevation axis
Tracking speed	1° to 15° per minute	On both azimuth and elevation
Maximum component weight	250 kg	Eliminates need for machinery during assembly

cations, an additional set of design requirements, to support some operational requirement, are listed in Table 3.3.

Table 3.3: Concentrating solar power system design requirements.

Design Requirements		
Design Guidelines	**Spec Dimensions**	**Design Implications**
Lightweight	aluminium frame	Structural stability in design and use of lightweight cables
Easy on site assembly	Kit components	Provision for jig to assemble ate remote rural sites
Azimuth hardware trip	adjustable $<\pm 270°$	Trip switch provision in hardware wiring to limit exceeding motion range
Elevation hardware trip	adjustable $<+120°$	Trip switch provision in hardware wiring to limit exceeding motion range
Azimuth cable wind-up protection	adjustable $<\pm 370°$	Software provision for cable wind-up trip
Elevation cable wind-up protection	adjustable $-10° < \alpha < +100°$	Software provision for cable wind-up trip
Windstorm protection (optional)	$Wind > 65km/h$	Windstow controller mode (plus wind sensor)
Tracking 10 hours	>140 Ah backup	Backup battery storage capacity
Modular off-the-shelf components	Components IP55 rating or equivalent	Factory and environmental specs of sufficient rating

Stellenbosch University http://scholar.sun.ac.za

As a product, the design should preferably incorporate off-the-shelf components to support local manufacturing. It is envisaged that the Stirling dish concentrating solar power system should be centrally manufactured and prepackaged into a number of smaller more easily handled boxes prior to leaving the factory. On delivery to the final operating site, the user should be able to easily assemble the solar power generating unit and connect the system in a plug-and-play type mechatronic platform assembly format.

3.5. Field Robustness

The failure of any component in the solar tracking mechatronic system would result in catastrophic operational failure from which the solar concentrator system would not be able to recover. Maintenance costs at remote rural sites are known to escalate due to slow reaction times combined with high logistical and replacement costs. Failures will further cause the system to lose its connection with the sun, eventually leading to battery drain and automation system communication failures and the system eventually becoming non-functional.

Apart from the mechanical structural movement and balancing challenges, the design choice for a mechatronic concentrating solar power system for rural Africa has to live up to harsh environmental conditions. Environmental effects such as ambient temperature, temperature variations, soil dust deposits (especially on the mirrors), high winds, snow, rain/rainwater and lightning may cause operational challenges. These effects need to be taken into account when the design robustness is considered since some of these solar generating systems might be deployed in areas that are not easily accessible to maintenance crews. Solar concentrator parts will have to be treated against rust while stainless steel components is preferred for critical subcomponents.

Control electronics will need to be housed in a watertight and properly earthed enclosure for protection against wet and dusty conditions. Preferably all components should have an Ingress Protecting (IP) rating of at least IP55 in order to remain intact when used outside in adverse weather conditions. The IP number rates the degree of protection provided against the intrusion of physical elements, chemicals or water into mechanical/electrical casings/enclosures (Bisenius, 2012). IP codes are of the format IPxy, where "x" describes the degree of protection against the entry of foreign solid objects, and the "y" describes the degree of protection against the entry of moisture/water.

Lightning is an important consideration in concentrating solar power system design as the system will be operating at remote and distant sites where downtime, maintenance and repair costs are typically very high. During storm conditions the solar concentrator dish would typically be directed to point 90° upward in order to reduce side wind exposure. This leaves the metal support structure of the solar receiver directly exposed to lightning (Lopez and Stone, 1993). Some design options to reduce potential lightning damage may include

Stellenbosch University http://scholar.sun.ac.za

manufacturing some dish components form fibre-glass, using fibre-optic communication wires where possible while proper earthing of the support pedestal, drives and electronic housing with stainless steel is essential.

3.6. Summary

This chapter presented the user requirements, quantitative design specifications and design considerations for a suitable solar concentrator design configuration. The required solar energy generating system must have the potential to collect 12 kW_t of energy during noon, at a typical site of installation in rural Africa. The present design should include the development of an appropriate altitude-azimuth drive tracking system and an electronic tracking and drive system. Design considerations based on environmental effects and control modes were also discussed while the design goals were summarised. The design has been conveniently subdivided into the following two broad project areas described in the next two chapters, namely the *mechatronic system and platform design* and the *electronic control integration*.

Stellenbosch University http://scholar.sun.ac.za

4. Mechatronic System and Platform Design

This chapter provides a detailed description of the solar concentrator mechatronic system, including the mechanical support and tracking platform as well as the actuator system designs. The electronic integration and electronic control aspects of the mechatronic system and platform design will be described in Chapter 5. The discussion elucidates the mechanical design challenges, solutions and system components chosen in the quest to develop a stand-alone electrical power supply system for off-grid rural communities.

4.1. Mechatronic System Components

A concept is presented to deal with solar tracking control from a dual axis cross-coupled mechatronic platform perspective. The aim is to implement a mechanical platform with a mechanical transmission or actuator system and digital PLC control strategy in order to realise smooth power input solar trajectory contour following.

In general, an electrically driven solar concentrator platform and tracking control system for driving the motion of a concentrating solar dish typically consists of the following elements:

1. Dish structure subsystem: Optical dish or reflector system with associated stirling engine/device mechanically mounted at the focal point of the parabolic dish;

2. Transmission/actuator mechanical drive subsystem: Linear actuators, worm gears, linear drives, slew drives, and planetary gear drives form part of the positioning system to move the reflector to face the sun;

3. Electric motors: DC or AC electric motors to drive the mechanical drives, through current, frequency or speed control;

4. Battery storage: Backup battery system for power storage and start-up power requirements;

Stellenbosch University http://scholar.sun.ac.za

5. Motion sensing subsystem devices: Linear or rotational shaft encoders, tilt sensors, inclinometers, photodiodes, photosensitive resistors to monitor the present position of the dish while it moves to the desired position;

6. Solar position algorithm: Algorithm to continuously calculate the sun vector $S_Q(\gamma_s, \theta_s)$, as solar azimuth and elevation angles;

7. Control unit subsystem: Programmable device to coordinate the modes of operation, as well as the control strategy to position the system according to the solar position algorithm or sensor coordinates;

8. Limit switches: Devices to prevent mechanical movement beyond predefined limits in order to prevent tracker or cable damage;

9. Environmental or atmospheric ambient sensing devices: Light intensity sensing, solarimeter, pyranometer, anemometer/wind sensor, ambient temperature sensor, humidity sensor and atmospheric pressure sensors to detect any emergency or threatening environmental risks.

The focus of this study is on the design and development of the solar concentrator and tracking control subsystems. From a holistic perspective, the design will also venture into certain aspects of the solar collector subsystem and the power subsystem in order to ensure technical compatibility. The detailed designs of the power conversion unit and grid interface/power electronics aspects of the system are the responsibility of other research team members.

4.2. Mechatronic System Layout

The aim of this study is to design a dynamic mechanical platform and concept parabolic dish configuration to realize a lightweight solar concentrator system which guarantees simplicity in terms of assembly and installation at remote rural-sites for unskilled support personnel. Starting with a system-layout, this section describes system-level aspects of the proposed mechatronic platform and concentrated solar power system for stand-alone rural power generation.

In Figure 4.1, a block diagram of the proposed mechatronic platform is illustrated, emphasizing the solar collector and self-tracking subsystems of the design. The proposed mechatronic platform consists of a solar collector subsystem (a lightweight, easy-to-assemble solar collector for concentrating solar energy onto a solar receiver), a power conversion unit (developed in an associated study, for converting solar thermal energy to electrical energy), a control and power subsystem (for dynamically steering the solar concentrator to pinpoint the concentrator on the sun, while managing onboard power), and an interfacing subsystem (for dispatching the generated solar electricity, and for interfacing with any remote control, monitoring, metering, time synchronization, or weather information systems).

Stellenbosch University http://scholar.sun.ac.za

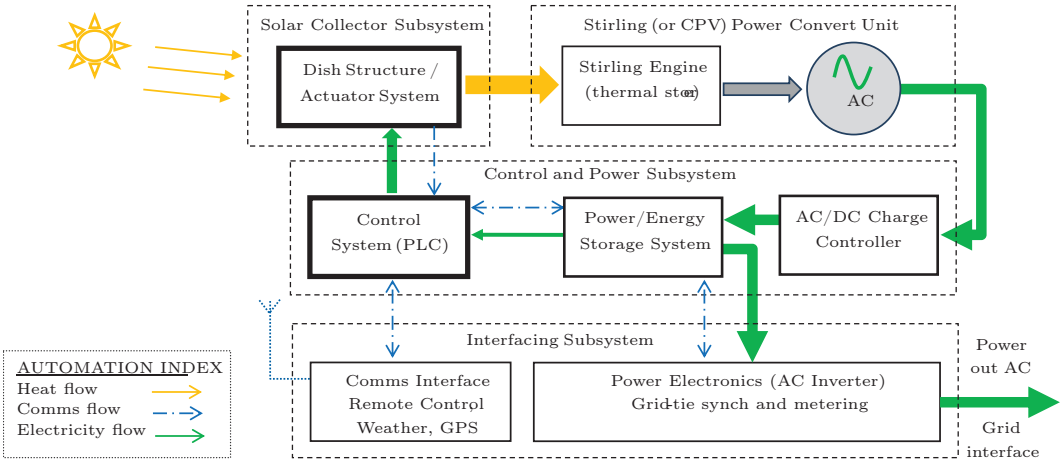

Figure 4.1: Block diagram of the proposed mechatronic platform for rural solar power generation, emphasizing the solar collector and control subsystems.

The rest of the discussion in this chapter will focus primarily on design considerations, design choices, and prototype implementation of the solar collector subsystem (Prinsloo *et al.*, 2013*b*). The control and solar tracking elements of the system are described in Chapter 5.

4.3. Solar Collector Subsystem: Parabolic Dish

User specifications detailed in Chapter 3 (Table 3.2) require a concentrated solar power system for Stirling solar power generation, with a capacity to collect 12 kW_t solar thermal energy during maximum solar altitude (MSA). In this section, details of the design of the parabolic dish as solar collector, including specifications and requirements to ensure a low maintenance self-assembly, with plug-and-play type self-tracking capabilities, are discussed.

A parabolic dish with a capacity to collect 12 kW_t thermal energy requires a calculated parabolic solar reflector area of around 12 m^2 (A =∼12 m^2), which is roughly equivalent to a dish diameter of 4 m (D =∼4 m) (Duffie and Beckman, 2006). Moreover, the user specifications call for a parabolic dish structure which meets the criteria in term of weight, simplicity, structural stability, ease of assembly at remote rural sites as well as transport to remote rural sites on rough dirt roads.

With a diameter around 4 m, the parabolic dish is not only the largest component of the concentrated solar power system but it is also the most sensitive and mathematically complex component. In conceptualising a concentrated solar power system for rural Africa, which is to be centrally manufactured and packaged in "knock down" form, the parabolic dish design should cater for the fabrication of the dish as modular units which can be packaged into a number of smaller more easily handled boxes for transport to a rural area. At the same

Stellenbosch University http://scholar.sun.ac.za

time, the dish design needs to cater for ease of assembly and installation at a remote rural site, without the use of complex optical alignment instruments.

Section 2.7 discussed the faceted or segmented ring-shaped solar reflector design developed by the IITM (Reddy and Veershetty, 2013) as well as the improvement (to flatten the mirror elements) by the Infinia Corporation (Infinia, 2012) (see Figure 4.2(a,b) respectively).

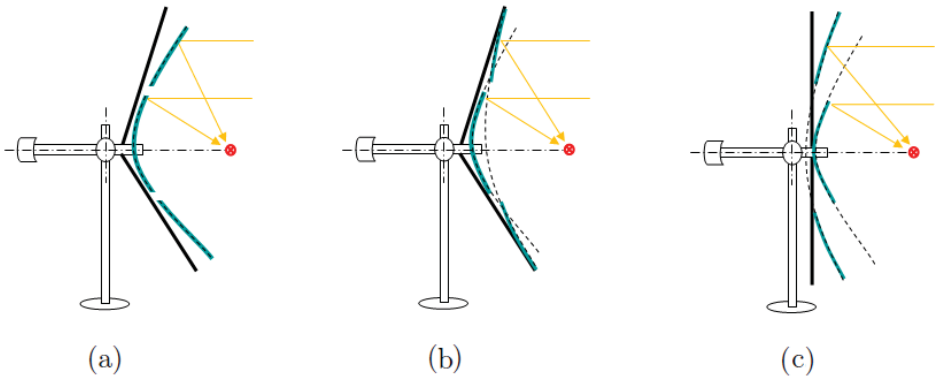

Figure 4.2: Circular cone-shaped load bearing structure to support (a) conventional parabolic dish, (b) staggered parabolic dish, and (c) the proposed flat load bearing structure with compact staggered parabolic dish.

This study proposes a novel approach to the design of a parabolic dish that would expedite and simplify the assembly and installation of the dish structure in the field. To help visualise the geometric shape of the proposed parabolic dish configuration, one should consider the surface of a conventional continuous parabolic dish being axially sliced into a series of circular differential strips/rings (see Appendix A, Figure A.2). Truncated differential ring sections for the same family of parabolic curves (with varying f/D ratios) are then collapsed and embedded onto the directrix plane of the main parabolic curve (Figure A.1), with this flat plane being supported by a metal frame that serves as the "load bearing structure" for the proposed dish configuration. The idea for such a flat parabolic configuration flowed from the designer's attempt to combine the features of the Fresnel-type HelioBooster, IITM and Infinia (Section 2.7) parabolic dish designs.

It was envisaged that such a rotating parabolic curve on a circular flat-plane load-bearing structure (Figure 4.2(c)) would greatly simplify the remote installation. The design presents non-complex procedures to simply assemble a circular support frame from triangular-shaped supporting ribs supplied in a kit form (flat load bearing structure kit), followed by the fitting of reflective panels (individual rugged reflective metallic elements) in differential parabolic ring patterns. With such a parabolic dish configuration, illustrated in Figure 4.2(c), the user is presented with a *modular* concentrator model that would

Stellenbosch University http://scholar.sun.ac.za

certainly help to guarantee simplicity in terms of assembly and installation at remote rural sites.

To expedite and simplify the installation of the parabolic dish at remote rural sites, the proposed parabolic dish configuration further comprises of modular parts, including a flat (lightweight) load-bearing structure fitted with an array of multiple parabolic reflector ring surfaces. The reflecting surfaces can be shaped/moulded as composite panels, or individual mirror petals can serve as optical reflecting surfaces (Figure 4.3). The support structure of the dish would be mounted onto the balancing boom of the mechantronic platform (Figure 4.3(a)) and has utility as a carrier structure for the concentrating (flat or slightly-curved) mirror facets. Multiple mirrors or a thin film of reflective material reflects and focus the solar energy onto the solar receiver. Alternatively, the flat frame can be fitted with reflective material in the form of one or more segments of moulded composite material panels (Figure 4.3(b,c)), aiming to further reduce the extent of field work assembly.

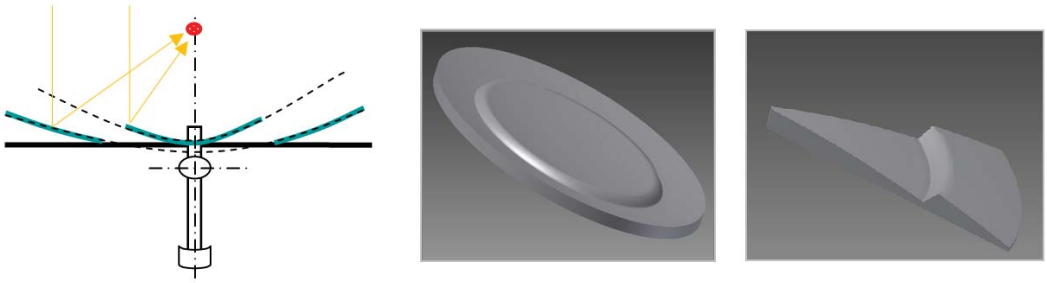

(a) (b) (c)

Figure 4.3: Parabolic design configuration, including (a) flat basis fitted with (b) curved composite material panels or (c) moulded reflective elements.

Striving towards producing a do-it-yourself CSP power generation kit, the design provides for on-site preassembly of dish parts by the user on a flat surface, easing the installation. Bolting the assembled dish structure onto the positioning system balancing boom is the next step, before finally mounting the completed assembly onto the pedestal pole (using pre-packaged bolts in the dish kit). A CAD drawing of the parabolic dish assembly as well as the *parabolic dish shape calculations* are available in Appendix A. The CAD drawing (Figure A.3) shows how the mirror facets are fixed onto the flat load bearing rib structure in two or more circular arrays, forming an inner ring of a first parabolic dish with a ratio $f/D = 0.6$ (Stine and Geyer, 2001), and outer rings with increased parabolic f/D ratios to ensure less curved parabolic segments on the outer parts of the dish (ensuring a flatter overall parabolic structure).

It should be noted that, in the CAD designs, the designer chose higher f/D parabolic ratios for the outer parabolic elements or circular arrays, with values such that the light reflection from each (collapsed) dish element converges on

Stellenbosch University http://scholar.sun.ac.za

the same optical focal point (solar receiver). The values for the parabolic f/D ratios of the outer arrays are computed such as to ensure that the basis of the inner-edge of the outer parabolic rim is mounted flush onto the flat load bearing structure (ensuring an optimally flat dish structure, see Appendix A).

Figure 4.4 shows the engineering prototype of the physically assembled dish arrangement in terms of the dimensions detailed in the CAD drawings (Appendix A), with (a) the construction of the prototype dish fully assembled; (b) the assembly of one of the modular parabolic dish rib segments; and (c) the hub or inner flange of the load bearing structure through which the dish structure will be mounted onto the actuator means. The resulting less-curved outer sections of the dish structure would potentially assist in ensuring a lower probability of dust fixation on the mirrors on the overall dish, helping to overcome a problem that is typically experienced with parabolic systems in agricultural and rural areas. This design configuration include improvements over the concentrators described before (Section 2.7), and aims to simplify assembly, installation and reduce field maintenance in remote rural sites.

Figure 4.4: Physical construction of proposed parabolic dish, showing (a) the reflector array ring elements, (b) modular dish segment, and (c) dish inner hub/flange.

To compensate for the optical shadowing losses caused by the physical orientation in the collapsing of the parabolic ring elements onto the same plane, and the resulting ring-like air gaps between the parabolic ring elements in the dish face (Figure 4.4), the dish diameter needs to increase from 4 m to 4.2 m (D=∼4.2 m) to allow for the system to maintain the same solar collection capacity of 12 kW_t. However, thanks to these ring-like air passages dividing or breaking the continuous surface of the parabolic dish face, the dish structure and mechanical actuator systems may be experiencing less load strain from head-on winds and wind gusts.

The final engineering prototype presents a dish configuration (Figure 4.5) comprising of an easy-to-assemble (a) truncated differential parabolic sections embedded onto, (b) a flat load bearing structure assembled from triangular-shaped rib elements, fitted with (c) reflective panels in a pattern to form (two, three or more) parabolic ring elements. To help ensure structural sta-

Stellenbosch University http://scholar.sun.ac.za

bility, the rib elements of the flat load-bearing structure can be compressed circumferentially by cable trusses between the concentrator outer rim and the counterweight, as well as the focal point, forming a diamond-like shape around the dish rim as shown with dotted lines in Figure 4.5(a), emulating the tensile spoke-wheel cable design of Shelef and Erez (2011).

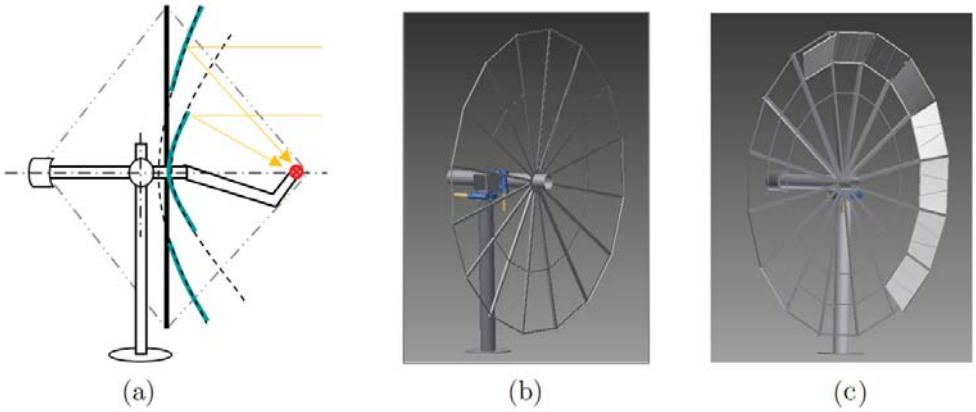

Figure 4.5: Conceptual design and CAD pictures of the proposed concentrator, comprising of a flat ribbed structural frame fitted with parabolic reflector array rings, pivotally supported on a pedestal through a balancing-boom arm.

Please note that the structural aspects of the parabolic dish structure does not form part of the main focus of this study. It will further be the responsibility of other researchers to continue with the required finite element analysis and further structural optimization in order to improve the wind loading and resistance effects of this dish configuration in terms of the user specifications (Table 3.2). It will also be their responsibility to obtain the required approvals from the university authorities, before the prototype parabolic dish model can be fitted onto the positioning system and outside onto the university's rooftop (i.e. liability requirements for rooftop installations at a public facility).

In this study, the solar concentrator parabolic dish needs a suitable mechatronic platform with gear drive mechanism to accommodate the solar tracking functionality for the solar concentrator power generating system.

4.4. Solar Collector Subsystem: Transmission

In this section, aspects of solar tracking functionality and the transmission solution required for the solar collector subsystem will be discussed. The transmission or actuator solution is detailed in terms of the motion platform concept, the transmission drive components, and the integration of the transmission system onto a mechanical drive mechanism suitable for accommodating solar tracking in rural power generation.

Stellenbosch University http://scholar.sun.ac.za

4.4.1. Transmission Drive Options

Various lines of modular gearbox systems are available for solar tracking movement control. This includes rotational type actuators, such as screw drives, worms drives, slew drives, spur gear drives, hypoid drives, helical gear drives, bevel gear drives and cycloidal drives. With Section 2.7 as background, this section introduces the features, benefits and disadvantages of the various transmission, actuator or gearbox components used in solar tracking applications.

The single worm slew drive (Figure 4.6) is used in many solar tracking applications. This slew drive inherently provides a self-locking solution to solar tracking and is presented by manufacturers as a drive with low backlash.

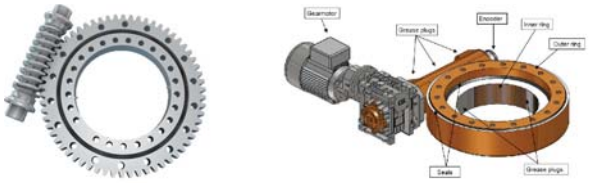

Figure 4.6: Single worm slew gear mechanism used as azimuth or elevation drive in some solar tracking applications (Fang, 2013).

Integrated dual axis gear drive mechanisms like those manufactured by Siemens/Nord (2013) (Figure 4.7) are typically used in renewable energy systems. These dual axis drives combine the azimuth and elevation movement in one gearbox, using two slewing drive mechanisms in one housing. For such combined dual axis drive systems to function efficiently, the structure should be balanced and light enough not to cause excessive wear or breakages in the combined drive system. In the McDonnell Douglas design (Figure 2.3) (Dietrich *et al.*, 1986), this problem was overcome by moving the elevation pivot point to the front of the optical reflector (reflector towards the back of the support pole), so that the weight of the dish structure and solar receiver could be balanced over the gearbox on top of the support pedestal.

Figure 4.7: Integrated dual axis drives supplied by Siemens/Nord (Siemens, 2013).

Worm drives (Figure 4.8) have been used in solar tracking applications in an attempt to solve the contact problem experienced by slew drives. However,

Stellenbosch University http://scholar.sun.ac.za

practical experience again proved that although these worm gears provide good gear-ratio's, the gear mechanisms still experience excessive wear when used in gusty wind conditions (Lopez and Stone, 1993). Limited load transfer can result in positional inaccuracies due to external influences such as wind. If the worm or king gear in this assembly is worn, wind gusts cause deviations as a result of the play on the gears, which can have an impact on the real-time solar tracking accuracy.

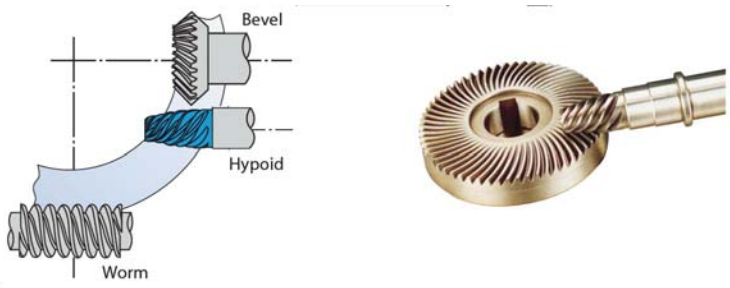

Figure 4.8: Worm hypoid or bevel drives (Lopez and Stone, 1993).

In order to overcome this problem, some solar concentrator manufacturers reverted to planetary gear systems where the contact is shared between three or more planet gears (Lopez and Stone, 1993). A planetary gear system may consist of one or more outer gears, or planet gears, revolving around a central sun gear (Figure 4.9).

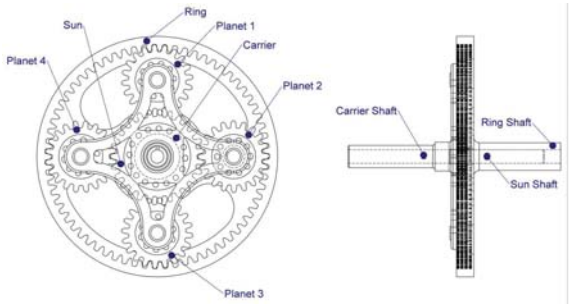

Figure 4.9: Planetary gear consisting of one or more outer gears, revolving around a central sun gear (Lopez and Stone, 1993).

Winsmith Planocentric drives (Figure 4.10) are commonly used in solar tracking applications (Lopez and Stone, 1993). One of the major advantages of the planetary gearbox arrangement in this application is the distribution of the load over a broader section of the ring gear on the circumference. The more evenly distribution of the load and increased rotational stiffness in the planetary gearbox system ensure greater stability than slew drives, and ensure

Stellenbosch University http://scholar.sun.ac.za

better transmission efficiency within a compact housing space. The transmission load is more evenly shared between multiple gears in the planetary system, which ensures increased torque capability, greater load ability and higher torque density.

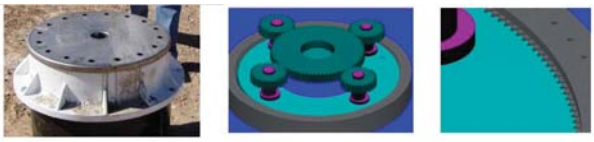

Figure 4.10: Winsmith planocentric drive commonly used in solar tracking applications (Lopez and Stone, 1993).

Another line of compact speed reducing gear motors with even better load distribution over the main gear section is the Cyclo gear drive (Figure 4.11). The design is fundamentally different from a planetary gear system and provides significantly better shock load absorption features, which makes this type of drive attractive for application in systems where robustness is required in terms of wind loading (Lopez and Stone, 1993).

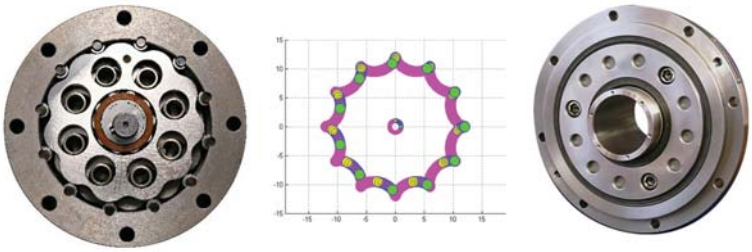

Figure 4.11: Cycloid drive operates by the principle of an eccentric cam driving a multi-lobed disc (Lopez and Stone, 1993).

The cyclo drive design includes only four components, namely a high speed input drive shaft, with an eccentric cam, a multi-lobed shaped cycloid disc, and a stationary ring gear fitted with roller pins on its inner circumference (Lopez and Stone, 1993). This gear drive transfers the rotating motion from the high speed shaft to a slow speed shaft through a multi-lobed cycloid disc. The disc is at the heart of the cycloid design as it is shaped to be smaller in diameter and with fewer lopes/teeth and a smaller diameter than the outer ring gear. An eccentric cam integrated onto the input shaft offsets the cycloid disc with reference to the centre of the rotating axis. The eccentric motion of the cam causes the lobed disc to rotate through the inner circumference of the outer ring gear housing, enabling a reduction of speed of the cycloid disc. During operation, the outer wheel turns slowly on its own axis in the opposite direction to that of the cycloid disc rotation.

Stellenbosch University http://scholar.sun.ac.za

In solar tracking applications, one benefit of the cyclo drive would be that is does not shear easily, as the load contact is shared over a larger angle span. In planetary or spur gearboxes, only a small section of gear teeth absorbs the entire shock load when subjected to for example wind gusts, leaving the potential for possible gear teeth breakage. When the cycloid drive is under load compression, more than two-thirds (66%) of the cycloidal disc lobes and ring gear rollers share the contact/shock. It can withstand intermittent shock loads of up to 5 times the torque rating of the drive (Lopez and Stone, 1993).

In the next section, the design of the integrated platform concept will be discussed, followed by the selection of suitable drives and transmission system components for the rural solar power generation system.

4.4.2. Integrated Platform Concept

The technology behind transmission systems for parabolic solar concentrator platforms and solar tracking movement shows some relation to concepts and components used in digital satellite tracking, military radar following, radio astronomy and radio telescopes. Tilt-and-swing type mechanisms are also used in the design of camera cranes, surveillance camera systems, pan-and-tilt type gun/cannon turrets, robotic arms and construction cranes. In digital satellite, radar or radio telescope systems, the payload typically includes a lightweight radio-antenna feed-horn or secondary optical telescope reflector, while in solar Stirling power generation systems, the payload comprises a complicated metal thermal to electrical energy converter of which the weight far exceeds that of any satellite or radar tracking payloads.

In dynamic behavioural systems, such as dual axis solar tracking control, the motion system should be designed around stable operating points. Ideally, the operating point must be in the region of a steady state. In robotic gun turret system design (Figure 4.12), the mechanical system is typically controlled around stable mechanical operating points, at least as far as static balancing is concerned, while robot arms and sections in turn are interlinked by slew drive or ring gear type mechanisms pivoting around operating points (IMO (Ingo Müller Oberflächentechnik), 2013).

Figure 4.12: Robotic gun turret and machine gun balance (Blain, 2010),(DoDaam, 2013).

Stellenbosch University http://scholar.sun.ac.za

A balanced camera crane design concept (Figure 4.13), ensures greater propensity towards stability and requires less energy to lift the heavy overhanging load on the end of the beam. This boom-type configuration mechanism is structured around a (counter) weight balanced device for moving, lifting and positioning of the camera payload on the long end of the boom. The mechanism allows unrestricted tilt action for elevation movement, as well as unrestricted pivoting azimuth movement. With constant aim azimuth movement combined with greater freedom of horizontal motion, this crane concept offers unique possibilities for motion control.

Figure 4.13: Balanced cantilever camera crane concept (VariZoom, 2013).

In a self-tracking solar concentrator system, the sheer physical weight, size and inertia of the movable parts of the mechanical structure (onto which the combined weight of the optical reflector/parabolic dish, solar receiver and PCU rests), requires a stable and balanced design in which the motion drives need to dynamically respond to the movement of the sun.

To accomplish solar concentrator movement for the proposed solar tracking system, the design of choice is on the robust dual-axis balanced boom movement principle, similar to the design of the camera crane shown in Figure 4.13. This design incorporates the responsive gun turret movement concept in combination with the stability benefits offered by camera crane counterbalancing movement. This type of mechanism is very attractive for concentrated rural power generation as it presents a simple yet robust dual-axis motion solution to dynamically move heavy payloads. The concept is also used in construction cranes and hoists in the mining and construction industries. In this tilt-and-swing motion platform principle, a balancing cross beam connects the optic reflector dish structure with the thermal receiver mechanism (solar power generator). The camera payload in Figure 4.13 represents the Stirling engine on one end of the boom, with the dish structure fitted in close proximity to the balancing point of the boom.

Stellenbosch University http://scholar.sun.ac.za

The McDonnell Douglas solar tracking design concept (Figure 2.5) (Dietrich *et al.*, 1986) is a good example of how a combination of steering movement concepts have been successfully incorporated in a solar tracking system. In such designs, the above principles have been successfully combined in the solar dish movement system to accomplish solar tracking, while payload motion is accomplished through large gear-ratio drives used in combination with an inherently stable weight balanced tilt-and-swing mechanism.

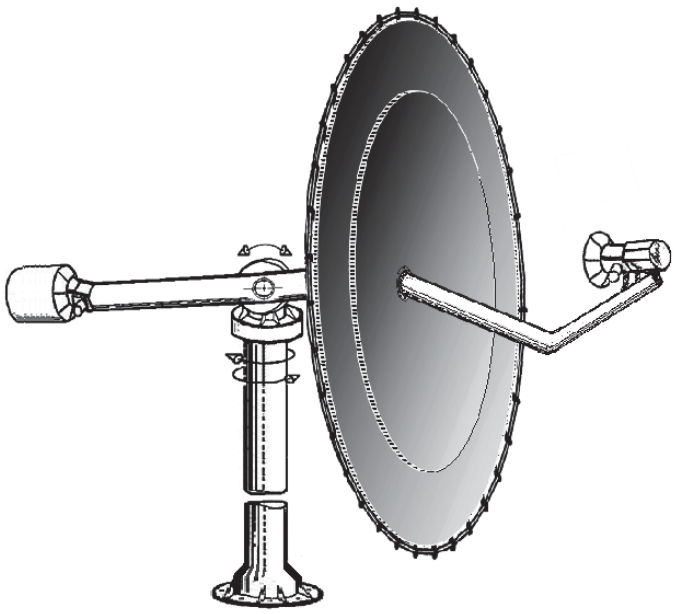

Figure 4.14: Isometric view of the concentrated solar power system concept, sketching the dish and transmission system with tilt-and-swing balanced cantilever actuation.

The present study proposes an integrated solar concentrator platform concept, with a tilt-and-swing balanced cantilever actuator system as shown in Figure 4.14. In such a balanced cantilever boom solar concentrator system assembly, the weight of the reflector and the weight of the receiver loads are balanced in a pendulum-like manner, with the beam hanging over the pivot point over the pedestal platform. The crossbeam balances on a pedestal such that the pedestal attachment point is located on the side of the balancing crossbeam. The point of attachment is located near the center of gravity balance point of the crossbeam/dish/counterweight assembly, so that the loads on the base pedestal and the attached solar tracking drive systems are minimized.

The mechatronic platform will be designed to slew the solar concentrator with the sun, as the concentrator is articulated about its rotational axis. A boom arm type slew configuration was chosen to realize solar tracking movement, as this type of design ensures a counterweight balanced device for mov-

Stellenbosch University http://scholar.sun.ac.za

ing, lifting and positioning of the solar concentrator. The proposed integrated platform concept (Figure 4.14) will incorporate a dual-axis altitude-azimuth actuator drive system, feedback sensing devices, and an electronic positioning and solar tracking control system to command the various modes of operation and states of control during accurate solar tracking and solar power generation.

Continuing along towards the physical implementation of the concentrated solar positioning system suitable for rural Africa (Figure 4.14), the main design considerations calls for simplicity, low-cost, rural maintenance, replacement considerations, environment considerations (lubrication, water, etc.), and for the stand-alone system to be driven from a backup battery power supply. Based on the proposed integrated solar concentrator movement concept of Figure 4.14, Figure 4.15 presents CAD drawings of the dish configuration integrated with the positioning means. The positioning means accommodates dual axis solar tracking through a cylindrical metal boom, which carries the parabolic dish with energy converting apparatus on the one end of the boom, and a balancing counterweight on the other end of the boom.

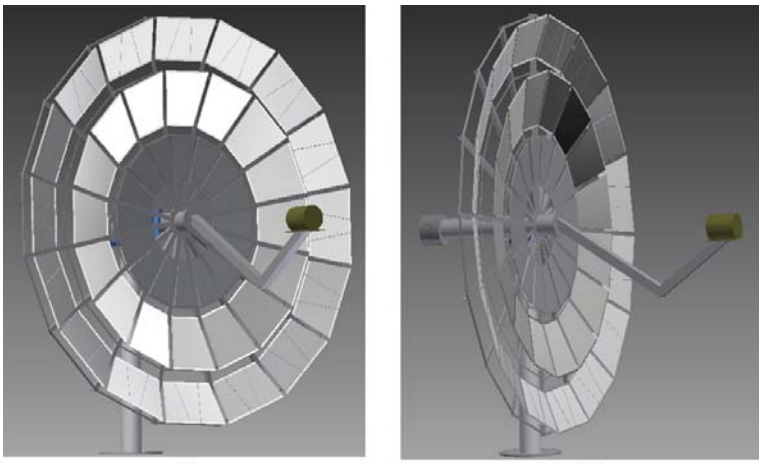

Figure 4.15: CAD drawings of the proposed solar concentrator fully assembled.

For solar tracking systems, the goal is to achieve dish movement through the desired rotational motion and with minimum torque. The sun progresses relatively slowly along a stable track (around 15° per hour), therefore tracking requires azimuth and elevation drives with high gear-ratios. Solar tracking systems typically employ actuator drives with gear-ratios in the region of 30,000:1 (Dietrich *et al.*, 1986). To achieve such high gear ratios, the gear-ratio multiplication factor in gear trains are often used in solar tracking actuator systems.

The proposed design configuration (Figures 4.14 and 4.15) offers a solar positioning mobility platform which ensures a robust yet simple mechanical mechanism suitable for rural solar power generation applications. Azimuth

Stellenbosch University http://scholar.sun.ac.za

and elevation axis tilt and rotating movements can be accomplished with slew drive actuators fitted on the pinnacle of the pedestal.

4.4.3. Integrated Actuator Design

In following through with the design strategy, this study proposes the integration of slew drive actuators in the dual axis solar tracking solution presented in Figure 4.15. Actuator slew drives (introduced in Section 4.4.1) provide an attractive solution for solar tracking applications. It has power efficient permanent magnet DC motors and due to its high gear ratios, it can be driven at a very low speed (Yedamale, 2003).

In a stand-alone CSP solar power system, solar tracking functionality would often be dependent on battery power. DC motors usually have linear speed current voltage relationships making it easier to predict power requirements when motor speeds must vary. DC motor driven slew drive actuators thus offer a better solution as these motors are typically more power efficient at lower speeds, when they produce higher torque (Yedamale, 2003). It further alleviates the problem of power losses due to DC/AC converter inefficiencies. By further driving the slew drive actuators (offering slew/planetary gear ratios around 12500:1) through power electronics and control techniques, such as pulse width modulation, the proposed slew actuation solution should provide a power efficient solution with the low rotational speeds required for solar tracking. The preferred design choice, in terms of mobility for the mechatronic platform for the solar concentrator system, is therefore on dual slew drive actuators in tandem with DC motor driven planetary gearboxes.

The gear ratio for slew drives (Figure 4.6) is typically in the range of (50-60):1, and a variety of torque levels is commercially available. The gear ratio of a slew drive can be increased significantly by connecting a small planetary gear drive (Figure 4.9) in series with the DC drive motor. With such planetary gear drives typically ensuring gear ratios in the range of (250-600):1, the compounded gear ratio of the combination would be able to deliver a gear ratio of at least 12500:1, a ratio desirable for low speed solar tracking. Sealed DC motor driven planetary slew drive actuation systems typically ensure high gear-ratio actuation in integrated self-locking and low backlash features.

When considering potential solutions towards ensuring an integrated design configuration that would accomplish dual-axis solar tracking with two individual slew drive mechanisms, the attention is turned to the best practice discussion in Section 2.7. The Siemens/Nord dual-axis solar tracking platform (Figure 4.7), the JuHuang dual-axis slew drive solar tracking mechanism (Figure 2.18(b)), and the Infinia actuator design (Figure 2.20), provide attractive concepts to integrate individual slew drives for dual axis motion control through metallic brackets or boxing. The most attractive solution for integrating two slew drive actuators in a configuration suitable for the concept presented in Figures 4.14 and 4.15, would be to use the side-mounted connect-

Stellenbosch University http://scholar.sun.ac.za

ing box solution introduced by Infinia in the Powerdish-IV (Figure 2.20). In this solution, the azimuth and elevation axis slew drive mechanisms are perpendicularly linked using a connecting box. The connecting box can be either square or triangular (Figure 4.16). This integration configuration presents an elegant but robust and simple dual-axis solution suitable for rural solar tracking applications and was chosen as solution in the present design.

In order to select a suitable slew drive system, the specifications of various systems were considered (see Appendix B and C). A slewing drive mechanism that meets the required specifications and is suitable for solar tracker applications was sourced from H-Fang New Energy Equipment Company (Fang, 2013). The Fang slew drive Model SE9A-61-R-24H.77.35-REV.B DC motor integrated slew drive (Fang, 2013) was selected on the basis of axial/radial load and torque specifications, required for the solar concentrator design. The design drawing and performance curve of the chosen slew drive are further explained in Figure C.2, shown in Appendix C. The chosen Fang slew drive includes a permanent magnet brush-less DC motor interfacing with the slew drive through a planetary gear reducer with a ration of 234:1. The DC motor performance curves are presented in Figure C.3 (Appendix C).

Due to the integration of the DC motors into the Fang slew drive models with the selected drive train gear ratios, the DC motors can run at low speeds. This is preferable in solar tracking applications where the large gear ratio makes it possible to use a smaller motor with less torque. The implemented solution (Figure 4.17) will thus be able to track the sun at relatively slow movement speeds. The price of using actuators, with low cost slew gear drive mechanisms and integrated power efficient permanent magnet DC motors, makes it possible to provide a cost effective transmission solution suitable for rolling out positioning systems at remote rural sites in rural Africa. Furthermore, the proposed slew drive and planetary gear actuator solution employs grease as lubrication medium, which means that there is no need for oil level

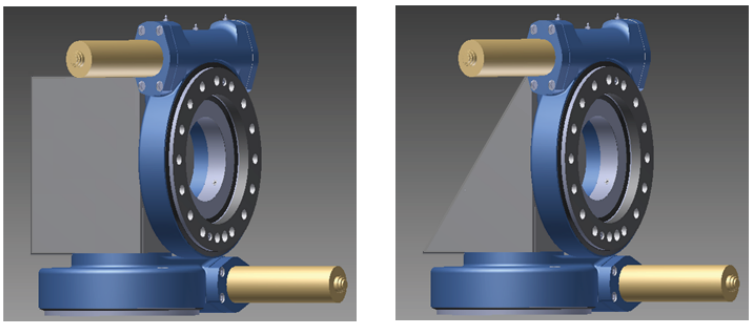

(a) (b)

Figure 4.16: CAD drawings of the proposed perpendicular dual-axis slew drive connecting box assembly in (a) rectangular and (b) triangular configuration.

Stellenbosch University http://scholar.sun.ac.za

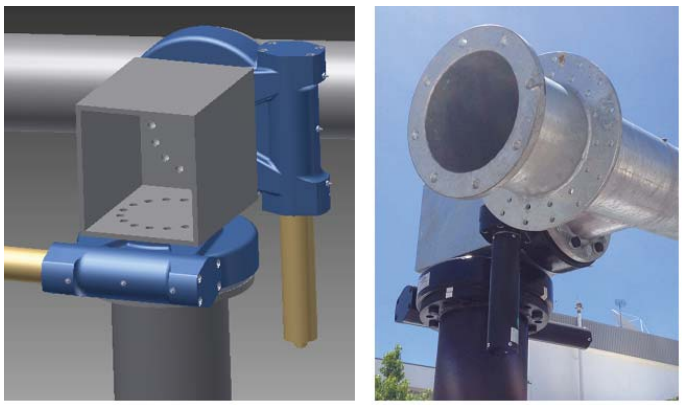

Figure 4.17: Actuators with DC motors fitted in perpendicular fashion shown in (a) CAD assembly and (b) as-constructed dual-axis configuration.

sensors since the solar power system will be less prone to lubricant loss through shaft seals when operating in hot rural environments, further reducing the risk of excessive concentrator dish soiling from oil leaks.

4.5. Engineering Prototype Assembly

The various sub-assemblies of the designed mechanical platform and positioning system is finally integrated and the engineering prototype is assembled. The dish is pivotally suspended on the pedestal and cross-beam acts as a cantilever to balance the weight of the dish structure with a counter-weight. CAD drawings (Appendix D) of the prototype platform (Figures 4.14 and 4.15, show how dual axis slew motion is accomplished through a dual element actuator drive unit fixed onto a pedestal pole readily configured to accommodate the parabolic concentrator motion through the main cylindrical boom element (Figure 4.18). This mechanism allows unrestricted tilt action for boom/concentrator elevation while ensuring a swing-pivot azimuth movement in the horizontal direction, as further detailed in CAD drawings of the prototype solar concentrator sub-assemblies (Appendix D).

A pedestal mounted solar concentrator system is subject to significant bending moments, thereby requiring a good support structure capable of withstanding turbulent- and shock-wind loads. A pedestal was therefore structurally designed in accordance with the weight and torque requirements, with special provision for shock loads such as wind gusts and wind turbulence influences on the solar reflector dish and structure. In this study, the pedestal was constructed from 230 mm mild steel piping with a 10 mm wall-thickness (Appendix B). The top of the pedestal includes a 15 mm thick flange for mounting the actuator mechanism, positioned at the pivot point of the balancing beam

Stellenbosch University http://scholar.sun.ac.za

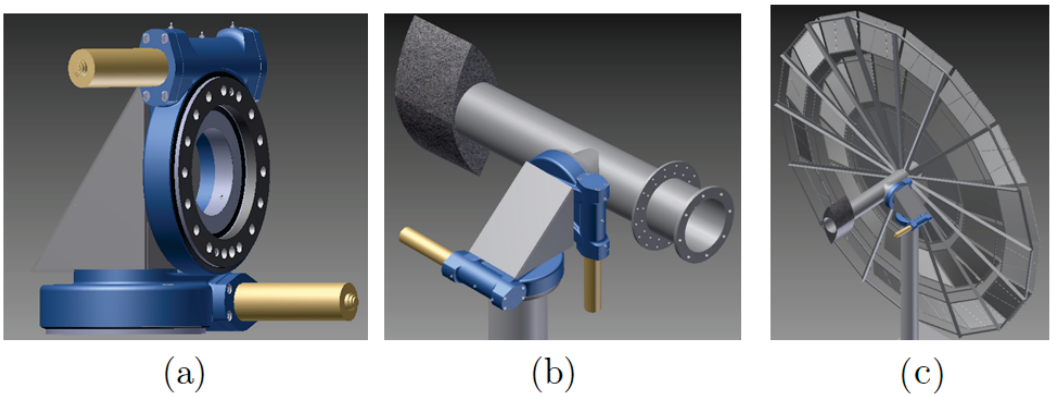

Figure 4.18: CAD drawings of (a) the proposed dual-axis pivoting slewing actuator mechanism with DC motor drive assembly, (b) actuator system fitted to the pedestal, and (c) solar concentrator dish with dual-axis actuator and pedestal system assembly.

which connects the solar dish and the counterweight elements. These elements are all galvanized to guarantee rust protection and long-term endurance.

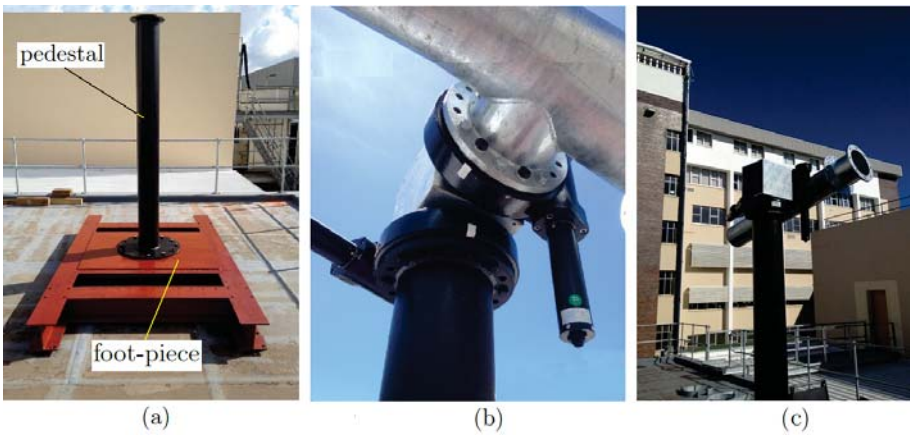

Figure 4.19: Photographs of (a) pedestal pole on rooftop at Stellenbosch University, (b,c) fitted with balancing boom type tilt-and-swing dual axis transmission system.

In order to host the pedestal and positioning system (Figure 4.19), a frame was specially designed by private structural engineers for the university, to prevent the drilling of holes in the rubberised waterproofing compound on the roof. The frame includes a flange-type foot piece to compensate for alignment adjustments due to foundation alignment inaccuracies. The roof mounting rests freely and firmly on the rooftop at the Faculty of Engineering at Stellenbosch University (installation site details in Figure E.2, Appendix E).

Stellenbosch University http://scholar.sun.ac.za

4.6. Summary

In this chapter, the mechanical design challenges, component choices and engineering prototype were discussed in the context of the challenges associated with a stand-alone electrical power supply system for off-grid rural communities, suitable for deployment into Africa. With the mechanical aspects of the mechatronic platform design concluded, a robust industrial grade electronic control automation platform is required to facilitate solar tracking. The primary task of the automation solution is to ensure that the thermal focus is maintained through the mechatronic platform and (parabolic) solar concentrator, which directs sunlight energy onto the Stirling receiver. In the next chapter, the digital electronic automation solution with the PLC control principle, and the architecture to achieve high accuracy solar tracking with optimum solar energy concentration and solar power generation, will be discussed.

Stellenbosch University http://scholar.sun.ac.za

5. Electronic Control Integration

The mechanical platform designed in the previous chapter provides a mechanical mobility means for a concentrated solar positioning system. The design aspects covered thus far includes a solar collector system that can be aligned to reflect incident solar energy towards the solar receiver, and an actuator system for dynamically moving the solar energy collector system to point towards the sun. In this chapter, the design and implementation of a digital electronic control system to move the solar collector system in response to the movement of the sun will be described. Such a control system requires field proven robust industrial standard automation hardware.

5.1. Automation Processing Hardware Selection

Digital electronic automation hardware can be classified as a mission critical component in a solar tracking system design, since any tracking automation defect or operational problems would cause the concentrator system to lose its connection to the solar resource. Any prolonged failure will result in battery drainage, causing wireless communication link failure, leaving a remotely located stand-alone CSP system being cut off from the control room or maintenance reporting centre.

Environmental influences are common problems experienced with electronic field systems operating throughout Africa. In such conditions, customised electronics could place the project and any associated business venture at risk. The possibility of custom-made automation hardware should preferably be avoided, while practical field experience taught that industrial grade power electronics should preferably be used as such electronics inherently provide for lightning protection (Lopez and Stone, 1993).

Being in pursuit of an industrial grade digital automation hardware platform, which offers robustness, self-assembly and plug-and-play features, the designer turned to the established automation industry for an industrial standard PLC platform. Amongst the electronic hardware platforms considered were the Rockwell Allen Bradley PLC platform (Rockwell Automation, 2012) and the Siemens Simatic PLC platform (Siemens, 2011). In this study, the

Stellenbosch University http://scholar.sun.ac.za

Siemens Simatic S7-1214C TIA industrial PLC platform (Figure 5.1) offers the processing power requirements to implement solar position algorithms in dual axis motion control mode and was chosen as automation platform for solar tracking hardware platform.

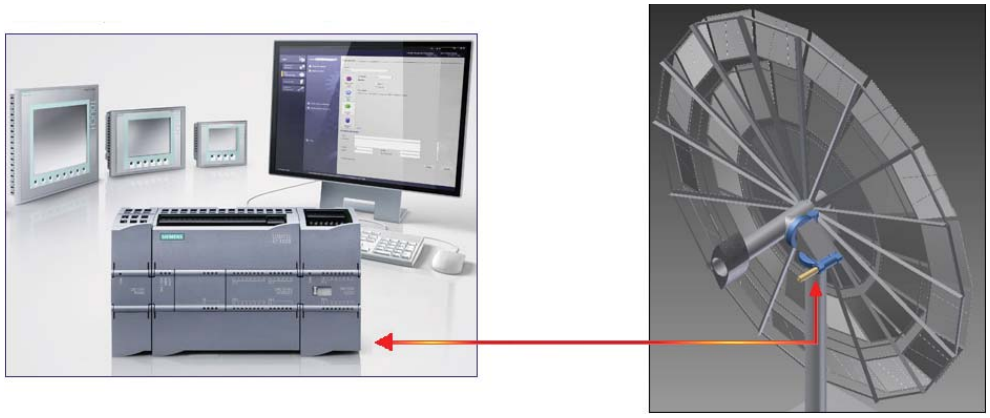

Figure 5.1: Siemens Simatic S7-1214 industrial PLC selected as automation processing platform for the proposed concentrated solar power system (Siemens, 2011).

The digital Siemens PLC processor provides for a range of analogue and digital inputs that can serve as input to analogue and digital sensors to assist with solar tracking error correction resulting from mechanical tolerances and installation deficiencies. The Siemens PLC further allows for a human machine interface (HMI) to be connected to the PLC processor to enable setting of the configuration parameters and calibration of control inputs as well as for the monitoring of the status of the PLC controller.

In the next section, the decision logic and control concepts chosen for the concentrated solar power generation solution will be discussed.

5.2. Control and Power Subsystem

The control and power subsystem elements of the system will be described with reference to the block diagram of the concentrated solar power system given in Figure 4.1. The discussion includes the selection of the solar tracking and control strategy, the integration of tracking control onto the automation hardware, as well as the carbon footprint and battery capacity analysis.

5.2.1. Solar Tracking and Control Strategies

Solar tracking control is required to continuously reflect the maximum amount of incident solar energy towards the concentrator focal point where the solar receiver is located. Solar tracking accuracy and stability are two of the primary

Stellenbosch University http://scholar.sun.ac.za

design parameters for a CSP solar tracking system. In order to improve solar tracking accuracy, various control strategy options can be followed, including open-loop control systems, closed-loop control systems and in some cases an integrated or hybrid-control system where open-and closed- loop control configurations are combined.

5.2.1.1. Open-loop Control

The block diagram in Figure 5.2 shows the operational principles of an open-loop solar tracking control strategy according to the principles described in the literature study (Section 2.5). In this control mode, the PLC controller keeps record of the angular positions of the actuator drives to determine the present solar concentrator position and compare this to the sun angles in order to determine any required motor control signals. In this configuration, the PLC can perform solar tracking in open-loop controller mode, where the solar position can be calculated from an astronomical algorithm (Reda and Andreas, 2008) (see Appendix F).

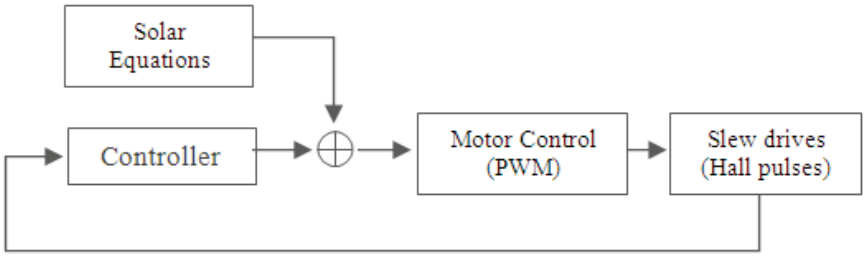

Figure 5.2: Operational principles of open-loop solar tracking control.

Given the longitude and latitude coordinates of any position on the earth, the position of the sun can be calculated with the aid of the astronomical algorithm as a solar vector. The solar vector $S_Q(\gamma_s, \theta_s)$ describes the required concentrator azimuth angle for the horizontal alignment and zenith angle for the vertical alignment. Solar position algorithm software is available for the Siemens Simatic S7-1200 series controller. This algorithm is based on NREL SPA and ensures 64-bit arithmetic accuracy with precise azimuth and zenith solar positioning control through an accurate astronomical algorithm. The algorithm is specified with leading edge accuracy of $\sim 0.0003°$ and supports solar tracking accuracies better than $\sim 0.05°$ (Reda and Andreas, 2008).

The software essentially implements the SPA on an S7-1200 controller as a function block with inputs shown in Figure 5.3(a) (Siemens, 2011), through which the PLC software compute solar vectors $S_Q(\gamma_s, \theta_s)$ for a specified location and time in relation to a high-accuracy PLC time-clock. The SPA function block can also be used to generate a sun-path diagram as shown in

Stellenbosch University http://scholar.sun.ac.za

Figure 5.3(b). This diagram reflects the solar trajectory during the summer solstice, winter solstice and solar equinox. This diagram is helpful in setting up and configuring a solar tracking controller for a particular site as it provides a visual representation of the required solar concentrator movements and stipulates the border regions and angular motion safety margins.

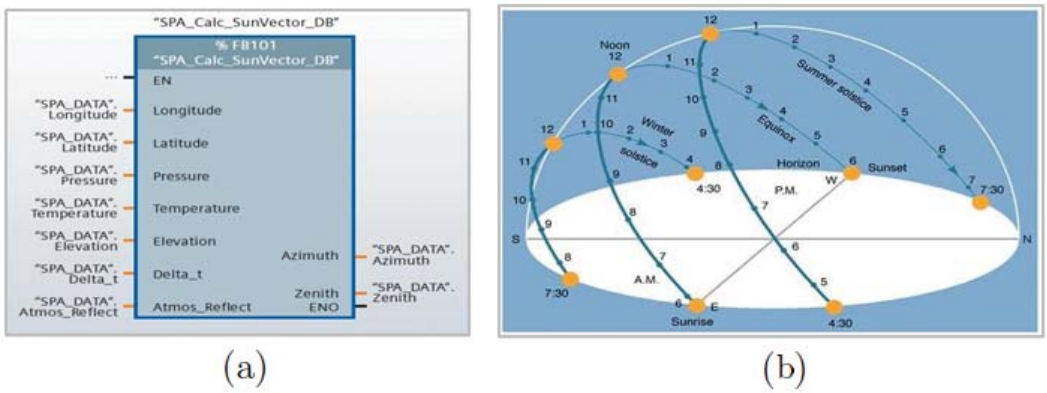

Figure 5.3: Block diagram of (a) Siemens S7-1200 function block *CalcSolarVector* to calculate (b) the solar vector and sun path diagram (Siemens, 2011).

The flow chart in Figure 5.4 represents the decision logic and software sequences used in open-loop control mode. In this mode, the PLC uses the logic in Figure 5.4 to verify day/night mode before monitoring the present position of the dish and compare this to the solar vector calculated through the SPA (check sensors on flow diagram). Should a calculated positional correction be required on any of the axes, the decision logic issues PLC commands for the DC motors on the relevant axes actuator drives to move the solar collector system to the new position (Figure 5.5).

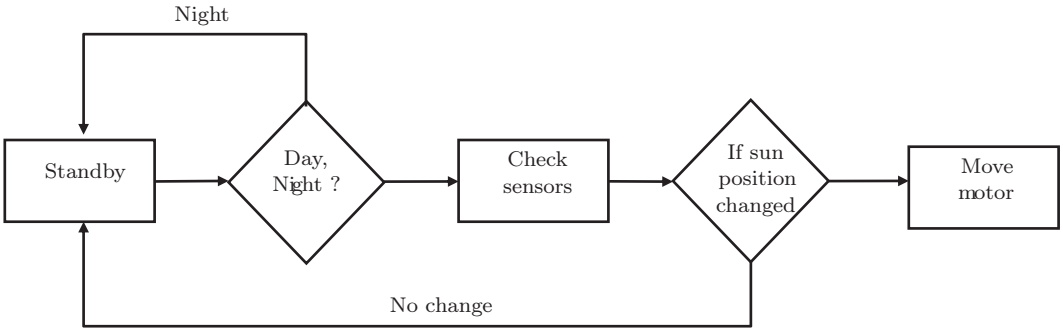

Figure 5.4: Flow diagram used in PLC decision logic to conduct open-loop solar tracking control through an astronomical algorithm.

A major disadvantage with open-loop solar tracking control using only astronomical algorithm parameters, is that the PLC control system is unable to

Stellenbosch University http://scholar.sun.ac.za

detect or correct disturbances caused by an imperfect installation, calibration, setup or time-clock parameters. In the absence of an optical observation means, the PLC control system simply accepts all parameters to be correct and blindly follows the sun path based only on solar vector parameters computed by the astronomical algorithm.

The underlying solar tracking control concept programmed into the PLC controller to command the physical slew drive actuator motors during solar tracking will be discussed in more detail in Section 5.2.1.2, while operational principles of the PLC solar tracking controller in closed-loop mode as well as the component section for optic hardware interfacing with the PLC for closed-loop mode will be discussed in Section 5.2.1.3 and Section 5.2.1.4.

5.2.1.2. Solar Tracking Control Concept

An underlying solar tracking control concept is required to command the physical slew drive actuator motors during solar tracking control and is programmed into the PLC controller to manage the hardware interfaces underlying the PLC solar tracking control intelligence and decision logic presented in Figure 5.4. The solar tracking concept physically commands the collector movement by way of defining PLC signals sent to the actuator DC motors for each new sun position in accordance with the angle deviation between the sun and the solar concentrator pointing direction.

A precise control concept, such as proportional integral and differential (PID) control, is not really suitable for slew actuator driven solar tracking control since the sun movement is quite slow and the large gear-ratios of the slew drive actuator ensures very slow dish movements. The integrated actuator DC motors in the slow response actuator drives can be easily controlled in on-off control steps through pulse width modulated (PWM) control signals.

In this approach the tracking resolution parameter (termed Δ) sets the travel interval of the solar concentrator and describes the approach to logically realise concentrator movement by intermittently driving the actuator DC motors within a certain allowable angle deviation window. The solar tracking resolution window (angle intervals) are specified for each of the azimuth and elevation axes as part of the software configuration set-up. Figure 5.5 presents an illustration of how this approach achieves solar tracking motion with the PLC solar tracking controller and how this approach is logically realised during the solar tracking process (Figure 5.4).

In the solar tracking approach (Figure 5.5), the PLC essentially moves the solar concentrator slightly ahead (angle $\Delta/2$) on the sun track, waiting for the sun to "catch up" with the concentrator position. When the sun "catches up", and progresses on its track beyond the last solar concentrator position (by an angle larger than $\Delta/2$), the solar concentrator in turn "catches up" with the sun by subsequently moving it to a new position slightly ahead (angle $\Delta/2$) of the sun on its track. In following this solar tracking approach throughout

Stellenbosch University http://scholar.sun.ac.za

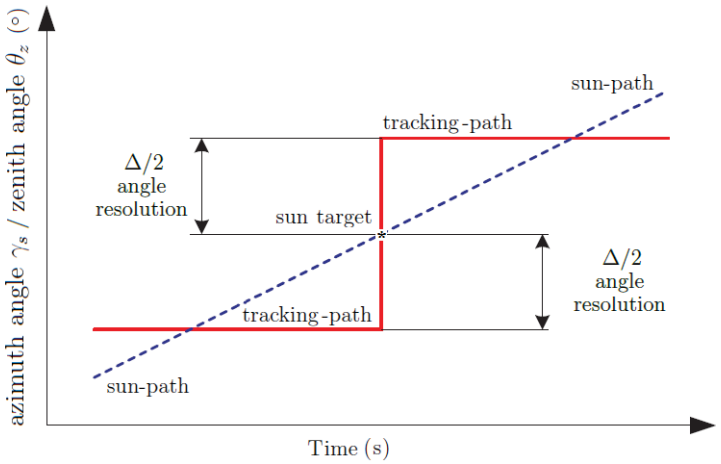

Figure 5.5: Illustration of decision logic used to control the actuator DC motor in following the sun path at tracking resolution $\Delta/2$ on each control axis.

the day, azimuth and elevation slew drive actuators (under PLC control) are constantly driven in a step-wise fashion and in such a way that the pointing direction of the solar concentrator physically overtakes the sun position by a very small pre-configured angle margin on both axes ($\Delta/2$), waits for it to pass by the same margin ($\Delta/2$), before the concentrator again overtakes the sun again by the predefined margin ($\Delta/2$), waiting for the next passing of the sun, continuing in this way in a step-wise incremental fashion. The optical solar tracking error sequences resulting from this approach is anticipated to be a slowly varying oscillating-type saw-tooth pattern, slowly varying up and down within the pre-configured error band of $\pm\Delta/2°$.

In more technical terms, the tracking resolution parameter Δ sets the travel interval of the solar concentrator slewing drive actuators in terms of an angle resolution Δ. During the solar tracking process (Figure 5.4) the PLC will independently activate the slew drive actuator motors during every control cycle on either the azimuth or elevation axis, but only if the concentrator on that axis lags behind by the sun angle by an angle of $\Delta/2$ (i.e. $\Delta = 0.25°$ then $\Delta/2 = 0.125°$). The PLC will end that cycle of concentrator movement on that particular axis when that actuator axis movement exceeds the sun position by an angle $\Delta/2$ on that axis. During the next PLC control cycle, the process is repeated, carrying along in the same fashion in following the sun movement throughout the day.

This PLC driven control concept, in combination with PWM signal control, reduces the energy requirements for moving the solar concentrator through the DC motor on each axis since the DC motors are not moving continuously throughout the day, but intermittently in pre-configured error margin increments. By further using PWM control technology, the slew drive on each axis is fed in time intervals associated with the solar contour movements to en-

Stellenbosch University http://scholar.sun.ac.za

sure that each DC motor only draws current during the required movement intervals. PWM is an efficient method to control and vary the power and speed of the DC motors, while the DC motors in-turn controls the azimuth and zenith/elevation angles of the solar concentrator through the slew drives in accordance with the approach described above (Figure 5.5). Compared to continuous solar concentrator actuator DC motor movement (which may drain a stand-alone solar tracker's energy reserves), the tracking approach described above has the benefit of reducing solar tracking energy consumption in proportion to the parameter Δ.

In this study, the tracking resolution is set to $\Delta = 0.2°$ on both azimuth and elevation/zenith axes. This resolution is comparable with similar field tested systems and provides for efficient use of power resources (Mancini, 1997). It further ensures sufficient error margin when the system operates in open-loop control, helping to circumvent the effects of mechanical tolerances, and subtle mechanical defects (Kinoshita, 1985). Although outside the scope of this study, a future opportunity is seen in experimenting with a slight improvement to this control concept, wherein the PLC could adjust solar tracking power consumption levels through (dynamic) variation of the angle resolution Δ. In future. such a feature may be beneficial in a stand-alone system that operates in overcast conditions, as it will be able to sacrifice accuracy in exchange for preserving backup energy reserves.

In order to evaluate the solar tracking accuracy of the proposed solar concentrator movement in open-loop control mode, a diagnostic instrument would be needed for measuring the tracker accuracy performance. Such optical solar tracking-means can also be employed as input sensor in the PLC closed-loop control mode, as shown in the next section.

5.2.1.3. Closed-loop Control

In closed-loop solar tracking control, optimal solar tracking precision is ensured with the aid of light sensitive electronics to enable the controller to observe the movement of the sun. Through optical feedback, the solar concentrator system can be directed in a dynamic fashion to achieve the optimal sun pointing position. The level of intelligence of the controller system as well as the type and sensitivity of the sensors are crucial in these systems.

This method of control is typically implemented to give feedback to the PLC under closed-loop solar tracking control mode and optically assists to eliminate or at least reduce some of the tracking errors brought on by an imperfect installation, minor mechanical defects or small misalignments. Optical or image processing techniques described in the literature study (Section 2.5) may be used to direct the solar tracking controller to observe and lock onto the position and movement of the sun. An optical solar observation means, such as the MEMS ISS-CYPA sun sensor (SolarMEMS, 2013), can be used.

Stellenbosch University http://scholar.sun.ac.za

In a closed-loop solar tracking control application, the MEMS analogue sun sensor (model ISS-AX detailed in Appendix G) is installed in a small housing and mounted onto the frame of the solar concentrator system. In this way, the PLC controller can monitor the present position of the dish and compare this to the true position of the sun observed/measured through the sun sensor. The sun sensor is then used as input means to closed-loop solar tracking control.

Instead of calculating the solar vector/position of the sun through an astronomical algorithm, the PLC control algorithm in closed-loop control mode computes the sun position $S_Q(\gamma_s, \theta_s)$ from sun sensor signals (Appendix G) and compares this to the sun vector (Figure 5.4) to direct the solar tracking motions of the concentrator platform (Figure 5.5). The solar collector movement approach is still used by the PLC solar tracking controller (Figure 5.5) to drive the actuator DC motors by way of intermittently moving the solar collector system for each new sun position in accordance with the angle resolution window parameter setting Δ (see Section 5.2.1.2).

By using the MEMS ISS-CYPA sun sensor, the difference in angle between the position of the solar vector can also be recorded on a personal computer (through a PIC processor and a USB interface), in order to store or log the azimuth and zenith elevation "pointing error" using optical measures and the sun sensor calculations (SolarMEMS, 2013).

Camera image processing, instead of light sensitive devices, can be used in robotics to control complex movements along directed paths. Image processing techniques determine the solar vector $S_Q(\gamma_s, \theta_s)$ from web camera images for closed-loop camera based solar tracking evaluation (Appendix H). Camera based augmented tracking systems offer some benefits in terms of accuracy, but these systems are not popular in industrial scale commercial solar tracking systems. Most robust industrial PLC based control systems simply does not always have the processing capability to perform complex image processing required to determine the position of the sun more accurately. Typical operating environment hazards such as dust, rain, static electricity and lightning are all enemies of camera based solar tracking augmentation systems.

One disadvantage of closed-loop solar tracking control is that the PLC system would find it problematic to recover from prolonged periods of cloud cover. In the absence of guidance from an astronomical algorithm, the optical observation means may find it difficult to determine the solar vector once the sun moved outside the field of view of the sun sensor/imaging camera, or if the sun path is no longer in the field of view of the optical device. To overcome this problem, an optical feedback means can be employed more efficiently in hybrid-loop control strategies.

Hybrid open-loop/closed-loop tracking control, as a means of overcoming the limitations of closed-loop control, will be discussed in the next section.

Stellenbosch University http://scholar.sun.ac.za

5.2.1.4. Hybrid-loop Control

Hybrid-loop control mode systems are used to control the dynamic behaviour of a solar collector system, using a combination of both open-loop and closed-loop control strategies. The control system may be driven by discrete-valued signals or continuous signals, while some of these input/output signals may be time-driven or event-driven. Optical light sensing devices, such as those used in the closed-loop control system.

The hybrid control approach follows the sun path with the assistance of an astronomical algorithm, while simultaneously using the sensors to monitor and improve solar tracking pointing accuracy. The hybrid-loop mode of control has the advantage over open-loop and closed-loop systems in that the positioning of the solar collector remains in close proximity to the real-time position of the sun.

In this hybrid mode of control the PLC receives input on the sun's position $S_Q(\gamma_s, \theta_s)$ from both the astronomical algorithm and optically, by means of a sun sensor or imaging camera. The block diagram in Figure 5.6 illustrates the flow diagram used by the PLC to achieve solar tracking with better accuracy in an integrated open-loop/closed-loop control mode.

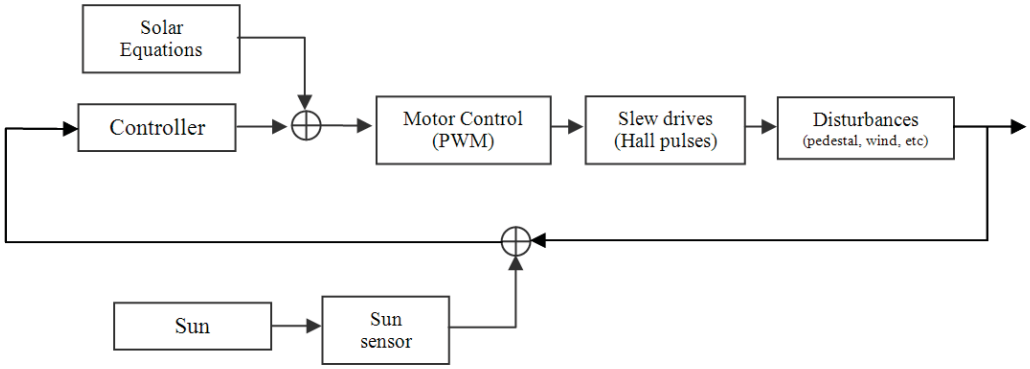

Figure 5.6: Operational principles of hybrid open-loop/closed-loop motion control.

In the hybrid open-loop/closed-loop control mode, the PLC uses the logic in Figure 5.4 to verify day/night mode before monitoring the present position of the dish and compare this to the solar vector calculated through the SPA and the solar vector provided by the MEMS sun sensor. Should positional correction be required, the decision logic issues PLC commands to the DC motors and actuator drives on the relevant axes. The flow chart given in Figure 5.7 represents the decision logic and software sequences typically used in the hybrid open-loop/closed-loop control mode.

Once again, the solar collector movement approach of Figure 5.5 can be used by the PLC solar tracking controller to drive the actuator DC motors

Stellenbosch University http://scholar.sun.ac.za

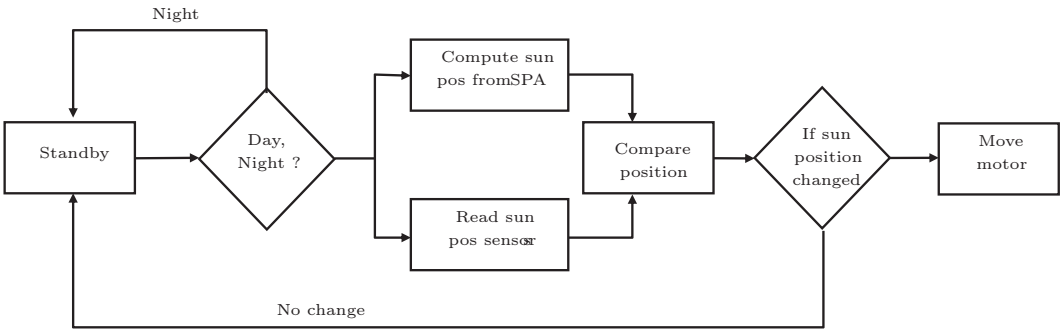

Figure 5.7: Flow diagram used in PLC decision logic to conduct hybrid open-loop/closed-loop solar tracking control.

by way of intermittently moving the solar collector system for each new sun position in accordance to the angle resolution window setting (Δ).

5.2.2. Automation Hardware Integration

The first slew drive element to direct the motion of the concentrated solar power system is mounted on the main boom (Figure 4.18). It has a rotary output shaft aligned with the elevation pivotal axis and accordingly controls the solar concentrator up-and-down movement. The second slew drive element is mounted to the pedestal pole and has a rotary output shaft aligned with the azimuth pivotal action, accordingly controlling the solar concentrator left-right movement. Each slew drive element includes a DC electrical motor and a planetary gear unit to drive the main ring gear of the slew units.

The attention of the discussion is now directed towards the PLC hardware integration of the software control logic principles discussed above. Figure 5.8 shows a layout of the interfacing between the PLC automation software and the hardware for the slew drive positioning and tracking mobility mechanism described in Chapter 4. With reference to this layout, the current azimuth and elevation angle positions of the solar concentrator can be detected using either a tilt sensor, angle sensors, shaft encoders, or Hall magnetic pulse encoder. Each of the slew drives selected in Section 4.4.3, and shown in Figure 5.1(b), includes a brushless DC motor with its own integrated Hall magnetic pulse position encoder. The number of Hall pulses can thus be recorded via the digital PLC controller and corresponds with the distance the drives has moved. The PLC control signals for determining the travel distances of the azimuth and elevation axes are computed from the Hall encoder pulses through the formulas detailed in Appendix I.

Digital interfacing on the PLC controller (Figure 5.8) includes Hall encoder input ports and motor driver output ports to communicate with the azimuth and elevation actuator brushless DC motors. The specifications and performance curves of the DC motors integrated with the slew drive mecha-

Stellenbosch University http://scholar.sun.ac.za

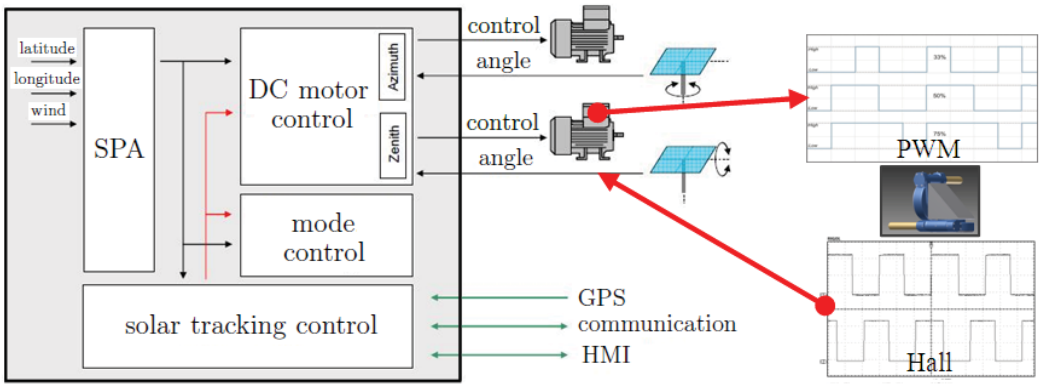

Figure 5.8: Siemens S7-1200 control block commanding the solar concentrator through DC motor driven slew drives (Siemens, 2011).

nisms (Appendix C) (Fang, 2013) needs to be stored as parameters upon PLC configuration, as these setup parameters are used in the slew actuator/DC motor travel distance computations (Appendix I). During the solar tracking operation each DC motor movement is commanded by the PLC using 24 Volt DC PWM signals. Figure 5.9(a) shows an oscilloscope display of a sequence of PWM pulses generated by the Siemens PLC, to be used as a DC motor control signal on one of the axes. Two such PWM signals are fed into two discrete MOSFET H-bridge motor drivers, which enables bidirectional control on each of the two high-power DC slew drive motors. This motor driver supports 5.5 V to 24 V voltage range and can deliver a continuous 15 A without a heat sink (see details in Appendix J). Figure 5.9(b) shows the datalogged PWM time sequences sampled at the azimuth and elevation MOSFET H-bridge motor driver outputs, measured where the motor drivers feed directly into the azimuth and elevation axes slew drive motors. The power levels in these real-time measured PWM time sequences highlight the power output delivered at the motor driver PWM signal outputs, and represents the slew drive actuator DC motor's power consumption levels.

In the PLC software, the control speed of the DC motor is varied around the optimum set-point speed of the motor (see Figure C.4, Appendix C). DC motor PWM control signals should be wired through a shunting capacitor to the ground in order to reduce radio frequency interference commonly caused by PWM control (Lopez and Stone, 1993). During the solar tracking control operation each of the two slew drive DC motors is powered on independently through each of the two the PWM interfaces, while high-speed axis counters monitor the feedback from each slew drive DC motor Hall encoder. The counted encoder pulses correspond with the desired travel path, while the particular motor movement will immediately be stopped when the desired slew angle has been reached. Following each slewdrive movement sequence, or during power down, the final axis counters are stored in order to continue with

Stellenbosch University http://scholar.sun.ac.za

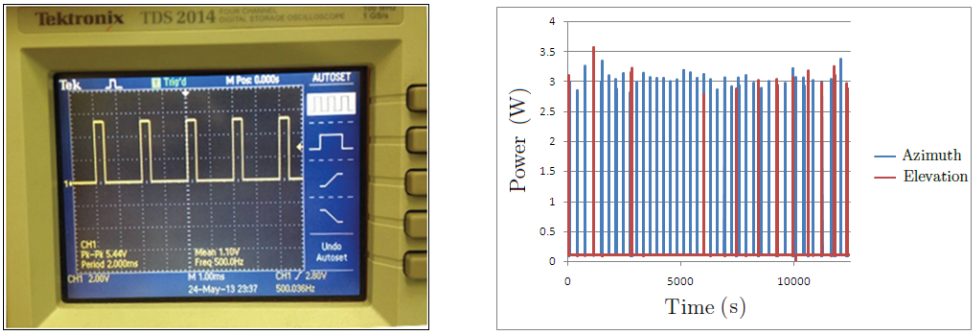

Figure 5.9: PWM control signals driving slew actuators shown on (a) oscilloscope at PLC output port and (b) power datalogger at motor current driver output port.

subsequent travel instructions from the previous angular positions.

The PLC keeps record of the absolute azimuth and elevation axis angular positions, if the solar concentrator pointing position is accurately referenced relative to the sun-vector position during configuration. Sun position setup synchronization is done by moving the concentrator's azimuth and elevation axis actuator slew drives until the concentrator position is absolutely orthogonal to the sun vector $S_Q(\gamma_s, \theta_s)$ at the moment of synchronization. At this instance, the absolute azimuth and elevation axis angular positions are saved as sun vector reference points. From that point onwards, the PLC controller can determine the travel distances of the azimuth and elevation axes slew drives, in terms of the Hall encoder pulses through the formulas given in Appendix I, in terms of the absolute pointing angles of the solar concentrator relative to the sun vector angles (Figures 5.4 and 5.5).

The PLC software configuration process includes the step of configuring the PLC parameters and referencing the solar position. The gear ratios of the actuator system (planetary and slew gears) are programmed in the PLC configuration setup (see Appendix I), while the PLC control system is referenced and synchronised relative to the true sun position. The physical installation was done in such a fashion that the control electronics and equipment could be disconnected from the main structure at any point to be stored. The control electronics are housed in a panel box that can be mounted onto the pedestal or balancing boom. The PLC and the mechatronic platform are thus stand-alone units that can be connected in a plug-and-play fashion.

While the DC motors draw current during each motor start-up phase, the Stirling engine also requires kick-start power to enable PCU operation with each sun re-appearance. These surges of energy may drain the backup battery, especially if the system operates in cloudy conditions and engages through multiple stop/start sequences. The next section describes the final part of the automation design process, namely a power analysis to estimate the operating times of the system elements in order to determine the backup battery capacity.

Stellenbosch University http://scholar.sun.ac.za

5.2.3. Power Budget and Battery Capacity

A battery backup system is most effective when used in conjunction with permanent magnet DC motors as these motors are more power efficient. However, continuous engagement and disengagement of the dish of a stand-alone system and in the absence sufficient solar irradiation (i.e. cloudy conditions) can drain the backup power supply. This calls for a power demand and power budget analysis to ensure that there is sufficient power storage capacity to feed the system components (Figure 4.1) in such conditions. The power demand analysis for the proposed concentrated solar power system is detailed in Appendix K, where Table K.1 presents the list of automation control hardware components as well as an estimate of the time needed to perform its duty during clear-day and cloudy-day conditions. The relevant percentage of time dedicated to each task is used to estimate the automation power requirements. The user specifications in Table 3.2 calls for a backup battery capacity (BBC) of at least 140 Ah for 10 hour user/solar tracking operation. The calculations presented in Appendix K, shows that a standard deep-cycle-type backup battery with a capacity of around 200 Ah is required to meet both parts of this specification.

Moreover, a demand-side power budget analysis also provides a foundation for determining the CO_2 footprint/impact of the concentrated solar power system. Table K.1 in Appendix K presents a detailed analysis of the CO_2 impact of each of the system components and shows that the total estimated CO_2 impact of the overall mechatronic platform and automation system hardware is around $CO_2 = 214.6$ g/h (grams of CO_2 per hour).

5.3. Summary

In this chapter, details of the digital electronic automation hardware and software, the electronic control system, control logic and the hardware/software integration, were provided. With the mechatronic platform and digital automation aspects of the complete automatic positioner and control system for a motorized parabolic solar reflector now designed and engineering prototypes of each successfully constructed, the system needs to be evaluated in terms of performance accuracy and solar tracking accuracy. In the next chapter, the experimental work and test results will be discussed.

Stellenbosch University http://scholar.sun.ac.za

6. Experimental Evaluation

Test-ready engineering prototypes of the mechatronic platform and digital electronic controller components for the 12 kW_t stand-alone self-tracking solar concentrator system were prepared and ready for evaluation. Since the percentage of collected thermal energy in a concentrated solar power system is most sensitive to solar tracking accuracy, strict error margins have been set in the design specifications for solar tracking accuracy (Table 3.2).

Three experiments are conducted in this chapter to validate the real-time optical performances of the designed prototype positioning system in terms of the predefined design specifications. To compare optical solar tracking accuracies for the as-built system in open-loop and closed-loop PLC control modes, an astronomical algorithm, an optical sun sensor device, and a camera imaging device are respectively used to determine the position of the sun in each of the three experiments. *Safety precautions* taken during the experiments are documented in Appendix L, while experiments are conducted on the rooftop of the Engineering Faculty at Stellenbosch University, South Africa (GPS coordinates: $Q = (33°S55'43.13", 18°E51'56.16)$, site details in Appendix E).

6.1. Experiment 1: Evaluation of Open-loop Tracking Accuracy

The mechatronic platform and control system for the solar concentrating system should be able to control and manage the physical movements of a parabolic dish structure with a tracking accuracy sufficient to collect 12 kW_t around noon. Solar tracking accuracy with self-tracking capabilities are therefore the primary criteria for evaluation of positioning system performance as it impacts directly on the optical focus and concentration levels of solar energy.

6.1.1. Goal

The goal of experiment 1 is to determine the positional accuracy of the tracking system controlled in open-loop solar tracking mode. In this mode, the PLC commands the solar tracking operation under guidance of the NREL solar position algorithm. The optical solar tracking accuracy should meet the error

Stellenbosch University http://scholar.sun.ac.za

criteria in terms of azimuth and elevation sun pointing errors measured with an optical means over the course of a full day.

6.1.2. Equipment

Table 6.1 presents a list of equipment required to determine solar tracking optical deviation errors on the azimuth and elevation axes of the solar concentrator mechatronic positioning platform. The SolarMEMS sun sensor (ISS-A25) measures precise optical tracking accuracy as angular on-sun pointing errors with a pointing accuracy resolution of 0.04° (Appendix G), while the azimuth and elevation tracking error sequences are recorded in real-time on a personal computer using the Labview (LArVa) digital data acquisition system.

Table 6.1: Equipment required to determine solar tracking optical deviation errors on azimuth and elevation axes of the solar concentrator positioning platform.

Equipment	**Function**
SolarMEMS sun sensor ISS-A25	Precise determination of sun position, see Appendix G.
HP-PC with Labview LArVa data acquisition system	Digital datalogger to monitor, record and display real-time measurements.
CMOS web camera LY208C with ION Video2PC converter	Precise determination of sun position through image processing software, see Appendix H.
Purpose-built instrument platform & sun-vector reticle means	Housing solar tracking test instruments and telescopic sun-vector observation means, see Appendix M.

The prototype parabolic dish component could not be fitted outside before passing wind-load tests. Therefore, on-axis azimuth and elevation optical measurements are taken directly on the sun-pointing axis of the cantilever boom. For this reason, the purpose-built instrumentation platform listed in Table 6.1 was developed to facilitate optical measurements on the pointing boom axis of the positioning system, as shown in Figure M.1 (Appendix M).

6.1.3. Experimental Setup and Procedure

Two sets of results is generated in this experiment. The first set is intended to create a feel for the solar tracking control concept described in Figure 5.5 (see Section 5.2.1.1), and presents simulated data for a desk-top experiment wherein the PLC SPA generated solar vectors $S_Q(\gamma_s, \theta_s)$ are used to compute simulated *solar tracking movement patterns*. The second set represents real-time recorded data for the physical engineering prototype positioning system controlled by the PLC in open-loop control mode, with the system physically tracking the sun over the course of a full day. The azimuth and elevation axes *solar tracking error angles* are measured in real-time through the high

Stellenbosch University http://scholar.sun.ac.za

precision SolarMEMS sun sensor device and digitally recorded through the Labview digital data acquisition system.

6.1.4. Results

Using the PLC generated SPA solar vectors, the simulated azimuth and elevation slew drive *movement patterns* are computed over a one-day period and is presented in Figure 6.1. These simulated *movement patterns* are important as it explains certain trends that will eventually translate into optical solar tracking errors when physically running the prototype system in the open-loop control mode (prediction of the true optical performance of the system).

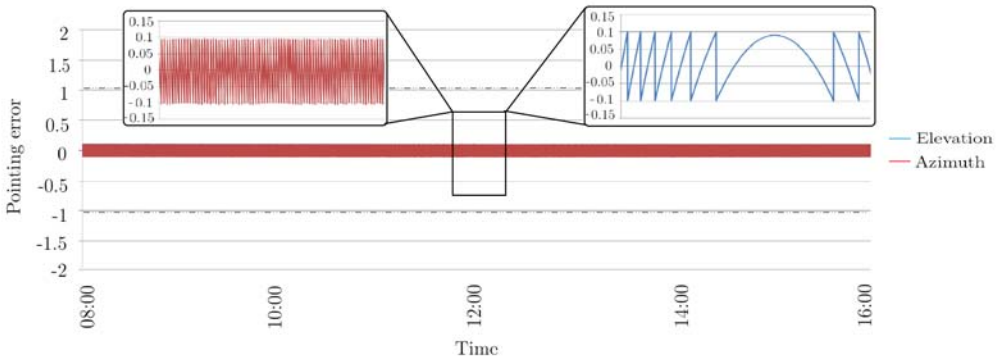

Figure 6.1: Mathematical simulation of the dish tracking movement patterns on the azimuth and elevation axes, computed using SPA solar vectors.

The short-term oscillating pattern in the tracking *movement patterns* (swinging movement), observed in the azimuth and elevation error time sequences of Figure 6.1, reflects the characteristics of the PLC solar tracking control concept in Figure 5.5. It should be kept in mind that the amplitude of these oscillations relates to the tracking resolution (Δ) in the PLC control concept, and was specified as part of the system configuration in Section 5.2.1.1. Other identifiable characteristics in the simulated/anticipated actuator movement patterns in Figure 6.1 are the relatively high rate of activity in azimuth slew drive movements around noon (highest rate of sun movement on the azimuth axis), compared to a relatively slower rate of azimuth slew activity in the morning and afternoon. Conversely, on the elevation axis, the relatively slower rate of slew drive activity around noon (slowest rate of sun movement), compared to a faster rate of elevation slew drive activity in the morning and afternoon.

Figure 6.2 presents the recorded on-axis solar tracking errors optically measured by the sun sensor on the azimuth and elevation axes over the course of one day, for the PLC commanding the physical prototype solar positioning

Stellenbosch University http://scholar.sun.ac.za

system in real-time and on the basis of the SPA algorithm in the open-loop mode. Figure N.2 (Appendix N) displays the same azimuth and elevation solar tracking error sequences on an expanded/zoomed scale. Specific attention should be given to three main features on these graphs. Firstly, the high amplitude noise-like patterns measured simultaneously on both the azimuth and elevation axes (Figure 6.2, especially around 10:00, 12:30, 13:30) are simply the effects of clouds eclipsing the sun and influencing with the optical device's ability to measure the true sun position. Secondly, the small amplitude sawtooth patterns in the tracking error sequences (Figure 6.2) were anticipated from the simulations (Figure 6.1), since it represents the characteristics of the PLC control concept (Figure 5.5).

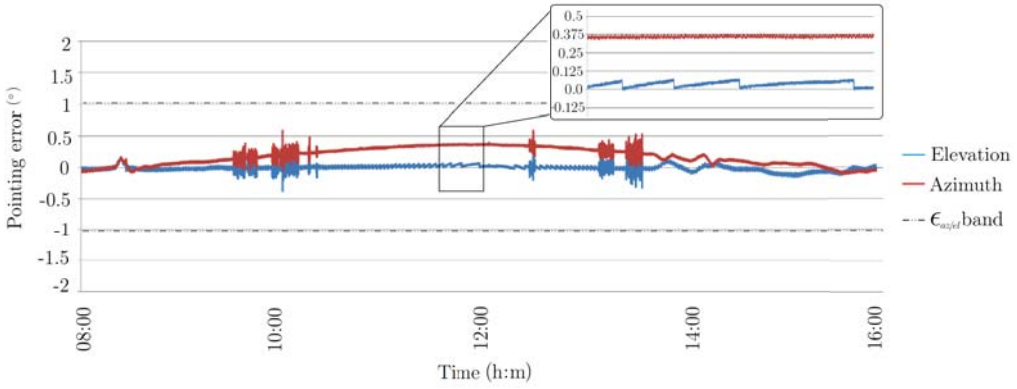

Figure 6.2: Optically measured azimuth and elevation solar tracking/pointing errors using the solar position algorithm in the PLC open-loop control mode.

Thirdly, both the azimuth and elevation axes solar tracking error sequences (Figure 6.2) show long-term time-varying average offset errors, both axes offset error patterns reaching a peak deviation around noon (12:00). In the early hours of the day (around 08:00), the azimuth and elevation axes errors are swinging around the average of $\overline{\epsilon_{az}} = -0.125°$ and $\overline{\epsilon_{el}} = -0.06°$ respectively. Around noon (12:00), the long-term average/offset tracking error on the azimuth error increases to around $\overline{\epsilon_{az}} = +0.375°$, while the elevation axis tracking average/offset tracking error increases to around $\overline{\epsilon_{el}} = +0.06°$. On the azimuth axis, the slow varying solar tracking offset errors around noon turns relatively close to the maximum allowable error band of $-1.0° < \epsilon_{az/el} < +1.0°$ (see demarcated band in Figure 6.2. Such slow time-varying average/offset errors in the open-loop solar tracking control mode may be indicative of subtle mechanical defects or slight installation misalignments.

Due to a lack of optical feedback, the open-loop electronic control system is unable to circumvent these effects on its own. In this case, the concentrated solar power system was synchronised with the true sun position at around 08:00 in the morning, explaining why the average azimuth solar tracking error is at a

Stellenbosch University http://scholar.sun.ac.za

minimum around 08:00 (concentrator pointing direction relatively close to the configuration reference). As continuous solar tracking progressed throughout the day, the average/offset azimuth tracking errors increased to a maximum around noon and then decreased again to a minimum in the afternoon (16:00). The nature of the azimuth/elevation offset error patterns in Figure 6.2 (time varying, smooth, peaking simultaneously around noon on both axes), may suggest that the cause could be slight misalignments, predominately towards the north/south direction. However, time varying offset solar tracking errors could emanate as a result of one or more of a variety of factors, factors that may typically be experienced with rural installations. The range of known inter-dependent factors that could cause such time-varying errors include: pedestal tilt errors, reference biases, linear azimuth and elevation errors (gear drive ratios and configuration settings), non-orthogonality in the slew drive axis mountings or bore-sight errors (optical axis misalignments). These factors would often be too complex to isolate as it may vary throughout the day, season or year, typically showing a non-linear dependence on the intended sun pointing angles.

Sandia National Laboratories's engineers (Khalsa *et al.*, 2011) found that it is rarely feasible to isolate the cause and repair minor installation errors or fabrication defects on any installed concentrated solar power system, because the complexity caused by the inter-dependency between the range of potential defects would require prolonged analyses and precise (laser) measurements stretching over several seasons. Furthermore, complex mathematical modelling would still be required to quantify each contributing factor, while any attempt to mitigate any one factor on its own would require the prolonged analysis process to start all over again. Their attempts towards a control solution that includes mathematical models to overcome subtle disturbances showed limited success. A more viable solution to circumvent the effect of minor defects on solar tracking inaccuracies with stand-alone rural power systems would be to include an optical feedback means in the solar tracking control solution.

Nevertheless, despite the effects causing minor time-varying offset errors in this rural power system positioning mean, the optically measured solar tracking accuracy for the system (Figures 6.2 and N.2) shows that the tracking errors on both axes are just about in compliance with the solar tracking error specification ($\epsilon_{az/el}$) and are within the boundary of $\pm 1.0°$ (Table 3.2).

6.1.5. Summary and Conclusion

With the PLC controller commanding solar tracking under guidance from the NREL SPA astronomical algorithm, this experiment evaluated the solar tracking accuracy of the solar concentrator positioning system in the open-loop control mode. Experimental results in Figures 6.2 and N.2 show that, contrary to the simulated data (Figure 6.1), the real-time optically measured solar tracking error data for both the azimuth and elevation axes shows a smooth

Stellenbosch University http://scholar.sun.ac.za

time-varying average/offset error pattern. Despite these potential defects or installation errors, the system achieves azimuth and elevation axes solar tracking accuracies within the set overall error band of $-1.0° < \epsilon_{az/el} < +1.0°$. This means that system performance in the open-loop mode is in compliance with the user accuracy specifications (Table 3.2). The conclusion from this experiment is that a rural power generating system with an open-loop electronic control system would be unable to circumvent the effects of typical rural installation errors, and that the control solution should compensate for such defects through an optical feedback means (e.g. using a sun sensor/web camera to determine the sun's position or solar vectors $S_Q(\gamma_s, \theta_s)$.

6.2. Experiment 2: Evaluation of Closed-loop Sun Sensor Tracking Accuracy

Installation defects or minor errors in the manufacturing processes will often cause offset errors in open-loop solar tracking. With the objective to overcome such errors and to ensure that solar tracking accuracy remains within the desired specifications, a closed-loop control experiment needs to be performed in order to compare solar tracking accuracy with optical feedback solar tracking control to that of open-loop astronomically based tracking control.

6.2.1. Goal

The goal of this experiment is to determine the positional accuracy of PLC controlled closed-loop solar tracking, with the PLC commanding the solar tracking operation under guidance from the Solar MEMS ISS-AX sun sensor (SolarMEMS, 2013). This device uses a micro-electronic sensor to determine the position of the sun (see principles in Appendix G). Measured solar tracking accuracy sequences reflect the solar pointing misalignments as azimuth and elevation sun pointing errors over the course of a full day.

6.2.2. Equipment

All of the equipment listed in Table 6.1 is used for this closed-loop tracking control evaluation experiment, with the exception of the web camera which would only be used in the next experiment. In this experiment, the sun sensor is used both as optical error recording means as well as optical feedback device for closed-loop tracking control. The optically measured solar tracking errors are recorded in real-time using the Labview (LArVa) digital data acquisition system (see Appendix M).

Stellenbosch University http://scholar.sun.ac.za

6.2.3. Experimental Setup and Procedure

The solar concentrator configuration remains the same as for the previous experiment, except for the fact that the solar tracking control system now includes an optical device with the PLC and the slew drive elements. With the open-loop solar tracking experiment, the panel box, PLC control electronics, and the slew drives were linked with two separate eight-core shielded wires. In this control configuration, an additional seven-core shielded wire cable relay feedback sun vector signals (with a resolution accuracy of 0.04°) from the sun sensor to the PLC. Solar tracking is thus accomplished in the closed-loop control mode and on the basis of the solar vectors $S_Q(\gamma_s, \theta_s)$ computed from the sun sensor signals (see Section 2.6.3 and Section 5.2.1.3).

It needs to be stressed that an optical sun sensor can easily be soiled in dusty operating conditions. Sun sensor soiling would significantly affect the sun sensor output and tracking ability of the PLC controller and care should be taken while conducting the experiment as to the condition of the sensor and its ability to return reliable results. Moreover, the presence of clouds could impact on the accuracy of this optical device and therefore, for reasons of comparison, the experiment is conducted on a clear day in order to reduce environmental influences on the experiment. As part of the procedure to compare open-loop and closed-loop solar tracking, the PLC will remain in the last visible sun position, should cloud cover interferences be experienced in the experiment.

6.2.4. Results

With the PLC commanding solar tracking on the basis of feedback from the Solar MEMS ISS-AX sun sensor, the results presented in Figure 6.3 show the optically measured on-axis solar tracking error sequences for the azimuth and elevation axes recorded over the course of one day. The same azimuth and elevation tracking error sequences are shown on expanded/zoomed scale in Figure N.3 (Appendix N). As with the open-loop solar tracking control, the short-term oscillating nature of the optically measured tracking error time sequences (Figure 6.3) reflects the characteristics of the PLC solar tracking control concept (Figure 5.5), wherein the tracking resolution ($\Delta = 0.2$) is specified in the pre-programmed PLC configuration setup (Section 5.2.1.1). The sun sensor experiment was conducted on a clear day, but the effects of individual passing clouds are noticeable (between 12:00 and 14:00), causing individual spikes in the tracking error sequences (Figure 6.3).

Experimental results in Figure 6.3 indicate that the optically measured solar tracking accuracy on both the azimuth and elevation axis remains within certain error bands throughout the day. On the azimuth axis, the solar tracking error (Figure 6.3) continuously swings around the average $\overline{\epsilon_{az}} = -0.01°$ within an error band of $-0.1° < \epsilon_{az} < +0.1°$. On the elevation axis, the solar tracking error continuously swings around the average of $\overline{\epsilon_{el}} = +0.02°$, within an error

Stellenbosch University http://scholar.sun.ac.za

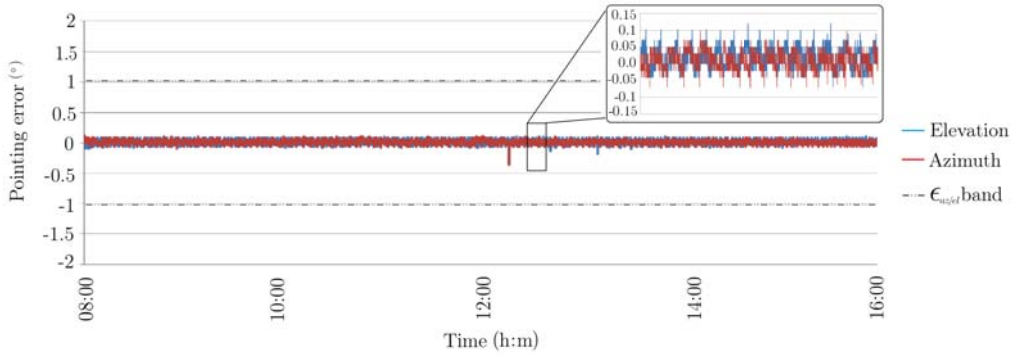

Figure 6.3: Optically measured azimuth and elevation solar tracking/pointing errors using the sun sensor in the PLC closed-loop control mode.

band of $-0.07° < \epsilon_{el} < +0.13°$. Both the azimuth and elevation tracking error rates remain comfortably within the allowable error band of $\epsilon_{az/el} = \pm 1.0°$ (see demarcated error boundaries in Figure 6.3).

Compared to the time-varying average/offset solar tracking error observed in open-loop solar tracking (Figure 6.2), the average/offset error sequences for sun sensor-based closed-loop tracking remains remarkably constant throughout the day. The results indicate that the sun sensor enables the PLC to track the sun with greater accuracy, despite potential subtle mechanical defects or slight installation misalignment errors (anticipated in a typical rural installation), provided that clear sky conditions prevail. Sun sensors are robust devices developed for high-precision satellite applications that operate on the principle of sun-ray pin-pointing, yielding extremely high accuracy in determining sun the vector $S_Q(\gamma_s, \theta_s)$. It uses a mask-plate with a small aperture(s) to direct a sun-ray(s) onto a minute substrate screen, deriving the solar vector very precisely from the illuminating pattern(s) of the sun-ray(s) detected on the pixels of the silicon detector substrate screen. This technique enables the device to measure the solar vector with a resolution in the order of 0.04° (Appendix G), meaning that the sun sensor is able to direct the PLC controller in a closed-loop tracking mode with extreme accuracy.

The experimental results (Figure 6.3) indicate that the PLC control system operating in the closed-loop control mode, with feedback from the sun sensor device, is able to circumvent the effects of installation/mechanical defects in the prototype positioning system. In general, this means that the PLC control solution would be more suitable for stand-alone concentrated solar power generation in rural areas, since the control system would have the ability to overcome any potential installation misalignment errors.

Stellenbosch University http://scholar.sun.ac.za

6.2.5. Summary and Conclusion

In experiment 2, it was determined that the prototype concentrated solar positioning system yields better solar tracking accuracy in the closed-loop control mode, when compared to open-loop solar tracking control. This is especially true for the *average error offset* and *error band limits*. The optically measured average solar tracking error rate, as well as the solar tracking error band in a closed-loop PLC control mode configuration (Figure 6.3), show that sun sensor directed closed-loop solar tracking errors oscillate around a fairly fixed error offset band ($\overline{\epsilon_{az/el}} = \pm 0.1^{\circ}$, yielding improved results compared to open-loop solar tracking (Figure 6.2). Sun sensor-based closed-loop solar tracking control comfortably achieves azimuth/elevation axes solar tracking accuracies within the set overall error band of $-1.0^{\circ} < \epsilon_{az/el} < +1.0^{\circ}$, which is in compliance with the user accuracy specifications (Table 3.2). The sun sensor is thus capable of assisting the PLC in compensating for apparent subtle installation and mechanical disturbances anticipated in a typical rural system installation. Although closed-loop control would be preferred in stand-alone concentrated solar rural power systems, one disadvantage with sun sensor based closed-loop solar tracking control is that the system is dependent on solar visibility. Other than with astronomical algorithms, the optical observation means on its own is unable to determine the solar vector if the sun is eclipsed by cloud cover (even moderate cloud cover) or if the sun path is out of the viewing angle of the sun sensor. The SolarMEMS sun sensor (ISS-A25) has a $\sim 50^{\circ}$ viewing angle (Appendix G), which allows for maximum $\sim$1.5 hours of continuous cloud cover or loss of view of the sun (25° forward view, $\sim$12 hours over horizon, $\sim$4 minutes/degree), before the sun sensor tracking and control system would lose its synchronization with the sun and would be unable to recover from lost synchronization on that particular day.

6.3. Experiment 3: Evaluation of Closed-loop Web Camera Tracking Accuracy

A further closed-loop control experiment is performed to determine whether solar tracking accuracy can be improved with a web camera as optical input device in the controller feedback loop. In this experiment, a web camera faces the sun directly to continually capture sun-images and determine the sun vectors as the sun progresses during the day. These vectors are fed back to the PLC controller in the closed-loop mode in order to evaluate camera performance in circumventing the cause of average solar tracking error variations.

Stellenbosch University http://scholar.sun.ac.za

6.3.1. Goal

The goal of this experiment is to determine the positional accuracy of PLC controlled closed-loop solar tracking, with the PLC commanding the solar tracking operation under guidance from a web camera that uses image processing to determine the position of the sun (Arturo and Alejandro, 2010). The optically measured solar tracking accuracy should once again reflect the solar tracking/pointing error measurements in terms of azimuth and elevation axes errors over the course of a full day.

6.3.2. Equipment

All of the equipment listed in Table 6.1 are used in this closed-loop tracking evaluation experiment. The PLC controller and slew drive actuators used in the open-loop experiment would once again be used along with the sun sensor for tracking evaluation, while the web camera would now serve as a sensing device to determine the solar vectors $S_Q(\gamma_s, \theta_s)$ (Appendix M).

6.3.3. Experimental Setup and Procedure

Other than a sun sensor, a web camera determines the position of the sun through image processing. In this experiment, image processing is done on an Arduino development board where solar vector computations are processed from frame captured camera images (Appendix H). The Arduino processor feeds the solar vectors to the PLC in the closed-loop control mode, while the PLC in turn steers the solar concentrator on the path of the sun throughout the day (see Sections 2.6.4 and 5.2.1.3).

As with the previous two experiments, the SolarMEMS sun sensor (ISS-A25) is used to measure the true optical tracking accuracy as angular sun pointing errors. The azimuth and elevation tracking errors measured with the MEMS sun sensor are recorded in real-time using the Labview digital data acquisition system. Although negative effects on web camera lens soiling would be less than for sun sensor soiling, cloud-cover could influence camera image processing and sun position accuracy. Thus, for reasons of comparison, the experiment is conducted on a clear day in order to reduce the environmental influences on the experiment. As part of the procedure to compare open-loop and closed-loop solar tracking, the PLC will remain in the last visible sun position, should cloud cover interferences be experienced in the experiment.

6.3.4. Results

Figure 6.4 represents the optically measured on-axis solar tracking error sequences for the azimuth and elevation axes, with the solar positioning system operating in the closed-loop control mode under guidance of a web camera

Stellenbosch University http://scholar.sun.ac.za

imaging means. The same on-axis azimuth and elevation solar tracking error sequences are shown on expanded/zoomed scale in Figure N.4 (Appendix N).

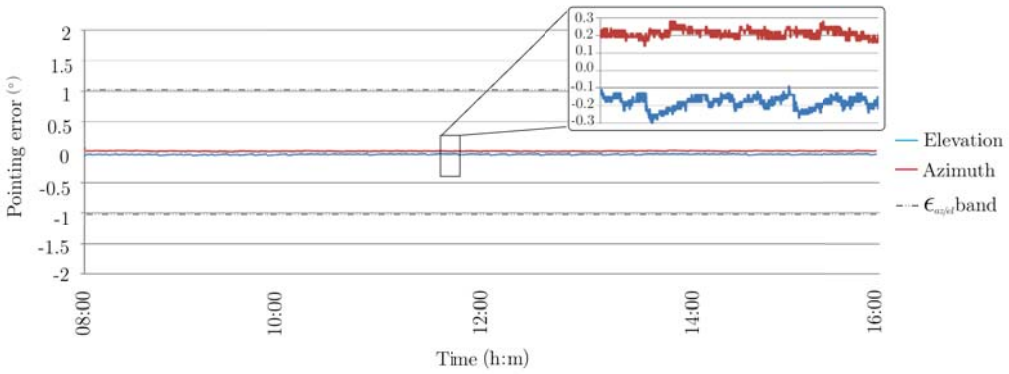

Figure 6.4: Optically measured azimuth and elevation solar tracking/pointing errors using the web camera in the PLC closed-loop control mode.

Experimental results in Figure 6.4 indicate that the solar tracking accuracy for camera based closed-loop solar tracking control varies within a fixed error band on both the azimuth and elevation axis. The short-term oscillating nature in the tracking error sequences (Figure 6.4) still reflects the characteristics of the PLC solar tracking control concept (Figure 5.5). On the azimuth axis, the tracking errors (Figure 6.4) swing around a relatively stable (non-time-varying) average of $\overline{\epsilon_{az}} = +0.2°$ and within an error band of $+0.1° < \epsilon_{az} < +0.3°$. On the elevation axis, the solar tracking error swings around an average error of $\overline{\epsilon_{el}} = -0.2°$ and remains within an error band between $-0.1° < \epsilon_{el} < -0.3°$. Both the azimuth and elevation tracking error rates are comfortably within the marked/allowable error band of $\epsilon_{az/el} = \pm 1.0°$ (see band in Figure 6.4).

By comparing the solar tracking error sequences obtained with the web camera to that of the sun sensor, the web camera error sequences appear to vary to a greater extent, while calibration bias errors causes the azimuth and elevation error sequences to swing around different averages (Figure 6.4). These variations are all due to the fact that camera-based solar position technology is inherently more complex than sun sensor-based solar position technology. The more expensive camera technique computes the sun centroid coordinates from frame-to-frame sun-blob images, while the more cost effective satellite quality sun-sensor technique detects the coordinates of the sun from individual sun-rays directed onto micro-substrates. The camera's contrast setting would sometimes be responsible for introducing very small average/offset deviation errors in camera-based closed-loop tracking in the early morning and late afternoon, basically because sunlight brightness variations between noon and afternoon/morning interferes with the image processing accuracies.

Stellenbosch University http://scholar.sun.ac.za

Some of the noise and offset error fluctuations in the solar tracking error patterns (Figure 6.4) emanate from the camera-based solar vector computations. It can be explained in the context of the technical details and steps used in the camera-based image processing technique. Keeping in mind that an industrial PLC is unable to provide sufficient computing power to support the mathematical complexities of image processing, a graphical illustration of the image processing hardware and sequence of steps required to determine the solar vectors through a web camera device is presented in Figure H.1. Firstly, the web camera faces the sun while external digital hardware captures individual pictures of the sun. Image processing software then performs complex processing to box the outline of the most apparent solar disc/blob within the captured image frame, though a process termed "sun-localization", typically using edge detection or object tracking techniques (Arturo and Alejandro, 2010). With a fixed web camera contrast setting, variations in the brightness of the sun over the course of the day (morning, noon, afternoons, clouds, etc.) does influence the sun-localization process, introducing potential sun localization errors. Continuing along with the (apparent) solar disc boxed/localized within the image, further processing in the next step determines the pixel coordinates of the centroid in the localized sun disc on each picture frame (see Figure 2.7(b, c)), followed by a step to determine and convert the sun vector pixel coordinates (x,y) into sun vector angles (°) using calibration parameters. In the final step, solar tracking azimuth/elevation axes errors are computed from the solar centroid image pixel displacement values. The sun-localization step is typically responsible for inconsistent/fluctuating daytime and frame-to-frame (noisy/biased) sun centroid pixel coordinates, especially since a camera image can be distorted when pictures of the sun are captured in varying sunlight levels and interferences from haze, clouds, wind or dust.

To help overcome distortions and contrast sensitivity problems experienced with the camera solar vector processing system, it is anticipated that a more expensive infra-red camera would help to improve sun-localization that will result in more accurate sun centroid calculations (especially in cloudy or dusty conditions). Furthermore, inter-frame sun centroid coordinate fluctuations/noise could be smoothed by progressively passing the determined output coordinates through a digital low-pass filter (i.e. Kalman moving average filter). The risks in meeting environmental requirements with additional sensitive hardware, as well as the technological complexities associated with camera-based solar tracking control, suggests that robust and simple sun sensor-based open loop solar tracking control would be more cost-effective in rural power generation applications. However, it should be noted in the context of a concentrated solar power system for rural power generation, that the web camera-based solar tracking control system showed superior capabilities in tracking the sun in moderate cloud cover, which the sun sensor was unable to do. This suggests that future developments towards developing a dedicated camera sun positioning solution, with integrated low pass filtering and potential infra-red

Stellenbosch University http://scholar.sun.ac.za

capabilities, may provide a solution capable of outperforming the sun sensor.

6.3.5. Summary and Conclusion

This experiment determined the levels of solar tracking accuracy achieved with the prototype concentrated solar positioning system using a web camera device in the closed-loop control configuration. In this experiment, an image processing system is used to determine the sun vectors $S_Q(\gamma_s, \theta_s)$ from web camera images (see Appendix H). Experimental results (Figure 6.4) show that the average on-sun azimuth and elevation axis solar tracking error sequences shows both short term and long-term noise-like variations throughout the day, with the average/offset errors at a minimum around noon. These smooth time-varying tracking offset errors are the cause of a fixed camera contrast setting throughout the day, which is unable to compensate for sunlight brightness variations. When compared to open-loop control solar tracking in the first experiment, the web camera device yields superior results as the optical feedback from the web camera is able to compensate for installation and mechanical disturbances and deficiencies.

Overall, camera -based closed-loop solar tracking control achieves azimuth and elevation axes solar tracking accuracies within the set overall error band of $-1.0^\circ < \epsilon_{az/el} < +1.0^\circ$, which is in compliance with the user accuracy specifications (Table 3.2). However, in comparing the solar tracking error sequences obtained with the web camera to that of the sun sensor, the web camera sun tracking error sequences appear to vary to a far greater extent. This is primarily as a result of inconsistencies in determining the exact position of the sun through relatively inaccurate image processing techniques. Web camera-based closed-loop solar tracking control also depends on the sun being directly within the view of the camera, meaning that the system would find it difficult to recover from prolonged periods of cloud cover. However, the web camera has an advantage over the sun sensor in still being able to locate the sun's position in moderate cloud cover, while the camera's zoom function could in future be used to dynamically adjust or broaden the camera's field of view. In this respect, a camera with an adjustable viewing/zoom angle between 50° and 90° (Appendix H) allows for an adjustment between ∼1.5 to 3 hours of continuous cloud cover or loss of view of the sun (45° forward view, ∼12 hours over horizon, ∼4 minutes/degree), before such a camera based tracking and control system would lose its synchronization with the sun and would be unable to recover from lost synchronization on that particular day.

6.4. Summary

This chapter presented three experiments to evaluate the optical performances of the mechatronic control system for the proposed self-tracking solar reflector

Stellenbosch University http://scholar.sun.ac.za

positioning system in two different control modes. The main objective of the three experiments was to validate whether the positioning system meets the design specifications, and to compare the optical performances of the PLC control system with sun vectors obtained from an astronomical algorithm, a sun sensor device, and a web camera imaging device respectively. Figure 6.1 to Figure 6.4 uses the same scale to display the the solar tracking error results for the SPA (open-loop), sun sensor (closed-loop) and web camera (closed-loop) control strategies, allowing for a quick visual comparison of the results between the various control methods.

Table 6.2: Summary and comparison between the three solar tracking control strategies, on the basis of the optically measured solar tracking error results.

Control Strategy	$\overline{\epsilon_{az}}$ **Az error**	**Azimuth error band**	$\overline{\epsilon_{el}}$ **El error**	**Elevation error band**
Open-loop SPA	0.18°	$-0.125^\circ < \epsilon < +0.395^\circ$	-0.06°	$-0.175^\circ < \epsilon < +0.125^\circ$
Closed-loop sun sensor	-0.01°	$-0.1^\circ < \epsilon < +0.1^\circ$	$+0.02^\circ$	$-0.07^\circ < \epsilon < +0.13^\circ$
Closed-loop camera	$+0.2^\circ$	$+0.1^\circ < \epsilon < +0.3^\circ$	-0.2°	$-0.1^\circ < \epsilon < -0.3^\circ$

To support the visual comparison of results between the various control methods, Table 6.2 presents a summary of the numerical results for the three control methods used in the experiments. The table details the solar tracking error results for the azimuth and elevation axis in the SPA based open-loop control, as well as the results for the sun sensor and camera based closed-loop control strategies.

In comparing open-loop solar tracking control with closed-loop solar tracking control, the results in Table 6.2 indicate that closed-loop control is superior to open-loop control in terms of accuracy. The average/offset deviation error for closed-loop tracking remains fairly stable throughout the day, provided that there be no cloud cover, while the width of the error band for the sun sensor is more consistent than that of the web camera device. It was anticipated that closed-loop tracking would yield better results since the closed-loop control receives optical feedback on the position of the sun from the sun sensor and is able to compensate for minor installation or mechanical disturbances. In comparing sun sensor based solar tracking with web camera based solar tracking, the results show that sun sensor tracking is more accurate. Compared to web camera image processing, the sun sensor is a pin-pointing device which is inherently more accurate in determining the sun's position. The web camera

Stellenbosch University http://scholar.sun.ac.za

approach has the disadvantage that sun brightness, atmospheric and environmental effects could influence the image processing accuracy, which in turn effects sun-vector accuracy calculations. With the camera device, complex image processing calculations are required to determine the position of the sun, but this comes with the advantage that the camera is able to still track the sun in moderate cloud cover while the camera's zoom function may in future be used for dynamically increasing or decreasing the field of view of the camera (should the sun move out of the field of view of the camera).

The experiments in this chapter show that the implemented concentrated solar positioning system delivers optical solar tracking accuracy within the accuracy range of $|\epsilon_{az/el}| < 1.0^{\circ}$ on both the azimuth and elevation axis despite apparent minor mechanical defects or installation errors. The as-built system meets the prescribed user specifications in Table 3.2. The proposed positioning system design achieves azimuth and elevation axes solar tracking optical accuracies within the required accuracy margins and will be able to compensate for slight installation errors anticipated with rural power system installations. Conclusions will be made in the next chapter and suggestions for future research towards improving the designed system will be made.

Stellenbosch University http://scholar.sun.ac.za

7. Summary and Conclusion

7.1. Summary

Most rural African villages enjoy high levels of sunlight, but rolling out solar power generation technology to tap into this renewable energy resource at remote rural sites pose some design challenges. To meet these challenges, a project has been initiated to design, build and test/evaluate a knock-down 3 kW electrical stand-alone self-tracking dual-axis concentrating solar power system. This study focused on the design and development of the dynamic mechatronic platform and digital electronic control components of the stand-alone concentrating solar power system. Chapter 1 highlighted the technological challenges associated with rural stand-alone power systems, while existing concentrated solar power generation solutions were discussed in the literature review in Chapter 2. User specifications, defined in Chapter 3, called for a mechatronic platform with automated solar tracking control for a parabolic solar concentrator with a thermal harvesting capacity of 12 kW_t at solar noon. This study presented the conceptual design and engineering prototype of a $\sim$12 m^2 lightweight parabolic solar concentrator with balanced cantilever tilt-and-swing dual-axis slew drive actuation, suitable for use in rural solar power applications, as detailed in Chapter 4. The design incorporates off-the-shelf components to support local manufacturing at reduced cost. Digital automation of the concentrated solar platform is realised on a Siemens S7-1200 Programmable Logic Controller (PLC), with Chapter 5 detailing the digital remote control interfacing, pulse-width-modulated direct-current driving with digital electronic open-loop and closed-loop solar tracking control. Real-time experiments evaluated the performance of the prototype positioning system in terms of solar tracking accuracy.

Chapter 6 presented three experiments in evaluating the optical performances of the mechatronic control system for the proposed self-tracking solar reflector positioning system in two different control modes. The main objective of the three experiments was to validate whether the positioning system meets the design specifications and to compare the optical performances of the PLC control system with sun vectors obtained from an astronomical algorithm, a sun sensor device and a web camera imaging device respectively. Interpretation of experimental results in Experiment 1 (Section 6.1) led to

Stellenbosch University http://scholar.sun.ac.za

the conclusion that subtle installation errors or mechanical defects may be the reason for minor band-limited average time-varying offset errors in the optic tracking accuracy observed with open-loop solar tracking control. Such defects/errors are typical in rural solar concentrator installations. Its effect was most noticeable on the azimuth axis, where the average/offset error increased from around $\overline{\epsilon_{az}} = -0.125°$ (in the morning and afternoon), to peak around $\overline{\epsilon_{az}} = +0.375°$ at noon, the latter being moving relatively close to the error boundary $\epsilon_{max} = +1.0°$ (see Table 3.2). Control mode experiments compared open-loop and closed-loop solar tracking accuracy with further two experiments. Experiment 2 employed a sun sensor (Section 6.2) while Experiment 3 employed a web camera (Section 6.3) to determine the effects of optical imaging devices in the feedback control loop of the PLC controller. Other than relatively small constant offset/bias errors in the azimuth and elevation axes solar tracking error sequences, these optical devices were able to support PLC-based solar tracking accuracies within a constant error band of $+0.1° < \epsilon_{az} < -0.1°$, as detailed in Sections 6.2 and 6.3. These results clearly confirmed superior solar tracking accuracy in the closed-loop control mode on clear day tracking, and demonstrated that the optical devices were able to circumvent the average time-varying offset errors experienced with open-loop solar tracking. In comparing sun sensor-based solar tracking with web camera-based solar tracking, the results (Section 6.2 and 6.3) showed that sun sensor tracking was more accurate. Compared to web camera image processing, the sun sensor is a pin-pointing device which is inherently more accurate in determining the sun's position. The web camera approach has the disadvantage that sun brightness, atmospheric and environmental effects could influence the image processing accuracy, which in turn effects sun-vector accuracy calculations. With the camera device, complex image processing calculations were required to determine the position of the sun, but this came with the advantage that the camera was still able to track the sun in moderate cloud cover. The camera's zoom function may in future also be useful in dynamically increasing or decreasing the field of view of the camera, should the sun move out of the field of view of the camera). Overall, the experimental results detailed in Chapter 6 showed that the implemented design performs continuous solar tracking actions to an optical accuracy better than 1.0° on both the azimuth and elevation tracking axes, meaning that the system complies with the solar tracking error specification of $|\epsilon_{az/el}| < 1.0°$ (Table 3.2).

7.2. Conclusion

In comparing the results from the three control strategies in the three experiments of Chapter 6, the summary of results in Table 6.2 was very useful. The results show that the open-loop SPA based tracking strategy yielded the poorest results, both in terms of average solar tracking error and solar tracking

Stellenbosch University http://scholar.sun.ac.za

error band, especially on the fast moving solar azimuth axis. In closed-loop solar tracking control mode, the sun sensor based solar tracking strategy outperformed both the open-loop SPA and the closed-loop web camera based solar tracking, and was found to be the overall preferred solar tracking control mode both in terms of accuracy and technical complexity.

7.3. Contribution

It was emphasized in Chapter 1 that the goal of this study was to utilize Africa's rich natural sunlight resource to deliver on socio-economic objectives in terms of providing solar electrical power to communities in deep rural areas. The hypothesis of this study postulated that it would be possible to develop an accurate automated positioner and control system for a stand-alone motorized parabolic solar reflector. Having the capacity to harness 12 kW_t of solar thermal energy at noon, which in turn is essential to provide off-grid rural communities with a stand-alone knock down 3 kW_e peak electrical power generation and supply system. This hypothesis supported the *energy and sustainable environment* research focus area of the Stellenbosch University HOPE Project.

Features of the implemented solar concentrator platform design include aspects such as a plug-and-play type automation platform, grease-lubricated actuator drives, tilt-and-swing pivot motion control, and a weight balancing boom over a pedestal pole. The proposed light-weight dish solar concentrator further ensures less wind resistance as a result of circular slots dividing the inner and outer rim mirrors, while a flatter dish structure ensures simpler installation and lower probability of dust fixation on the mirrors. The features and technical aspects of the solar concentrator design and digital control system automation were also presented at the international SolarPaces 2013 conference (Prinsloo *et al.*, 2013*b*).

Based on the findings of this study, and the experimental results presented in Chapter 6 (Sections 6.1, 6.2 and 6.3), it is concluded that the the study succeeded in designing and implementing a simple but accurate automatic positioner and control system for a motorized parabolic solar reflector to support the HOPE project. The degree of accuracy achieved with a relatively simple and modular design that supports the commercialisation objectives of the project, since the system has the potential to play a part in helping to meet the everyday electricity needs of rural citizens of South Africa. The design and prototype incorporates off-the-shelf components to support local manufacturing at reduced cost and generally meets the goal of delivering a dynamic mechatronic platform for a concentrating solar power system that is easy to transport, assemble and install at remote rural sites in Africa. The design further supports the goal of the university's joint research project aimed at producing a locally manufactured knock-down do-it-yourself concentrated solar power generation

Stellenbosch University http://scholar.sun.ac.za

kit, suitable for deployment into Africa. Structural aspects of the designed parabolic dish are further evaluated and optimized by other researchers, while the Stirling power unit and power handling subsystems are presently under development in parallel studies.

Stellenbosch University http://scholar.sun.ac.za

8. Directions for Future Research

The proposed mechatronic design configuration and solar tracking system allows flexibility to accommodate production demands and marketing potential in terms of commercialisation of the technology. Structural aspects of the prototype parabolic dish will in future be optimized by other researchers while the Stirling and power handling units are under development in parallel projects. A cost analysis and feasibility study are progressing in a parallel project. Other directions towards technically improving the system are highlighted in the recommendations below:

Hybrid Solar Tracking Control: Further research should be undertaken and experiments conducted in order to determine the most practical solution towards integrating generic optical feedback devices into an hybrid open/closed-loop PLC control mode. In such a development, the solar vector from a generic optical means $S_{optic}(\gamma_s, \theta_s)$ should optically augment the SPA solar vector information $S_{SPA}(\gamma_s, \theta_s)$, while the azimuth/elevation axes PWM sequences should be adjusted in relation to error inputs from the optical device. Ideally, the control signals of the optical device should be interpreted to measure solar radiation levels and predict cloud cover as part of the PLC-based hybrid tracking control solution.

Weather Prediction Intelligence: Weather effects are the Achilles heel of concentrated solar power generation systems, especially in stand-alone solar power systems. Solar tracking control in future stand-alone solar power generating systems would therefore require further intelligence in terms of awareness of weather patterns and overcloud weather conditions. In a stand-alone solar system, the effects of weather patterns directly impact on the power source to drive the solar tracking and power generation subsystems. Forecasting solar radiation, cloud cover and rain from light intensity, humidity or wind measurements will help to improve onboard energy management. With weather pattern intelligence provided through a wireless link, the automated control and tracking system will be able to further emulate the thinking processes of an operating engineer.

Carbon Footprint Management: The control system of the future could incorporate CO_2 impact management, power budget and smartgrid principles to establish smart rural microgrids in order to help enhance local power reliability and improve power quality. Dynamic engagement of intelligent modes

Stellenbosch University http://scholar.sun.ac.za

of operation through artificial intelligence and finite state machine principles could emulate the thinking processes of an operating engineer, helping the PLC to auto select different modes of operation under varying on-board, user-demand and external sunlight exposure conditions (Prinsloo *et al.*, 2013*a*).

Stellenbosch University http://scholar.sun.ac.za

Appendices

Stellenbosch University http://scholar.sun.ac.za

A. Parabolic Dish Configuration

In large diameter point-focussing solar concentrator reflectors, a continuous parabolic dish is not ideal. The slope angle of the parabolic curve gets very large further away from the parabolic vertex, meaning that a large volume of dish material and weight hangs over onto the sun-axis of the balancing boom, causing an uneven weight distribution and strain on the actuators drives. A continuous parabolic dish further complicates dish installation at remote rural sites, since great precision and competency is required to perfectly assemble a large continuous parabolic dish.

To meet the challenge of producing a simple, modular, easy-to-assemble and relatively flat parabolic dish structure suitable for rural applications, a compact multi-layered (Fresnel-type) dish configuration is being proposed in this study. The geometry of this compact dish configuration is illustrated in Figure A.1. It comprises of an array of differential parabolic sections (1.inner, 2.middle and 3.outer ring sections) embedded onto a flat plane located at the vertex of main parabolic curve. This plane is orientated perpendicular to the parabolic sun-axis, intersects with the parabolic curve at the vertex, and is known as the parabolic *"directrix"* plane.

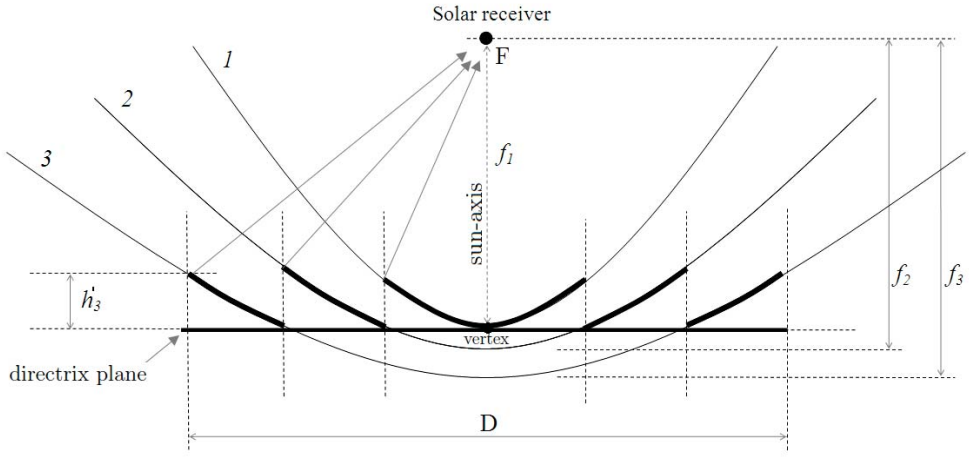

Figure A.1: Orthographic view of a family of parabolic curves with identical parameters and focal point F, but with increasing f/D ratios, axially embedded onto the main parabolic directrix plane, serving as flat load bearing structure.

Stellenbosch University http://scholar.sun.ac.za

A simplified way to help visualise the geometric shape of this parabolic dish configuration (Figure A.1), is to consider the surface of a conventional continuous parabolic dish being axially sliced into an series of circular differential strips/rings (Figure A.2). These truncated differential ring sections are then collapsed and embedded onto the directrix plane of the main parabolic curve (Figure A.1), which now serves as the "load bearing structure" for the proposed dish configuration.

Mathematically, this dish configuration can be described in terms of the parameters of an array of truncated sections of parabolic functions of the same family, parabolic functions with identical parameters but varying parabolic constants (f/D ratios). Parabolic equations can thus be used in the selective integration of differential ring-like strips/curves from members of the same parabolic family into a compound structure Figure A.1, while retaining a common focal point (F) through selected parabolic ratios (f/D). The parabolic equations for the family of curves/functions is best expressed in terms of the parameters in Figure A.2, with (a) showing parameters defining an individual truncated circular differential strip, and (b) showing a family of parabolic shapes for varying f/D ratios.

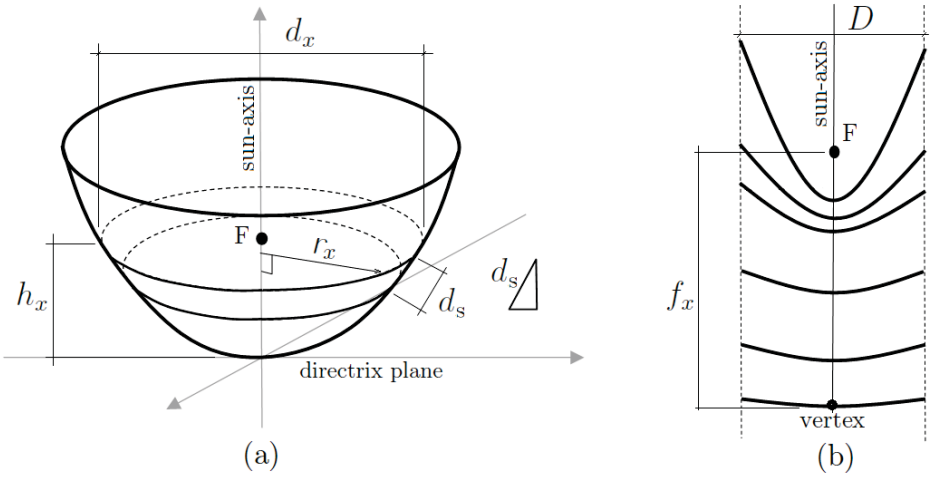

Figure A.2: Parabolic elements with (a) parameters defining a circular differential strip and (b) flatter curves for increasing f/D (Stine and Geyer, 2001).

Parabolic equations can now be engaged in a mathematical iteration process to select a set of three parabolic family members, which jointly guarantees an optimally flat parabolic dish geometry in a fashion that describes three reflective circular parabolic arrays embedded onto a flat load bearing structure (Figure A.1). This process starts with a centre/inner ring as first parabolic segment with a conventional parabolic constant of $f/D = 0.6$ (Stine and Geyer, 2001). Increased f/D parabolic ratio values should subsequently be computed for the middle and outer circular array elements, with values such that the basis

Stellenbosch University http://scholar.sun.ac.za

of the inner-edge of each subsequent parabolic ring can be mounted flush onto the flat load bearing structure (Figure A.1), while at the same time ensuring optimal physical separation from one array element to the next (ring-like air gap divisions between the three parabolic ring elements) to help minimize the effect of inter-element shadowing. Moreover, the selected set of three parabolic family members should at the same time guarantee an overall dish reflective surface area of A=12 m^2, for the system to deliver a solar collection capacity of 12 kW_t (also taking into consideration Stirling module optical shadowing losses). The complexity in optimally selecting three parabolic member sets to balance all of the requirements calls for an iterative process that involves the use of differential parabolic equations ((Stine and Geyer, 2001)):

$$h_x = d_x^2/16f_x \tag{A.1}$$

$$A_x = \pi d_x/12h_x^2 \times \left[(d_x^2/4 + 4h_x^2)^{3/2} - d_x^3/8\right] = 12\ m^2 \tag{A.2}$$

The parameters (d_x, f_x, h_x, h'_x) for the inner ($x = 1$), middle ($x = 2$) and outer ($x = 3$) parabolic dish elements was calculated iteratively through Equations (A.1) and (A.2). The parameters h'_1, h'_2 and h'_3 are key in ensuring the flattest possible dish structure, as it represents the height of the upper-outer edge rim of each respective parabolic segment above the load bearing plane (see Figure A.1). Table A.1 lists the parameters for the selected set of parabolic family members. Interesting to note is that inter element- and Stirling unit- optical shadowing losses increased the overall diameter of the compound dish from $D = 3908\ mm$ (conventional parabolic) to $D = 4274\ mm$, allowing for the system to maintain the specified collector capacity of 12 kW_t.

Table A.1: Parabolic ring element parameters (Figure A.3).

Parameter	**Inner ring** ($x = 1$)	**Middle ring** ($x = 2$)	**Outer ring** ($x = 3$)
d_x	2063.46 mm	3655.27 mm	4274.00 mm
f_x	2400.00 mm	2520.00 mm	2600.00 mm
h'_x	58.96 mm	176.87 mm	184.61 mm

Figure A.3 presents a two-dimensional CAD drawing, illustrating the multi-segment dish structure with selected dimensions (d_x, f_x, h'_x) computed above. This drawing shows how the three segments in the three element dish structure ensures a relatively flat compact parabolic dish configuration with uniform flux profile on the target plane. In order to simplify manufacturing and on-site installation, the inner, middle and outer parabolic ring elements can be fabricated as flat reflective surface panels that mounts onto the flat ribbed frame (load bearing structure), providing a slightly broader flux profile (533 mm x 533 mm) at the solar receiver area (Figure A.3).

Stellenbosch University http://scholar.sun.ac.za

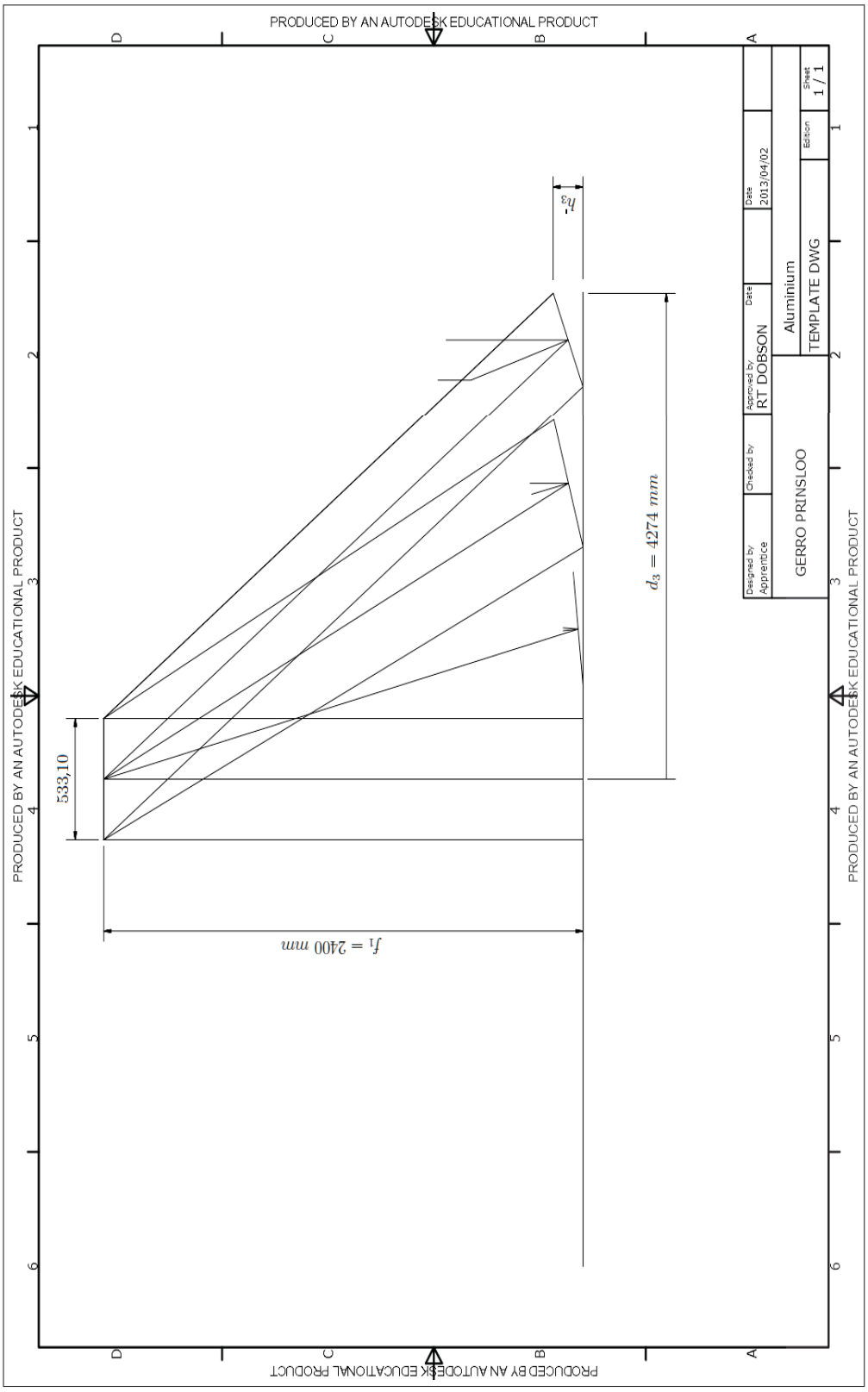

Figure A.3: Parabolic dish elements and calculated segments at different f/D ratios to concentrate on the same focal area.

Stellenbosch University http://scholar.sun.ac.za

B. Pedestal Pole Dimensions

Azimuth and elevation axis movement is accomplished through slew actuators fitted on the pinnacle of a pedestal support structure. Structurally, the pedestal should be designed around the weight and torque requirements, with special provision for shock loads such as wind gusts and wind turbulences impacting on the solar reflector dish and structure.

Table B.1: Pedestal pole dimension calculations.

Parameter	Value	Unit
F_{wind}	18000	N
T	5040	N.m
P	2265	N
Outside diameter	0.22	m
Inside diameter	0.196	m
c	0.11	m
A	0.007841415	m^2
Material yield strength	240000000	Pa
Safety factor	4	
Pipe length	2.2	m
I	4.25475e-05	
J	8.5095e-05	
$sigma_x$	102668498	Pascal
tau_{xz}	6515068.448	Pascal
$sigma^{'}$	103286779.5	Pascal
$sigma^{''}$	60000000	Pascal
n	2.323627488	

From the analysis and dimensions documented in Table B.1, the support pedestal is fabricated from 230 mm mild steel piping with a 10 mm wall-thickness. The top of the pedestal includes a 15 mm flange for mounting the actuator mechanism at the pivot point of the balancing beam which connects the solar dish and the counterweight elements. Elements are all galvanized to guarantee rust-protection and long-term endurance. Ideally a slewing drive actuator mechanism (Chapter 4, Section 4.4.3 and Appendix C) should be selected such that it meets the minimum torque specification in Table B.1 (T>5040 N.m) and should mount onto the pedestal pole flange with a mounting diameter of around 250 mm to 350 mm.

Stellenbosch University http://scholar.sun.ac.za

C. Slewing Drive Specifications

Depending on the location of the observer, the sun is moving on average at an angular speed of around 0.25° per minute (Stine and Geyer, 2001). Thus, on the fastest moving solar tracking axis, namely the azimuth axis, the solar concentrator dish should achieve an angular rate of movement of at least 0.25° per minute to keep up with the relative sun movement. To achieve this minimum angular movement rate of 0.25° per minute, a 360° minimum rotational motion speed of 0.000694 rpm ($0.25°/360° = 0.000694\ rpm$) is required to accomplish successful solar tracking.

Electrical motors normally move at a rate of around 1750-2000 rpm. These motors on their own would thus not achieve this slow rate of movement with adequate torque to drive solar tracking. Thus a gear drive or transmission system is required to gear-down motor speed while providing sufficient torque at slower solar tracking speeds. Equation (C.1) can be used to compute the required gear ratios, given the motor speed and the sun's angular speed.

$$Gear_{ratio} = \frac{(Motor_{input\ speed})}{(Gearbox_{output\ speed})} \tag{C.1}$$

From Equation (C.1), the maximum allowable gear ratio or reduction gearing allowed to convert a rotational speed of 1750 rpm (motor speed) to that of 0.000694 rpm (solar tracking speed) through a transmission or gear drive system is computed to be around 2,000,000:1 (1750/0.000694). With this gear ratio, the solar concentrator gear drive system will just be able to keep up with the sun movement.

Concentrated solar dish movement could also be faster than the rotational movement speed of the sun (0.000694 rpm) as typical gear drive systems with gear ratios between 10,000:1 and 30,000:1 are used for solar tracking. By way of example, with a gear ratio of 15,000:1 and a motor speed around 1750 rpm, the rotational solar tracking movement calculated from Equation (C.1) will be around 0.175 rpm, ensuring a rotational solar tracking speed roughly 250 times faster than the movement of the sun on the azimuth axis. Using a slower DC motor, with a motor speed around 10 rpm and the same gear ratio of 15,000:1, the rotational solar tracking movement speed calculated from Equation (C.1) will be around 0.00067 rpm, ensuring a rotational solar tracking speed within the same order as the rate of movement of the sun on the azimuth axis.

Stellenbosch University http://scholar.sun.ac.za

Slew Drive Specifications and Datasheets

Figure C.1 shows a drawing of a typical slewing actuator mechanism with DC motor drive assembly to identify slewing drive components.

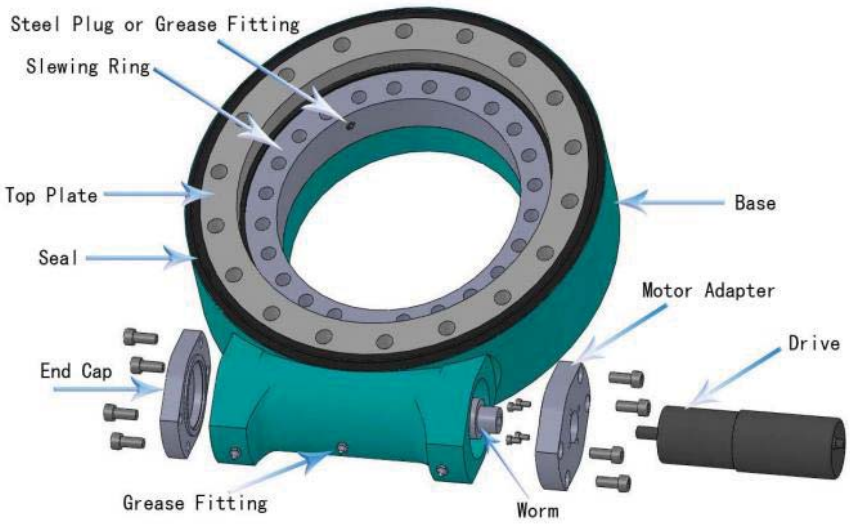

Figure C.1: Illustration of the slewing actuator mechanism with DC motor drive assembly to show the slewing drive components(Fang, 2013).

Any slew drive selected for this design needs to meet the torque and dimension specifications presented in Table B.1. The slewing drive selected in this design is the Model SE9A-61-R-24H.77.35-REV.B solar tracking slew actuator. This DC motor integrated slew drive is manufactured and supplied by Jiangyin Huafang New Energy Hi-Tech Equipment Company and the datasheet is presented in Figure C.2 (Fang, 2013).

This slew drive system integrates a DC motor with a planetary gear drive and provides a choice between a brushed and brush-less DC motor. The selected SE9A-SE enclosed slewing drive has a rated torque of 854 N.m (0.126 rpm) and a holding torque of 38.7 kN.m. The overall drive-train gear ratio of this enclosed slewing drive together with the integrated DC 24 V motor planetary gear system is 14,274:1 (slew gear ratio 61×234 planetary gear ratio). A brush-less DC motor is preferred as these motors require less maintenance and are more suited for multiple starts and stops when compared to brushed DC motors (Yedamale, 2003).

Figures C.3 and C.4 further present the mechanical performance charts and electrical performance curves of the 24 V DC motor and Hall position magnetic pulse encoder integrated with the slewing actuator mechanism Model SE9A-61-R-24H.77.35-REV.B (Fang, 2013).

Stellenbosch University http://scholar.sun.ac.za

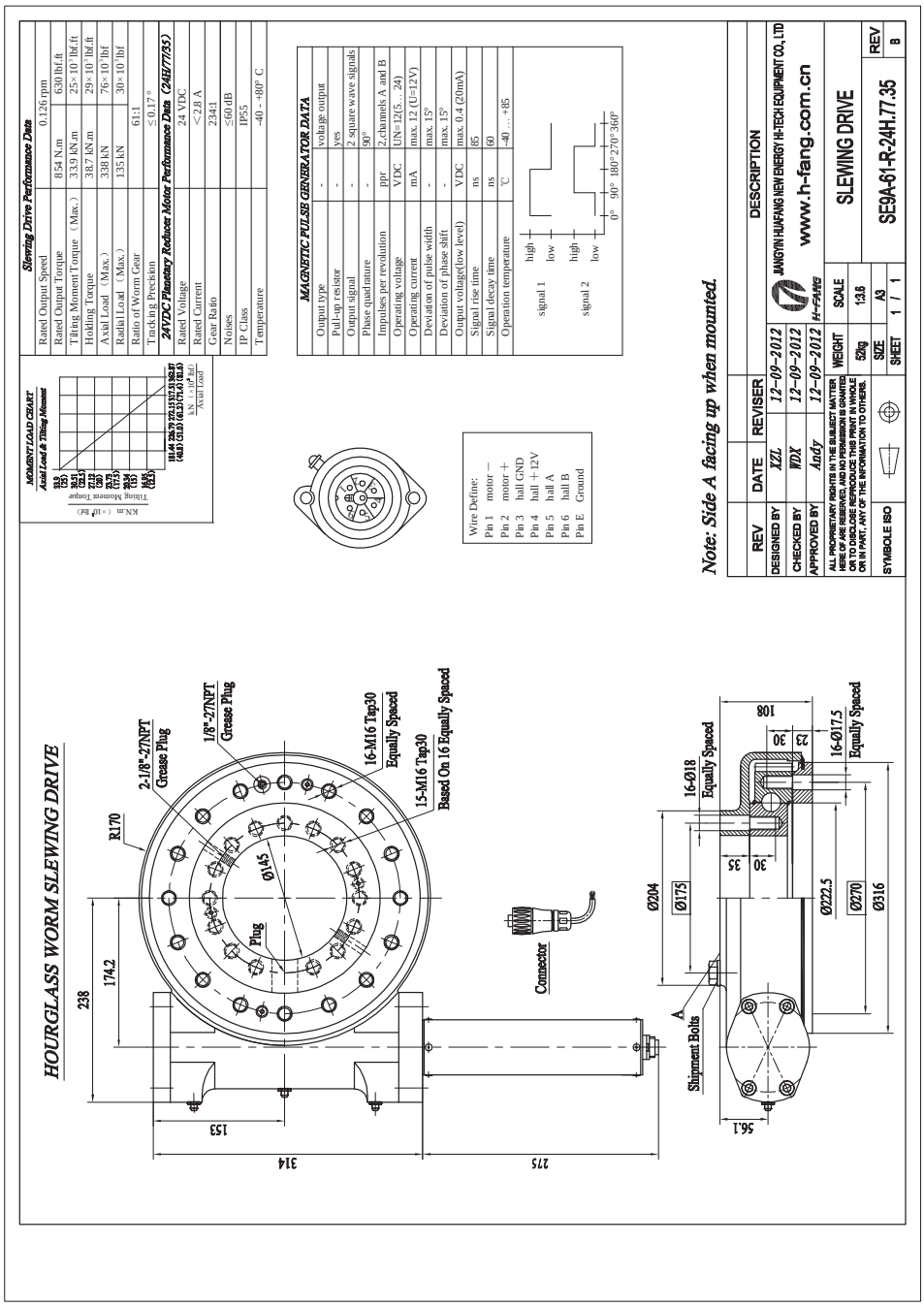

Figure C.2: Datasheet of the selected SE9A slewing actuator mechanism and DC motor assembly (Fang, 2013).

Stellenbosch University http://scholar.sun.ac.za

H-FANG

DC Motor testing data

Motor model		24H/77/35-REV.A				Rated Power			
Serial NO.						Rated Voltage	24V		
Tester		TiaoXH				Rated Speed	7.7r/min		
Test Date		03/05/2013				Rated Torque	35N.m		
NO.	Time(S)	Voltage(V)	Current(A)	Power Factor	Input Power(kw)	Output Torque(N.m)	Output Speed(r/min)	Output Power(kw)	Efficiency(%)
0	0	0	0	0	0	0	0	0	0
1	0	23.94	0.503	1	0.012	-1.4221	10.31	0.0015	12.5
2	5.4	23.88	0.552	1	0.013	-2.1721	10.16	0.0023	17.69
3	7.6	23.88	0.577	1	0.013	-3.4395	10.12	0.0036	27.69
4	11.7	23.88	0.772	1	0.018	-5.5747	9.99	0.0058	32.22
5	13.8	23.88	0.895	1	0.021	-7.6305	9.89	0.0079	37.62
6	16	23.94	0.993	1	0.023	-8.2654	9.8	0.0085	36.96
7	17	23.88	1.042	1	0.024	-9.6858	9.76	0.0099	41.25
8	18.1	23.88	1.09	1	0.026	-11.975	9.75	0.0122	46.92
9	20.2	23.82	1.237	1	0.029	-13.883	9.61	0.014	48.28
10	21.3	23.82	1.36	1	0.032	-15.587	9.53	0.0156	48.75
11	22.3	23.82	1.433	1	0.034	-16.251	9.38	0.016	47.06
12	23.5	23.82	1.531	1	0.036	-17.044	9.2	0.0164	45.56
13	25.7	23.82	1.751	1	0.041	-22.389	9.03	0.0212	51.71
14	26.7	23.82	1.898	1	0.045	-24.232	8.87	0.0225	50
15	28.9	23.82	2.045	1	0.048	-26.168	8.74	0.024	50
16	31	23.76	2.46	1	0.058	-31.653	8.52	0.0282	48.62
17	32	23.76	2.534	1	0.06	-34.771	8.41	0.0306	51
18	33.1	23.76	2.681	1	0.063	-37.197	8.18	0.0319	50.63
19	34.1	23.7	2.852	1	0.067	-37.581	8.16	0.0321	47.91
20	35.2	23.76	2.705	1	0.064	-36.132	8.25	0.0312	48.75

Figure C.3: Test data showing performance of the SE9A slewing actuator brushless DC motor (Fang, 2013).

Stellenbosch University http://scholar.sun.ac.za

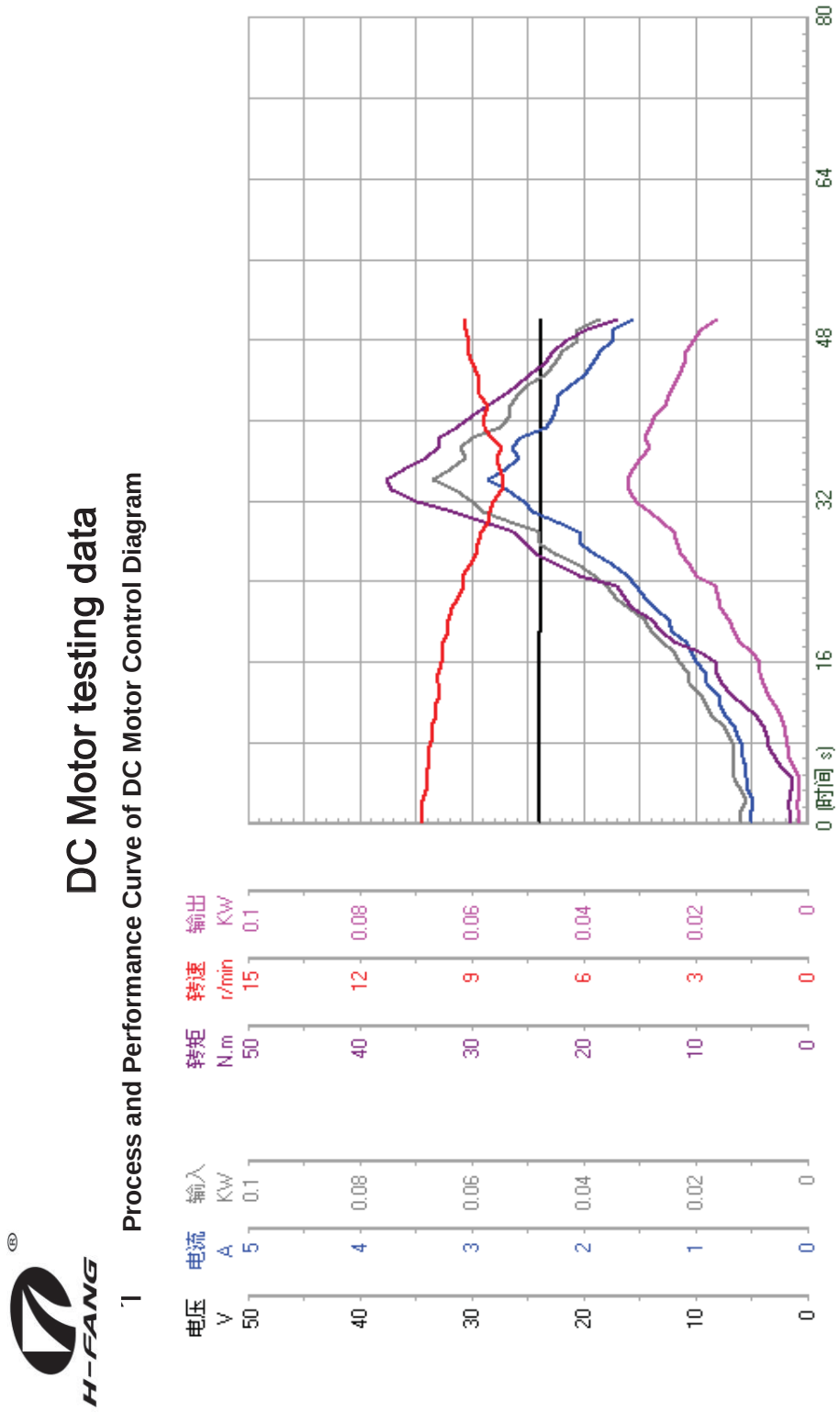

Figure C.4: Test data showing performance curves of the SE9A slewing actuator brushless DC motor (Fang, 2013).

Stellenbosch University http://scholar.sun.ac.za

H-FANG

DC Motor testing data

2

HALL Position Encoder waveform of control diagram

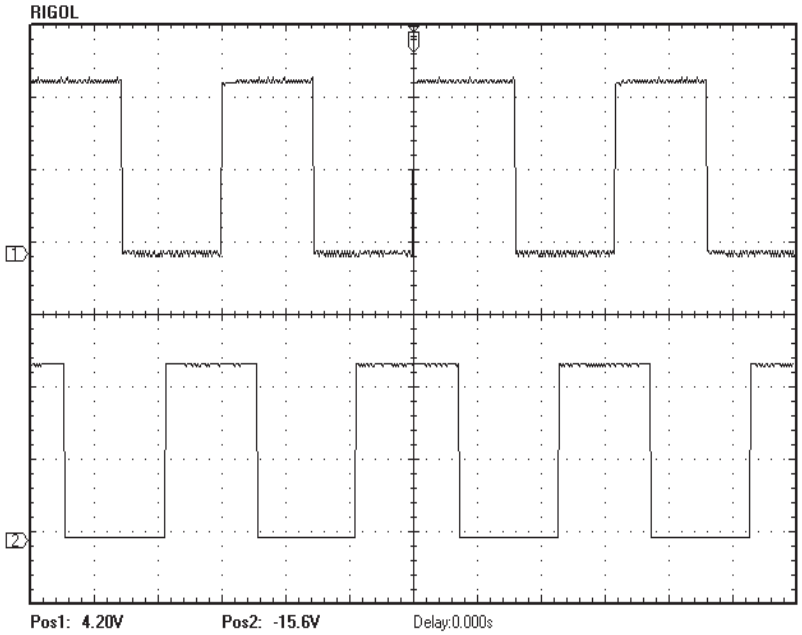

Check by: RenHL
Date:2013-5-3

Approved by: YuanH
Date:2013-5-3

Figure C.5: Output waveform for SE9A slewing actuator Hall magnetic position encoder (Fang, 2013).

Stellenbosch University http://scholar.sun.ac.za

D. Platform CAD Drawings

Figure D.1 to Figure D.4 shows CAD design drawings of the mechatronic platform system for the proposed concentrated solar power system.

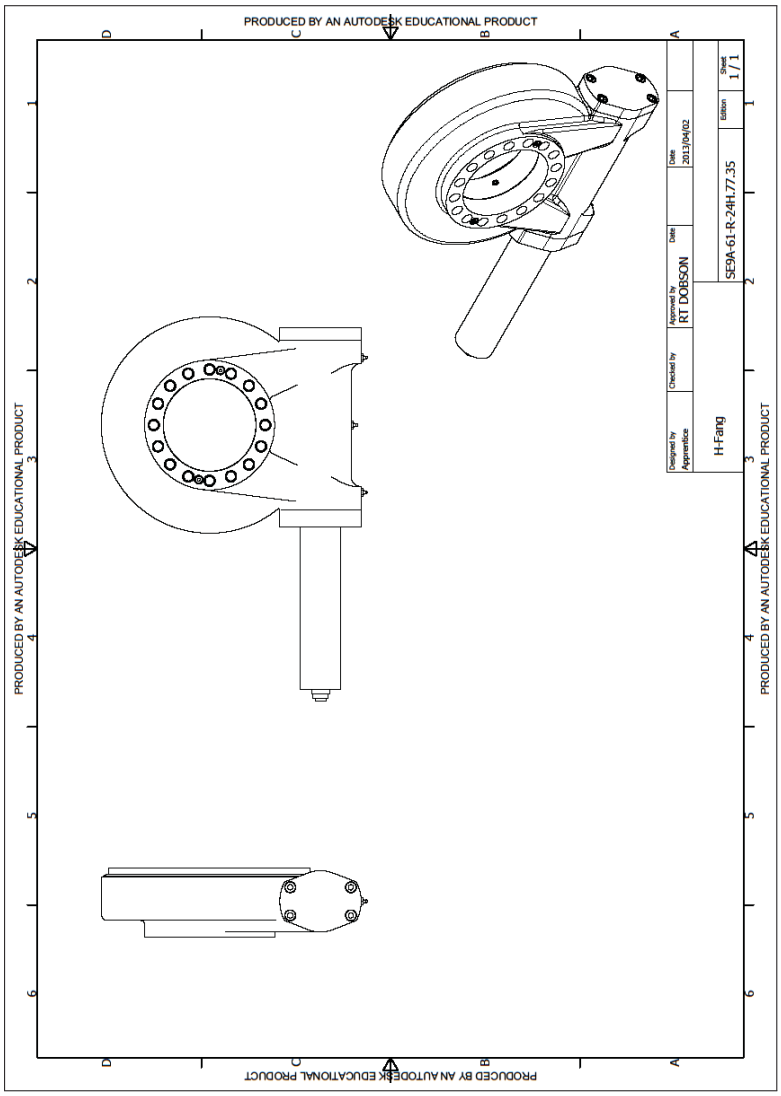

Figure D.1: CAD drawing slewing drive selected for the mechatronic platform.

Stellenbosch University http://scholar.sun.ac.za

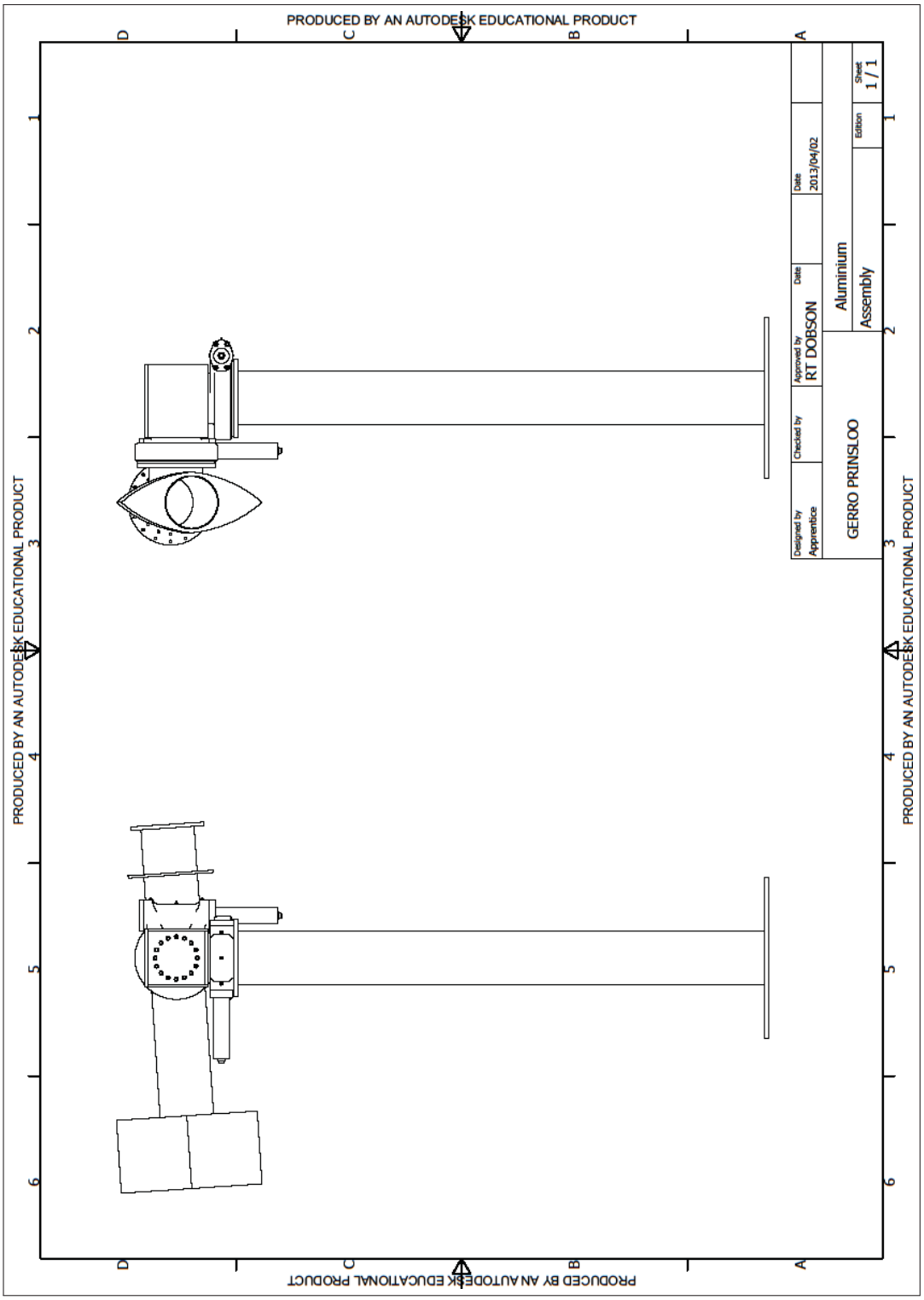

Figure D.2: CAD drawing of the complete solar concentrator mechatronic platform system assembly.

Stellenbosch University http://scholar.sun.ac.za

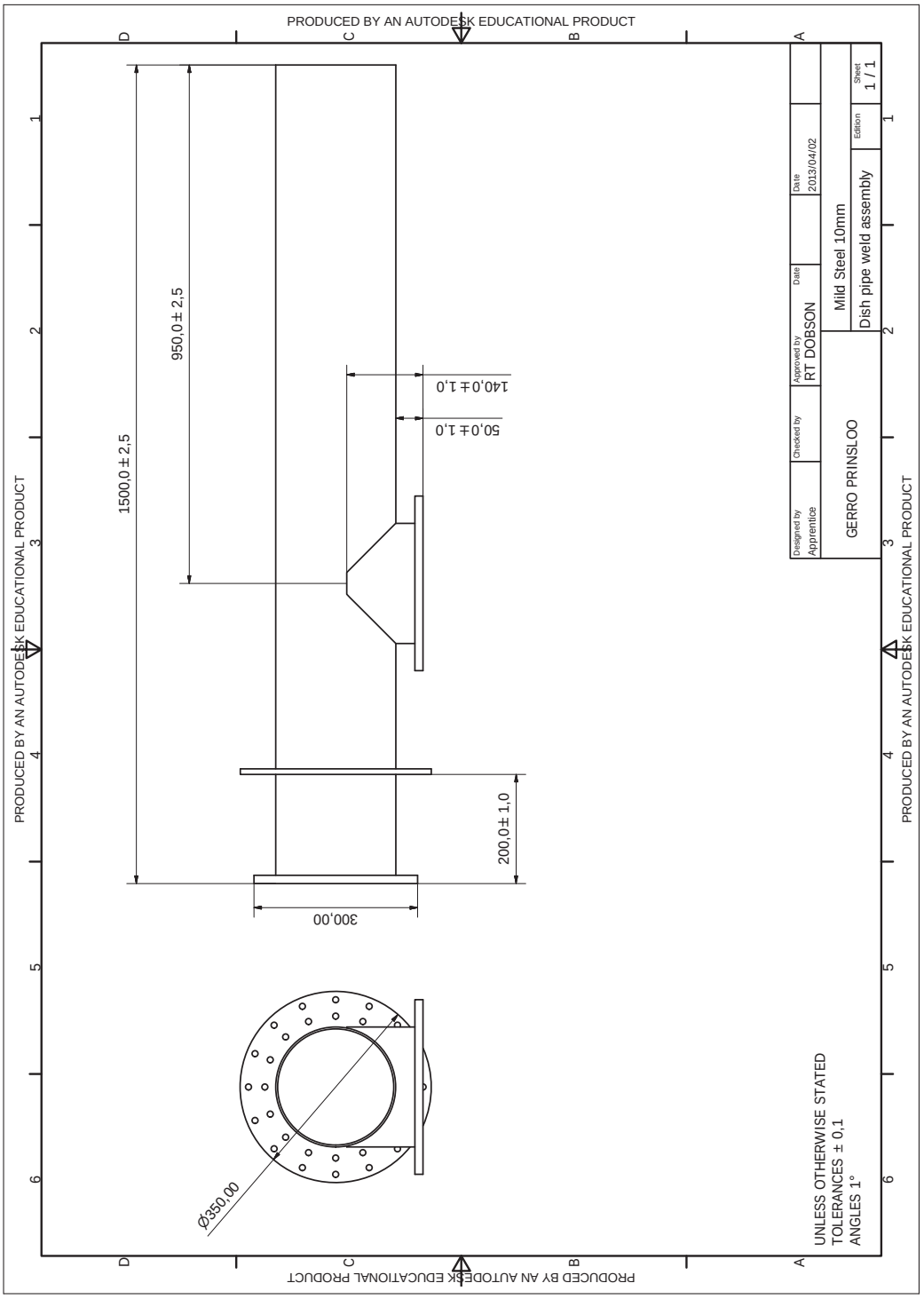

Figure D.3: CAD drawing of the solar concentrator mechatronic platform balancing boom assembly.

Stellenbosch University http://scholar.sun.ac.za

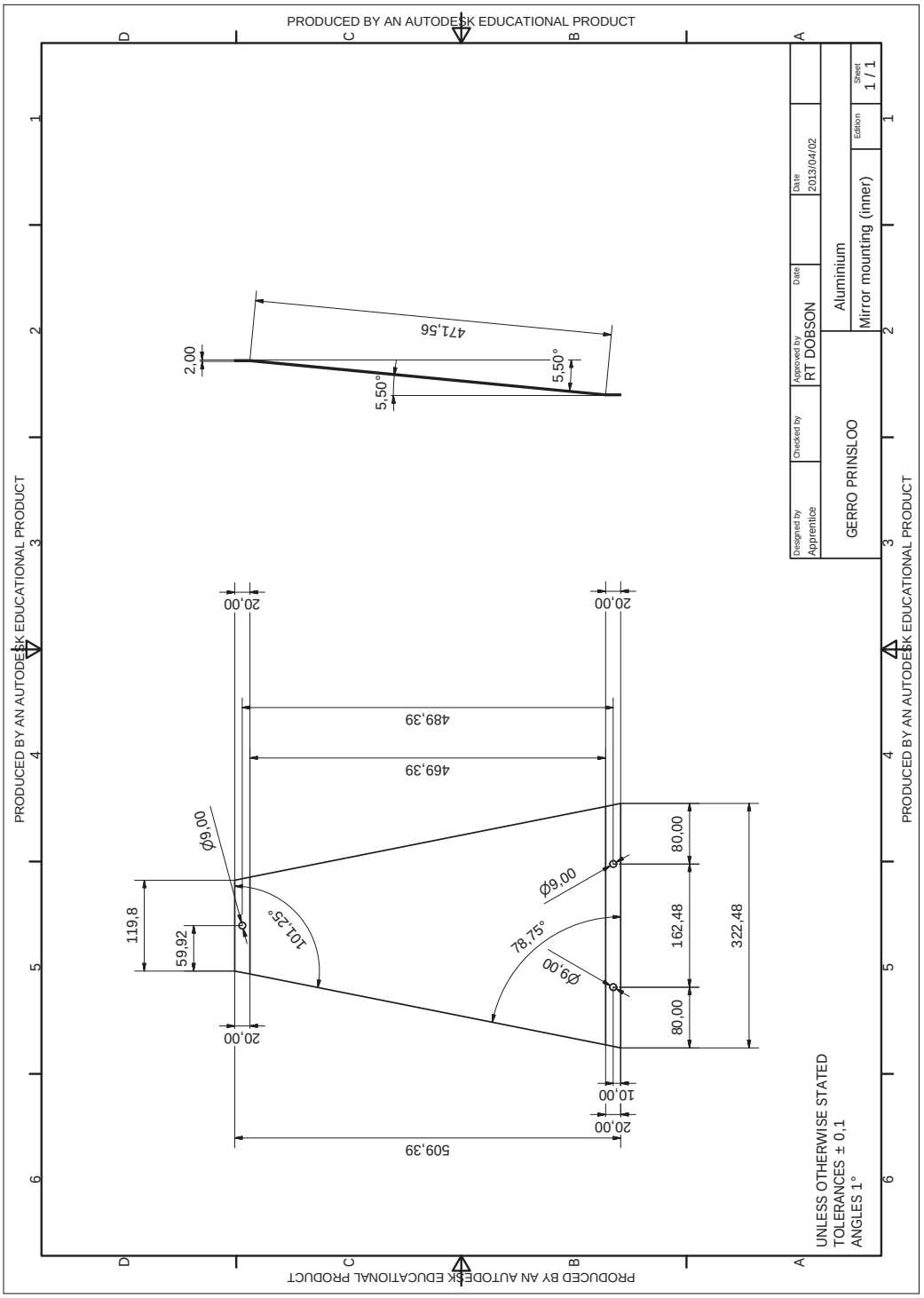

Figure D.4: CAD drawing of the solar concentrator mechatronic platform parabolic dish hub assembly.

Stellenbosch University http://scholar.sun.ac.za

E. Experimental Test Site

In order to conduct evaluation experiments on the performance of the designed solar concentrator system, the mechatronic platform was installed at a fixed evaluation site. The solar concentrator experimental test site is located in the region of Banghoek Road and Joubert Road, Stellenbosch, South Africa.

Figure E.1 shows pictures of both the STERG Kipp & Zonen Solys 2 UV-A/B solar radiometer (for measuring solar radiation spectrum) and the implemented mechatronic solar concentrator platform. Both these units are installed on the rooftops of two immediately adjacent buildings at the Department of Mechanical Engineering at the Faculty of Engineering complex on the Stellenbosch University campus. In future, solar irradiation readings from the Solys solar radiometer in close proximity to the concentrated solar power system could be used to validate thermal collection capabilities of the system.

Figure E.1: Site of experiments, showing the STERG Solys 2 UV-A/B solar radiometer and prototype solar concentrator installed on adjacent building rooftops.

Figure E.2 shows a satellite image of the site of installation of the implemented solar concentrator platform on the concrete rooftop of the Department of Mechanical and Mechatronic Engineering at the University of Stellenbosch. The exact GPS coördinates of the location of installation are: $33°S55'43.13", 18°E51'56.16$ $(-33.928646,\ 18.865601)$. Figure E.2 further shows the solar path contours at the installation and experimental site.

Stellenbosch University http://scholar.sun.ac.za

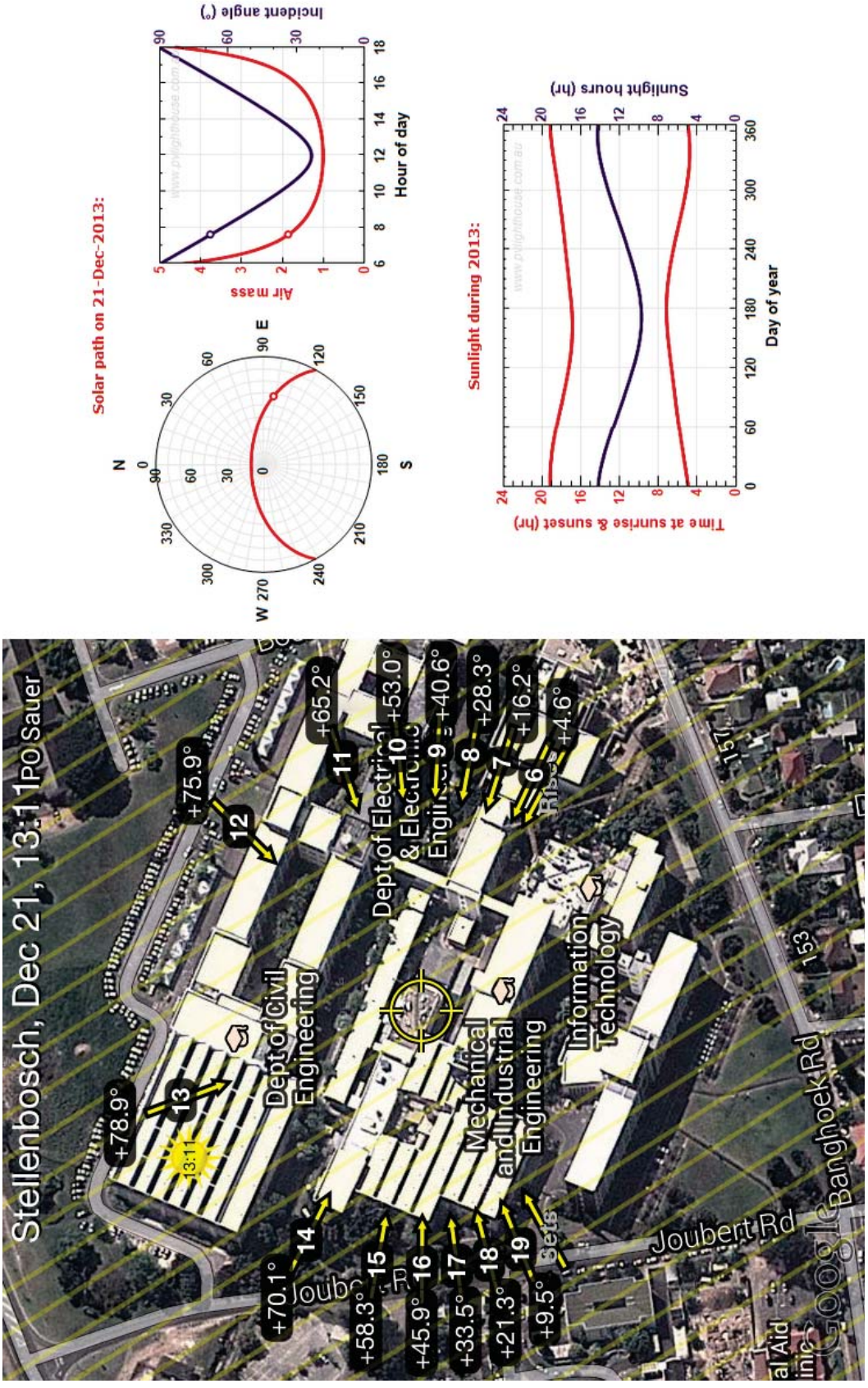

Figure E.2: Satellite image and solar path for solar concentrator at site of installation where performance experiments are conducted.

Stellenbosch University http://scholar.sun.ac.za

F. Solar Positioning Algorithm

Figure F.1 shows a typical illustration of a sun-vector and sun-angles to consider when a solar concentrator tracks the sun using any the digital electronic Siemens PLC hardware in conjunction with the SPA algorithm.

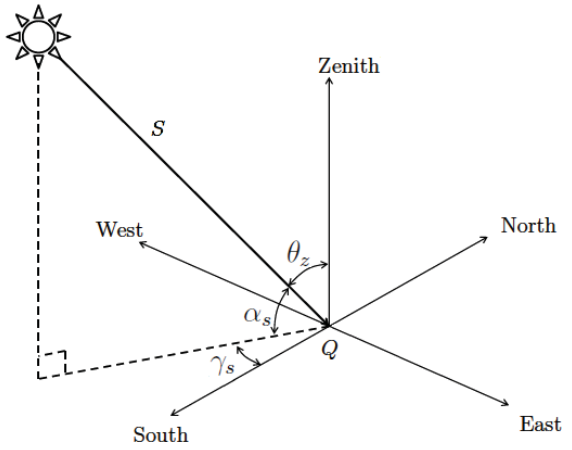

Figure F.1: Observer at location Q illuminated by sun ray observed along sun vector S_Q, showing solar tracking azimuth and elevation/zenith angles.

A solar position algorithm (SPA) implementation determines the position of the sun at any given time for a specific location. The calculations presented herein are based on the SPA of National Renewable Energy Laboratory (NREL) and is classified as an astronomical algorithm because of the high degree of accuracy. The earth angles described below are the angles required to determine the position of the sun with respect to a plane of any particular orientation (Reda and Andreas, 2008). The following list of parameters relates to the terms used in the calculation of the sun-vector given in Figure F.1:

- Latitude(ϕ): The angle north or south of the equator of the solar collector (measured in degrees);
- Longitude(ζ): The east-west position of the solar collector relative to the Greenwich (measured in degrees);

Stellenbosch University http://scholar.sun.ac.za

- Declination(δ_s): The angular position of the sun at solar noon with respect to the equator (measured in degrees);
- Surface azimuth angle(γ): Deviation of the direction of the slope to the local meridian (degrees);
- Solar azimuth angle(γ_s): Angle of the sun to local meridian or surface azimuth, clockwise from the south (degrees);
- Elevation angle(α_s): Solar-vector elevation from observer (degrees);
- Zenith angle(θ_z): Angle of incidence on a horizontal surface, solar-vector zenith ($90° - \alpha_s$) (degrees);
- Angle of incidence and reflection(θ): Angle between incident solar radiation and surface, solar-vector elevation (degrees);
- Hour angle based on the solar time(ω): Conversion of solar time to an angle where 24 hours = 360° and solar noon is zero.

The sun vector then represents the sun angle and elevation from the perspective of a specific Global Positioning System (GPS) orientation on the earth (Reda and Andreas, 2008). Depending on the longitude (ζ) and latitude (ϕ) position of the solar concentrator installation site on the surface of the earth, the PLC uses Equations (F.1) to (F.6) to calculate the solar vector $S_Q(\gamma_s, \theta_s)$ through astronomical principles (Siemens, 2011).

$$Solartime = Standardtime + 4 \times (\zeta_{st} - \zeta_{loc}) + E \tag{F.1}$$

$$E = 229.2(0.000075 + 0.001868 \times cosB - 0.04089 \times sin2B) \tag{F.2}$$

$$B = \frac{360}{365} \times (n - 1) \tag{F.3}$$

$$\delta = 23.45 \times sin\left(\frac{360}{365} \times (284 + n)\right) \tag{F.4}$$

$$\cos\theta_z = (cos\phi \times cos\delta_s \times cos\omega) + (sin\phi \times sin\delta_s) \tag{F.5}$$

$$\gamma_s = sign(\omega) \times \left| cos^{-1}\left(\frac{cos\theta_z \times sin\phi - sin\delta_s}{sin\theta_z \times cos\phi}\right)\right| \tag{F.6}$$

The solar vector $S_Q(\gamma_s, \theta_s)$ computed through Equations (F.1) to (F.6) describes the azimuth angle (γ_s) for the horizontal alignment and zenith/elevation (θ_s, α_s) for the vertical alignment of the solar concentrator at location Q to pin-point at the sun at any given time of the day.

Stellenbosch University http://scholar.sun.ac.za

G. MEMS Sun Sensor Datasheet

Optical accuracy during continuous solar tracking is a key performance criteria for the proposed solar concentrator system. A diagnostic optical instrument is required for measuring the solar tracking accuracy and to evaluate system performance on the azimuth and elevation axes. The SolarMEMS ISS-AX sun sensor provides extremely accurate optical measurements of sun ray incident vectors and are fabricated for high-precision satellite applications. It uses a high-precision substrate type integrated circuit sensing structure to measure sun-ray incident angles (SolarMEMS, 2013). This guarantees that the SolarMEMS ISS-AX device ensures reliable optical measurements at low power consumption levels. Such characteristics make the device suitable for high-precision sun-tracking and positioning systems, for example in aircraft altitude control, solar tracking/pointing systems, heliostat control, altitude control using light sources as well as for measuring solar radiation levels.

The operational principles of the SolarMEMS sun sensor is illustrated in Figure G.1. Interfacing between the sensor and the data acquisition system is accomplished through a four-core cable carrying analogue signals. The sun sensor datasheet is presented in Figure G.1 and explains how the zero degree position of the sensor is calibrated through a simple alignment process during installation. Continuous output signals allows for the measurement of the sun ray incident vector $S_Q(\gamma_s, \theta_s)$, and provides sun ray projection angles in two orthogonal reference axes suitable for solar tracking applications (SolarMEMS, 2013). The SolarMEMS ISS-AX sun sensor can also be integrated into a data acquisition system to operate as solar tracking error datalogger. Moreover, Chapter 5, Section 5.2.1.3 describes procedures to employ the SolarMEMS ISS-AX sun sensor in a hybrid open-loop closed loop Siemens PLC control philosophy wherein the solar reflector tracking system use solar positioning algorithms to direct the reflector system by computing the direction of the solar vector at any specific location at a particular time using astronomical coordinates as basis of computation. The sun sensor then assists with a homing sequence to focus any sun-tracking error remaining through the sun sensor.

Figure G.1 shows the technical specifications of the MEMS ISS-AX sun sensor device, which allows for the measurement of the incident angle of a sun ray by providing four analog outputs. By means of a simple computation (see formulas Figure G.1(page 3)) the solar vector $S_Q(\gamma_s, \theta_s)$ is computed.

Stellenbosch University http://scholar.sun.ac.za

Figure G.1: Technical Specifications of the MEMS ISS sun sensor (pages 1-3) (SolarMEMS, 2013).

Technical Specifications.pdf

Solar MEMS Technologies S.L.

Sun Sensor ISS-AX

Technical Specifications

Features

Two orthogonal axes sun sensor
Wide or narrow field of view
High accuracy in installation with calibration
4 analog outputs
Low power consumption
Wide operating voltage range: 5÷12 V
Industrial temperature range: - 40° to 85°
Reduced size
Low weight
IP65 protection
Reverse polarity protection

Applications

Sun tracking/pointing systems
Solar Trackers
Heliostats
Photovoltaic
CSP, CPV and HCPV
Stirling

ISS-AX sun sensor measures the incident angle of a sun ray in both orthogonal axes. The high sensitivity reached is based on the geometrical dimensions of the design.

Its characteristics make it a suitable tool for high accurate sun-tracking and positioning systems, with low power consumption and high reliability.

ISS-AX sun sensor has been designed with an unique and novel own technology based on MEMS fabrication processes to achieve high integrated sensing structures at low cost.

ISS-AX

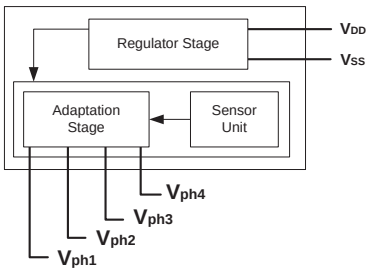

Fig 1. Block Diagram

Stellenbosch University http://scholar.sun.ac.za

Technical Specifications.pdf

1. General Specifications

Parameter	ISS-A60	ISS-A25	ISS-A15	Unit	Comments
Sensor type	2 axes	2 axes	2 axes	-	
Field of view (FOV)	120x120	50x50	30x30	º	
Accuracy without calibration	< 3	< 2	< 1	º	Average (*)
Accuracy in calibrated zero degrees	< 0,06	< 0,04	< 0,02	º	3σ (*) Chapter 4: Calibration.
Consumption					
Dark	12	12	12	mW	
Sun light	36	36	36	mW	
Dimensions					
Diameter	80	80	80	mm	
Height	21	21	21	mm	
Weight	100	100	100	g	
Level of protection	IP65	IP65	IP65		CEI 60529 Standard
Expected life time of 10 years + Pressure test at 0,05 mbar and 25ºC					

(*) Accuracy test in Laboratory: cable of 2 meters, collimated light source, radiation of 900 W/m^2, CAD resolution of 10 bits, and filter stage with sampling frequency of 50 Hz and bandwidth of 0,4 Hz.

Table 1. General Specifications

Different models of the ISS-AX are offered, differing in the field of view (FOV) of the sensor. The accuracy of the sensor is inversely proportional to the field of view. All these models have been tested on solar trackers with Solar MEMS Helios Controller.

2. Electrical characteristics

Symbol	Parameter	Min	Typical	Max	Unit
V_{DD}	Supply voltage	5	5	12	V
I_{DD}	Feed current	-	33	-	mA
Vph	Photodiode voltages (analog outputs)	0	-	4,5	V
Recommended					
V_{DD}	Supply voltage	5	-	12	V
V_r	Supply voltage ripple	0	-	100	mVpp
T_{OP}	Operating temperature	-40	-	85	ºC
Absolute maximum					
V_{DD}	Supply voltage	0	-	16	V
T_{OP}	Operating temperature	-40	-	85	ºC

Table 2. Electrical characteristics

Reverse polarity protection.

Stellenbosch University http://scholar.sun.ac.za

Technical Specifications.pdf

3.3. Measurements

The A*ngle X* and *Angle Y* specify the angular position of the incident sun ray inside the field of view of the ISS-AX sensor.

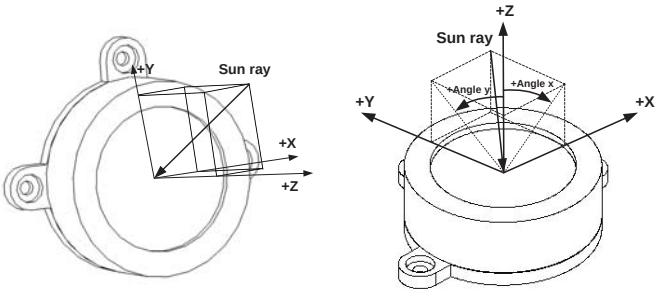

Fig 4. References for measured angles

Angle X and *Angle Y* of the incident ray can be obtained with a simple **set of equations** involving the four photodiode voltages generated by the sensor (V_{PH1}, V_{PH2}, V_{PH3}, and V_{PH4}):

$$X_1 = V_{PH3} + V_{PH4} \qquad Y_1 = V_{PH1} + V_{PH4}$$

$$X_2 = V_{PH1} + V_{PH2} \qquad Y_2 = V_{PH2} + V_{PH3}$$

$$F_X = \frac{X_2 - X_1}{X_2 + X_1} \qquad F_Y = \frac{Y_2 - Y_1}{Y_2 + Y_1}$$

$$Angle\ X = arctg\left(C \cdot F_X\right) \qquad Angle\ Y = arctg\left(C \cdot F_Y\right)$$

Type	Value
ISS-A60	1,889
ISS-A25	0,477
ISS-A15	0,273

Table 3. Values of the parameter C according to the type of sensor ISS-AX (Geometric Correction)

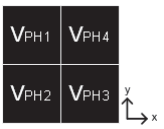

Fig 5. References for the photodiodes

The accuracy of the sensor increases when receiving a radiation perpendicular to the sensor, close to zero degrees in X and Y. This is an outstanding feature that makes it suitable for tracking applications. The **accuracy** can be **increased** in more than one order of magnitude by compensating the offset error after the installation of the sensor by means of **Calibration**.

The use of a **filtering stage is recommended** (for example: 50 Hz sampling frequency and 0,4 Hz bandwidth).

Stellenbosch University http://scholar.sun.ac.za

H. Image Processing System

Image processing techniques are used to determine the position of the sun from web camera images for closed-loop camera based solar tracking evaluation. Figure H.1 illustrates how camera images of the sun is sequentially captured with a CMOS LY208C web camera, while the position of the sun is determined from an image processing algorithm running on a Nootropic experimental development board. The captured image frames with the sun localization coordinates are relayed to the PC USB port and displayed on the PC screen through an ION video-2-pc video conversion system. In the computer display, the processed localization coordinates are continually overlaid onto the snapshot images of the sun as it moves across the sky.

An Arduino microcontroller (Figure H.1) reads the sun position coordinates from the Nootropic processor, converts it into solar vectors $S_Q(\gamma_s, \theta_s)$, and output this as digital control signals to the Siemens Simatic S7-1214 PLC processor. The PLC processor in turn controls the solar tracking process in accordance with the sun vectors received from this image processing system.

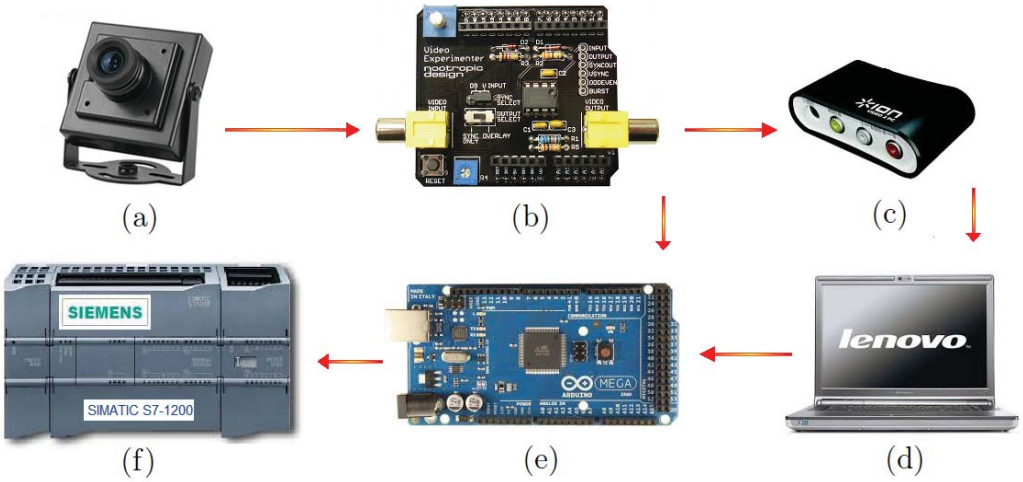

Figure H.1: Image processing system for determining sun position coordinates from camera images, includes (a) CMOS LY208C web camera, (b) Nootropic image processor, (c) ION video-2-pc USB interface, (d) personal computer, and (e) Arduino μcontroller relaying sun vectors to (f) PLC processor to control solar tracking.

Stellenbosch University http://scholar.sun.ac.za

I. PLC Control Calculations

The PLC controller needs to compute the required DC motor angular movement to point the solar concentrator towards the sun. By employing the known position of the sun (Appendices F,G and H), the PLC controller keeps record of the solar concentrator angular positions and compare this with the solar vector $S_Q(\gamma_s, \theta_s)$ to determine any required DC motor control signals. Through principles detailed in Section 5.2, the PLC moves the concentrator when the angle difference exceeds the pre-configurable tracking resolution ($\Delta/2°$).

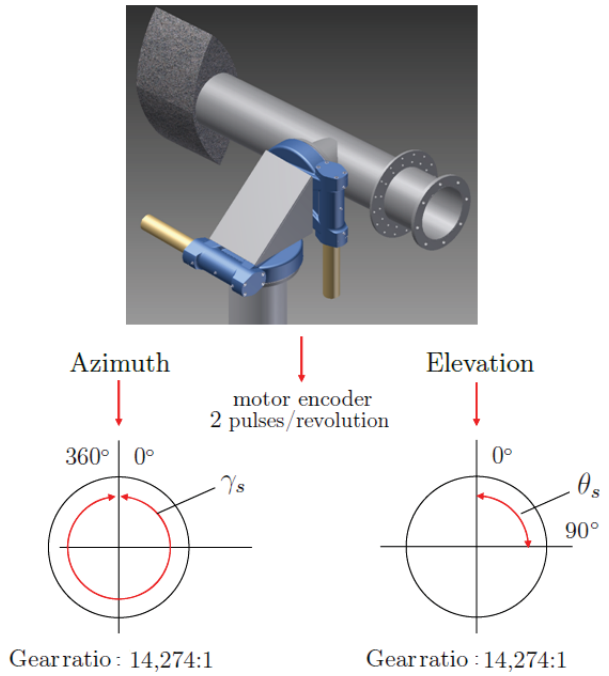

Figure I.1: DC motor azimuth and elevation axis angular travel distances computed from gear ratio and encoder pulses.

Figure I.1 shows the azimuth and elevation/zenith control ranges for the solar concentrator dual axes movement. Given the gear ratios ($slew_{ratio}$; $planet_{ratio}$) for the selected actuator (Appendix C), a mathematical calculation compares the solar angle to the number of Hall encoder pulses. In this calcula-

Stellenbosch University http://scholar.sun.ac.za

tion, the angle difference between the sun vector (γ_s, θ_s) and the concentrated solar reflector position is expressed in terms of azimuth/elevation Hall pulses, which in turn is used to command the DC motor travel distances for each of the azimuth/elevation actuators. Since the conversion of the required azimuth angle γ_s and elevation angle θ_z into DC motor travel distance (Hall pulses) is linear, the required DC motor revolutions can be calculated through Equations (I.1) and (I.2) respectively. These formulas relate the relative solar position to the required DC motor movement (Hall encoder pulses) to follow sun to its next position.

$$\gamma_{az} = \frac{\gamma_s}{360^\circ} \times slew_{az} \times planet_{az} \times Hall_{pulse/rev} \tag{I.1}$$

$$\theta_{el} = \frac{\theta_s}{360^\circ} \times slew_{el} \times planet_{el} \times Hall_{pulse/rev} \tag{I.2}$$

With the azimuth/elevation slew gear ratio (61:1), planetary gear ratio (234:1), and Hall pulses (2:1) per rotation known (Figures C.2 and I.1), the azimuth/elevation angular travel distances (in pulses) on each of the axes can be computed from Equations (I.3) and (I.4).

$$\gamma_{az} = \frac{\gamma_s}{360^\circ} \times 61 \times 234 \times 2 \tag{I.3}$$

$$\theta_{el} = \frac{\theta_s}{360^\circ} \times 61 \times 234 \times 2 \tag{I.4}$$

The main task of the PLC solar tracking positioning controller is illustrated in Figure I.2, where it is shown how the PLC control triggers and precisely controls the travel distance of the actuator DC motors in terms of the number of Hall encoder pulses. The PLC monitors and controls the moving dish process according to the solar tracking resolution ($\Delta/2^\circ$), upon inputs from the sun sensor or SPA parameters (Siemens, 2011).

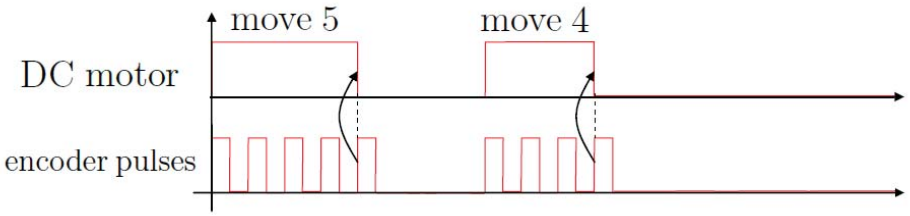

Figure I.2: Slew azimuth and elevation axis motor travel distances computed by PLC from encoder pulses and actuator gear ratio through Equations (I.1)&(I.2).

The travel distance computations in Equations (I.3) and (I.4) for the azimuth/elevation axes relates to the solar tracking movement. It can be logged/saved to show graphs of the azimuth and elevation axes solar tracking movement patterns as the solar dish follows the sun throughout the day.

Stellenbosch University http://scholar.sun.ac.za

J. DC Motor PWM Current Driver

Figure J.1 shows a circuit board picture of the Pololu 15 Ampere high-power motor driver with discrete MOSFET H-bridge which supports the Siemens PLC in digital PWM mode to drive the slew drive DC motors introduced in Appendix C. The motor driver contains one N-channel MOSFET per output (see datasheet Figure J.2), with circuitry to manage PLC driven user inputs. This circuit supports a wide output voltage range (5.5 to 24 V) and is able to deliver continuous current levels of 15 A with no heat sink, and 21 A with a proper heat sink.

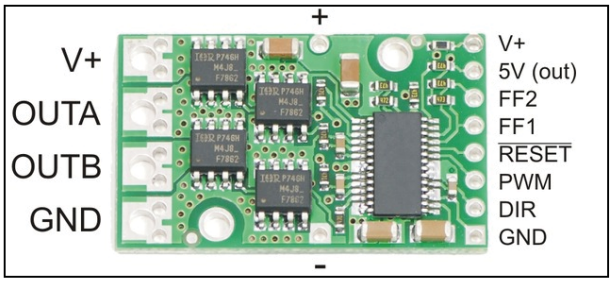

Motor channels:	1
Minimum operating voltage:	5.5 V
Maximum operating voltage:	30 V
Continuous output current per channel:	15 A[2]
Maximum PWM frequency:	40 kHz[3]
Maximum logic voltage:	5.5 V
MOSFET on-resistance (max per leg):	3.5 mΩ
Reverse voltage protection?:	N

Figure J.1: Pin assignment and specifications for discrete MOSFET H-bridge motor driver for bidirectional PWM control of a high-power DC motor.

The PWM pin in Figure J.1 should be held logically low to activate the brake operation and logically high for the motor output to be controlled through the DIR input. The current driver supports dual mode operation, namely (a) sign-magnitude for the PWM duty cycle to control the motor speed while the DIR pin controls the direction, and (b) locked-antiphase where the PLC control signal is applied to the DIR pin while the PWM pin is logically high. The motor driver supports PWM frequencies of up to 40 kHz, but requires a restoration time of around 3 microseconds per cycle. High duty cycles is therefore not available at frequencies above 40 kHz. Gradually ramping the PWM input from 0-100% will result in the output ramping from 0-88% after it will switch to 100%.

Stellenbosch University http://scholar.sun.ac.za

International
IOR Rectifier

PD - 97275A

IRF7862PbF

HEXFET® Power MOSFET

Applications

- Synchronous MOSFET for Notebook Processor Power
- Synchronous Rectifier MOSFET for Isolated DC-DC Converters

V_{DSS}	$R_{DS(on)}$ max	Qg
30V	3.7mΩ@V_{GS} = 10V	30nC

Benefits

- Very Low $R_{DS(on)}$ at 4.5V V_{GS}
- Ultra-Low Gate Impedance
- Fully Characterized Avalanche Voltage and Current
- 20V V_{GS} Max. Gate Rating
- 100% tested for Rg
- Lead-Free

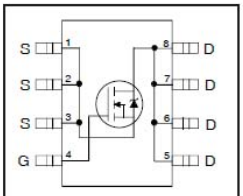

Top View

SO-8

Absolute Maximum Ratings

	Parameter	Max.	Units
V_{DS}	Drain-to-Source Voltage	30	V
V_{GS}	Gate-to-Source Voltage	± 20	
I_D @ T_A = 25°C	Continuous Drain Current, V_{GS} @ 10V	21	A
I_D @ T_A = 70°C	Continuous Drain Current, V_{GS} @ 10V	17	
I_{DM}	Pulsed Drain Current ①	170	
P_D @T_A = 25°C	Power Dissipation	2.5	W
P_D @T_A = 70°C	Power Dissipation	1.6	
	Linear Derating Factor	0.02	W/°C
T_J T_{STG}	Operating Junction and Storage Temperature Range	-55 to + 150	°C

Thermal Resistance

	Parameter	Typ.	Max.	Units
$R_{\theta JL}$	Junction-to-Drain Lead ⑤	—	20	°C/W
$R_{\theta JA}$	Junction-to-Ambient ④⑤	—	50	

Figure J.2: Datasheet for Pololu 15 Amp high-power motor driver HEXFET Power MOSFET.

Stellenbosch University http://scholar.sun.ac.za

K. Power Budget and Battery Capacity Analysis

Considerable attention is given to climate change. Internationally, governments are increasingly implementing measures to reduce the potentially devastating effects of climate change. The government of South Africa, for example, is of the view that *"in pricing the external costs associated with carbon-emissions, an incentive is created to change behaviour and encourage energy-efficiency measures"* (Treasury, 2010). Carbon footprint and power budget analysis are essential concepts in any off-grid stand-alone system as it relates to the survival of the system.

Power budget and carbon footprint analysis are linearly dependent concepts. Even in the design and operation of renewable energy systems, carbon footprint analysis of the as-built system is of importance and the demand side CO_2 footprint should be quantified. In this regard, Table K.1 presents a power budget analysis, namely a list of concentrated solar positioning system components plus an estimate of the relative times dedicated to each task. This information is used to analyse the power budget reserve as well as the CO_2 footprint of the concentrated solar power system, and is at the same time required for calculating the backup storage capacity required by the system in a stand-alone application. A summation of the estimated power requirements for each task represents the averaged power demand of the stand-alone concentrating solar power system and also needs to be accommodated for in the battery backup selection and electrical sub-system design.

The system and user demands presented in Table K.1 is equated to the carbon impact in terms of grams of CO_2 per hour. The CO_2 impact (grams) for each task, presented in the far right column of Table K.1, is computed by multiplying the Power (W) consumption with the GHG conversion rate of 0.70555 kgCO_2/kWh (Environmental Protection Agency, 2012). This CO_2 column gives an indication of the carbon impact or carbon footprint for each of the concentrated solar power system components during daytime operation. The added total gives the overall CO_2 footprint of the proposed concentrated solar positioning system and equates to a **concentrated solar power system demand side carbon footprint of around 214.6 g/h (grams of CO_2 per hour)**.

Stellenbosch University http://scholar.sun.ac.za

Table K.1: Power Budget and CO_2 impact analysis for the concentrated solar positioning system and components in Figure 4.1.

Power Budget and CO_2 impact analysis					
Task	**Current**	**% Time**	**$\overline{\text{Amp}}$**	**Power(W)**	**CO_2(g)**
Solar tracking subsystem					
PLC control	56 mA	100%	56 mA	1.34 W	0.95 g
Azimuth motion	2.92 A	50% PWM	7.7 mA	185 mW	0.13 g
Azimuth Hall encoder	0.8 mA	50%	0.4 mA	10 mW	0.007 g
Elevation motion	2.92 A	50% PWM	5.5 mA	132 mW	0.093 g
Elevation Hall encoder	0.4 mA	50%	0.2 mA	5 mW	0.003 g
Homing sensors	1.2 mA	50%	0.6 mA	15 mW	0.011 g
Communication	208 mA	1%	2.1 mA	50 mW	0.035 g
Subsystem Total			**72.4 mA**	**1.737 W**	**1.229 g**
Power subsystems					
PCU power up	1.5 A	0.2%	3 mA	72 mW	0.051 g
Charge control	6.0 mA	50%	3 mA	72 mW	0.051 g
Power inverter	65.0 mA	100%	65.0 mA	1.56 W	1.1 g
Subsystem Total			**71.0 mA**	**1.704 W**	**1.202 g**
User interface dispatch					
User supply/demand	12.5 A	100%	12.5 A	300 W	211.66 g
Subsystem Total			**12.5 A**	**300 W**	**211.66 g**
System total					
System Totals			**12.64 A**	**303.44 W**	**214.6 g**

In the power budget analysis of Table K.1, the power demand of the system is estimated to be around 1.737 Wh (Watt hours). With the estimated hourly energy demand for solar tracking control and automation to be around 1.737 Wh, and the total estimated system demand (with an assumed constant user load of 300 W) to be around 303.5 Wh (Table K.1), the battery power storage medium can be selected. As a practical consideration, it should be taken into account that theoretical battery capacity does not allow for 100% use of any battery. The actual battery life should rather be computed with an efficiency (η) of 75% of the battery capacity to allow for a 25% recharge reserve (Excide, 2013).

$$BBC = \frac{Demand\ load\ (W)}{Voltage\ (V)} \times \frac{Reserve\ capacity\ (h)}{\eta_{battery}} \tag{K.1}$$

Equation (K.1) can be used to calculate the required backup battery capacity (BBC). The first part of this equation computes the theoretical BBC for which the designer specifies the average demand load (Wh), the operat-

Stellenbosch University http://scholar.sun.ac.za

ing voltage (V) and the Reserve capacity (hours), while the battery efficiency ($\eta_{battery}\%$) is brought into the equation to calculate the actual BBC capacity.

For solar tracking system with an operating voltage of 24 V, a demand load of 303.33 W (computed in Table K.1), a required run-time operation reserve of 10 hours (specified in Table 3.2) and a 75% battery efficiency, the actual BBC is calculated as follows:

$$BBC = \frac{330\ W}{24\ V} \times \frac{10\ h}{0.75} = 183\ Ah \tag{K.2}$$

From Equation (K.2) the actual battery capacity is calculated to be at least 183 Ah. In the user specifications given in Table 3.2, the battery capacity should provide for 10 hours solar tracking capacity in the absence of available sunlight (the re-charging resource) and specifies the BBC to be at least 140 Ah.

A battery is normally rated in terms of Amp hours over discharge rate. For example, a battery specified as "100 Ah at C20" is able to produce 100 Ah when discharged over 20 hours. Other than car batteries designed to produce a short burst of power to start the engine, solar applications typically use heavy duty deep cycle batteries, such as deep cycle lead acid batteries. Deep cycle batteries are designed to provide power over a far longer period of time and is able to ensure deep discharges (Excide, 2013). These batteries are typically only available in terms of standard 50 Ah, 100 Ah, 150 Ah and 200 Ah ratings.

From Equation (K.3) the actual time of operation available with a backup battery capacity with a standard rating of 150 Ah is calculated to be 8.2 h, while a battery rated at a standard capacity of 200 Ah would deliver around 10.9 h of operation, computed in Equation (K.4).

$$OperatingTime_{hours} = \frac{150\ Ah \times 24 \times 0.75}{330\ W} = 8.2\ h \tag{K.3}$$

$$OperatingTime_{hours} = \frac{200\ Ah \times 24 \times 0.75}{330\ W} = 10.9\ h \tag{K.4}$$

The user specification in Table 3.2 requires a battery with capacity to ensure at least 10 hours of user and solar tracking operation and specifies a battery capacity to be at least 140 Ah. The calculated capacity requirement for the as-built system with an estimated 10 hours of user/solar tracking operation is 183 Ah. Although this capacity meets one part of the user specification, a cost-benefit analysis would be required by the user around fulfilling the second part of the specification, which centres around a choice between the available deep cycle battery capacity options, namely a standard 150 Ah or standard 200 Ah (24 V) deep cycle battery. Calculations above show that the **200 Ah battery** would be able to deliver an estimated 11 hours of operating time, compared to the estimated 8 hours of operating time with the **150 Ah battery**, both cases where the concentrated solar power system operates in the absence of sunlight (zero re-charging resource).

Stellenbosch University http://scholar.sun.ac.za

L. Safety Precautions

Before the experiments can proceed, the evaluation team should be made aware of the following safety considerations.

L.0.1. Thermal Protection

Thermal protection is one of the most important items to keep in mind when conducting experiments on any concentrated solar power system.

It is advisable to always wear gloves and use caution when working with solar concentrator parts during the daytime. Most of the solar concentrator parts and elements become very hot when exposed to bright sunlight. Extreme caution should thus be taken before handling any parts that have been exposed to sunlight. Figure L.1 shows the safety signs that needs to be fixed onto the pedestal pole of each solar tracking system.

Figure L.1: Safety signs to be set up at the site of installation and experiment.

When conducting tests, it its advisable to partially tile the dish with reflective elements for safety reasons. Alternatively, some reflecting surfaces should be covered to prevent heat concentration or build up when working on the system or when the system is maintained.

L.0.2. Glint and Glare Hazards

It is known that solar concentrators present glint and glare hazards to passing aircraft and pilots. Addressing these safety aspects during experimentation is an important requirement towards ensuring public safety. A glint is defined as a momentary flash of light reflected from the parabolic reflective elements, while a glare is defined as a more continuous source of excessive brightness relative to

Stellenbosch University http://scholar.sun.ac.za

the ambient lighting, usually radiated from the area of the solar receiver. The site of installation and experimentation on the university's rooftop is in close proximity to airports and aircraft flying routes, hence special care should be taken during test experiments. Partially tiling the dish with reflective elements will assist in limiting glint and glare hazards to passing aircraft and pilots.

Hazards as a result of solar concentrator glint or glare further poses a potential risk for permanent eye injury (retinal burn) and temporary disability or distractions (flash blindness). This may impact people working nearby, pilots flying overhead, or motorists driving alongside the site. Partial tiling of the dish during experimentation would once-again help reduce such risks in the initial tests, especially when testing the concentrator without a solar receiver mechanism (Stirling device) installed at the focal point.

L.0.3. Electric Shock and Lightning

It is important to emphasize that a solar concentrator system produces electricity when exposed to sunlight. Even overcast days can present enough sunlight for the concentrator to generate electrical energy. The soundest method of completely turning-off the power generation/electricity is to move the face of the concentrator away from the sun.

During experimentation, caution should also be taken when handling the electric system components of the concentrated solar power system, as backup power systems presents dangers that can still cause electrical shocks. Before touching any of the electrical parts or power connections on the concentrated solar power system, wait for a few minutes to give the bus capacitors time to discharge, as these can still cause electrical shocks after the system have been switched off.

It is important to ground the solar collector structure, including each module frame, control electronics, dish structure, the drive head assembly and the pedestal pole in order to make the solar collector and tracking system safer and less susceptible to lightning damage.

L.0.4. Emergency Procedures

A STOP function can be activated through a hardware emergency abort switch wired to the PLC digital input, providing for any emergency situations during experimentation. Irrespective of the mode of operation, activation of the STOP function will instantly halt all motion of the concentrator positioning system and power generation (i.e. Stirling device). Emergency soft(ware)-trip limits on the PLC configuration further allow for protection against cable windup. These soft trips limit the boundary movement positions of the solar concentrator to prevent overrun on pre-set safety angles for the mechanical actuator parts. Future implementation of alarm signals will help to alert an

Stellenbosch University http://scholar.sun.ac.za

operator in case of safety, especially when prompt reaction such as immediate disabling of the slewing drive motors is required.

Stellenbosch University http://scholar.sun.ac.za

M. Optical Test Instrumentation

With the dish reflector components still under construction at the time of the mechatronic system evaluation and validation, the solar positioning tracking system accuracies were evaluated without the parabolic dish component. On-axis azimuth and elevation tracking accuracy measurements were therefore taken on the sun-axis of the parabolic dish hub on the sun-pointing cantilever boom of the mechatronic platform. The purpose-built experimental test instrument housing (Figure M.1) was specially designed and fabricated to serve as physical platform for the installation of the solar tracking accuracy sensors (Appendix G). This instrumentation housing is fitted securely to the hub of the parabolic dish mounting located on the sun-axis of the mechatronic platform boom, to face precisely in the direction of the sun axis (see Figure M.1).

Figure M.1: Test experiments were conducted with a test instrument and sun sensor/camera mounted onto the sun-axis of the solar concentrator boom.

Stellenbosch University http://scholar.sun.ac.za

This instrument platform and orientation means (Figure M.1) was designed and precision fabricated to fit directly onto the sun-pointing hub of the cantilever boom, instead of the parabolic dish. One sun-facing end of this instrumentation platform includes a "telescopic sun-vector reticle means" comprising cross-hair sun-target patterns (laser cut onto the platform footplate) for illumination by sunbeams directed from a small aperture (laser cut through a circular mask plate mounted above the target), serving to provide a visual representation of the solar vector for mechanical system alignment and solar tracking observations. The centre of the instrumentation platform serves as housing for the optical sensors (sun sensor, camera), where a welding visor helps to enhance web camera image contrast and prevents camera CMOS saturation. These optical sensor devices monitor and communicate exact digital representations of the sun vector $S_Q(\gamma_s, \theta_s)$, the physical orientation of solar concentrator, and the solar tracking axes errors to the data acquisition system.

The optically measured azimuth and elevation tracking error sequences are recorded in real-time on a personal computer using the Labview (LArVa) digital data acquisition system. The data acquisition system networks with an Arduino microcontroller, which acts as hardware interface through six 12-bit analog to digital converters and 14-digital input/output pins (6 PWM outputs). It communicates through USB with a personal computer for data transfer and storage. Figure M.2 shows a typical screen display of the LArVa data acquisition system during experimental setup configuration.

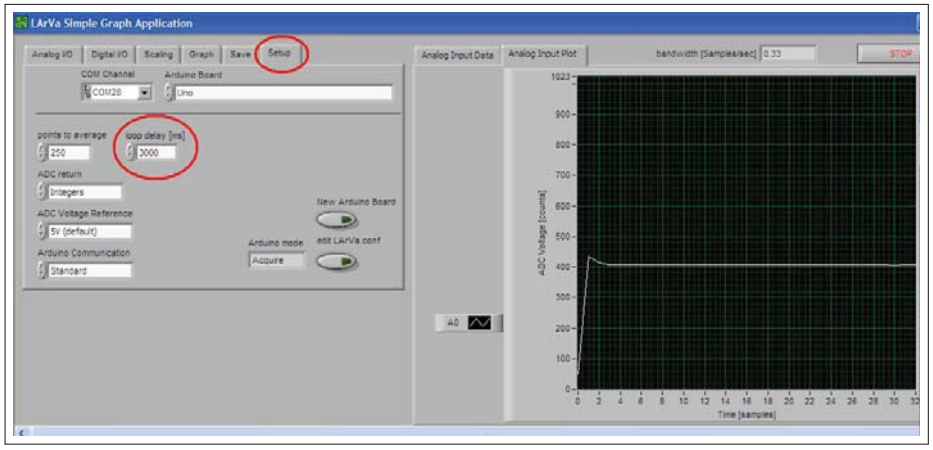

Figure M.2: Labview (LArVa) digital data acquisition system display.

The performance of the mechatronic platform and control automation for the self-tracking solar concentrator positioning system is evaluated on the basis of the on-axis optical sun pointing azimuth/elevation errors (off-target errors). Tracking errors are measured optically through the SolarMEMS sun sensor (Appendix G), while data is recorded on the Labview (LArVa) digital data acquisition system and displayed through the Microsoft Excel software package.

Stellenbosch University http://scholar.sun.ac.za

N. Solar Tracking Performances

Stellenbosch University http://scholar.sun.ac.za

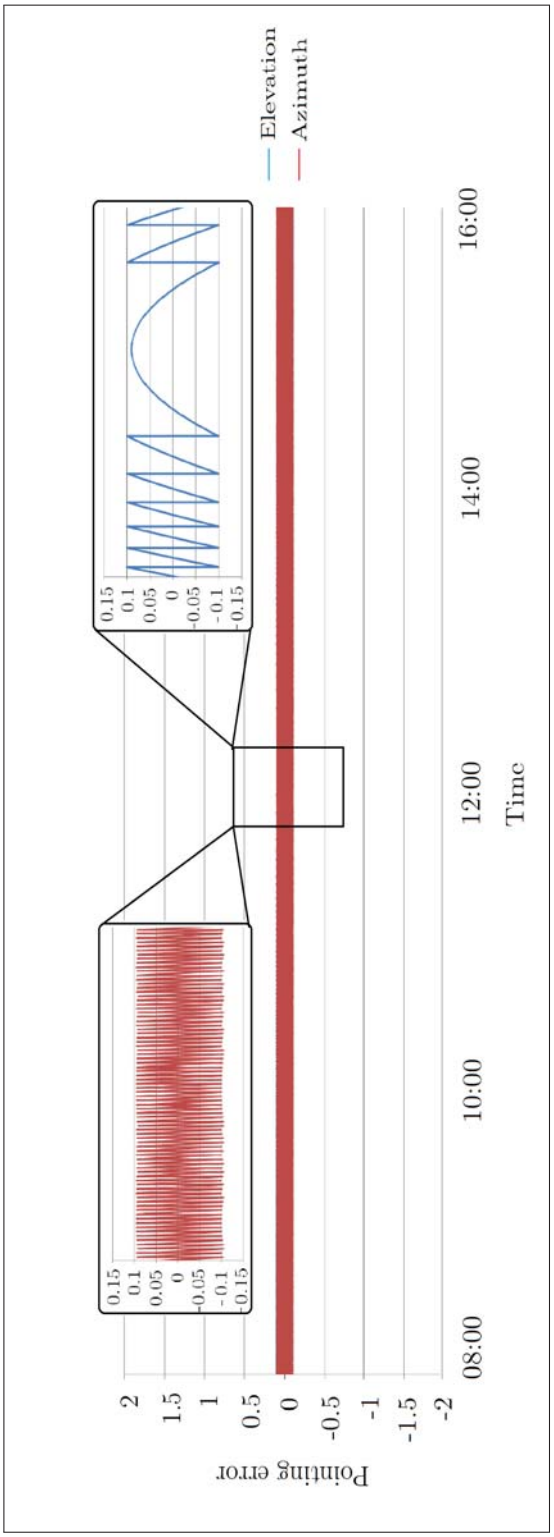

Figure N.1: Simulated solar concentrator movement patterns for the solar concentrator mechatronic platform on the azimuth and elevation axes, determined by the PLC on the basis the SPA calculated solar vectors (Chapter 6, Experiment 1).

Stellenbosch University http://scholar.sun.ac.za

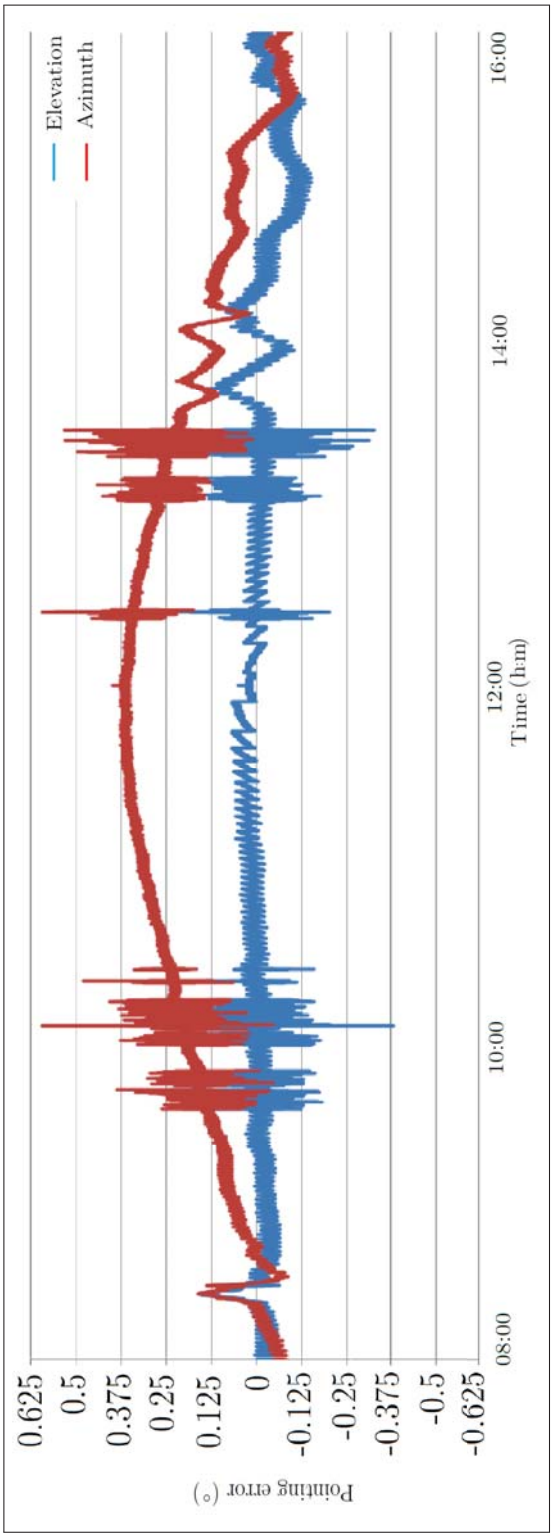

Figure N.2: Optically measured azimuth and elevation tracking error sequences (in degrees) for the solar concentrator mechatronic platform commanded by the PLC using the SPA in the open-loop control mode (Chapter 6, Experiment 1).

Stellenbosch University http://scholar.sun.ac.za

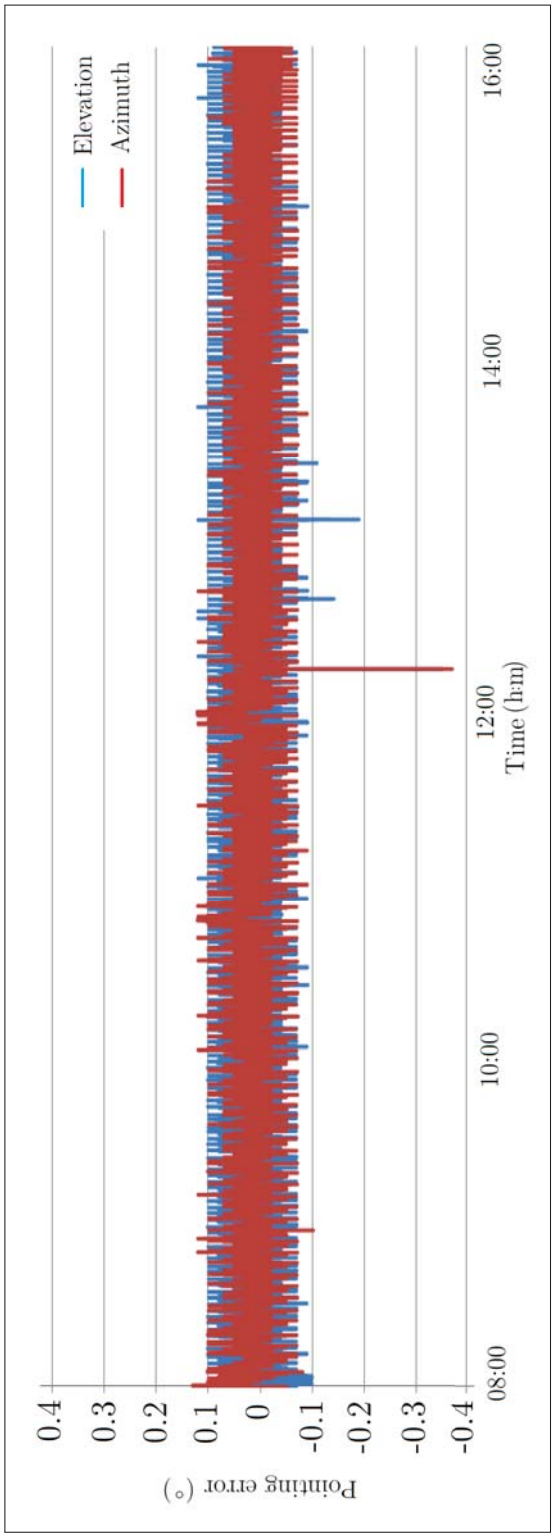

Figure N.3: Optically measured azimuth and elevation tracking error sequences (in degrees) for the solar concentrator mechatronic platform controlled by the PLC using the sun sensor in the closed-loop control mode (Chapter 6, Experiment 2).

Stellenbosch University http://scholar.sun.ac.za

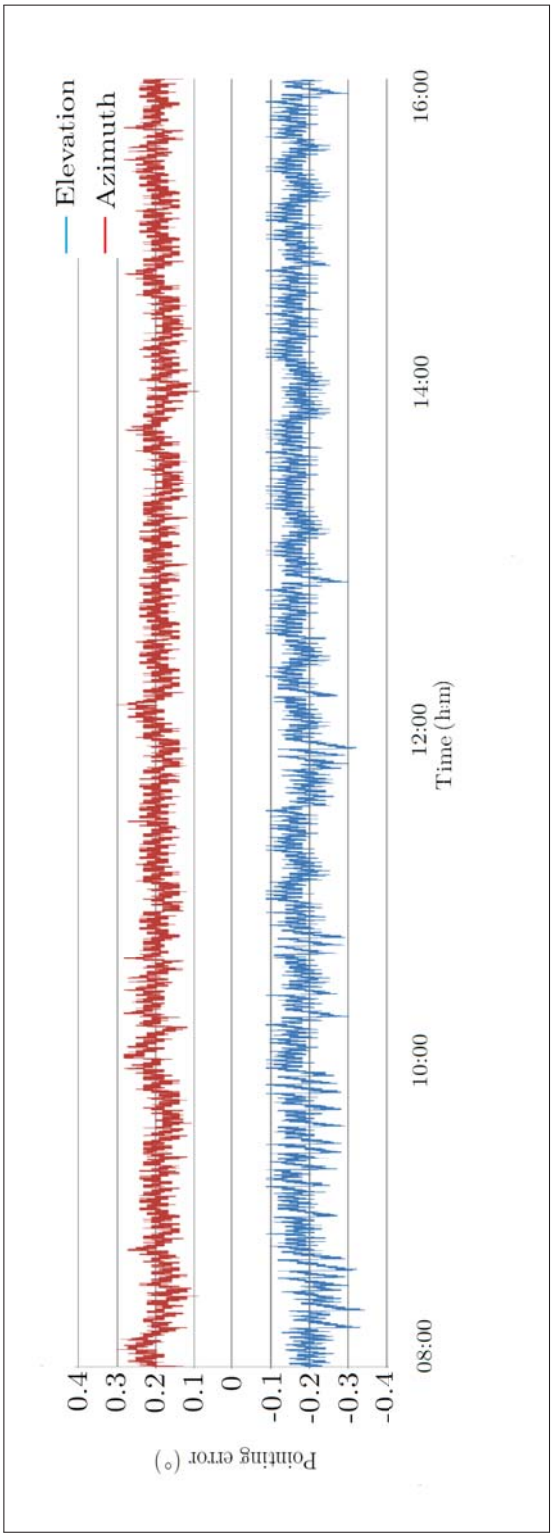

Figure N.4: Optically measured azimuth and elevation tracking error sequences (in degrees) for the solar concentrator mechatronic platform controlled by the PLC using the web camera in the closed-loop control mode (Chapter 6, Experiment 3).

Stellenbosch University http://scholar.sun.ac.za

List of References

Angel, R.P. and Davison, W.B. (2009). Solar Concentrator Apparatus with Large, Multiple, Co-axial Dish Reflectors, PCT patent WO2009140174.
Available at: http://www.google.com/patents/WO2009140174A3

Arturo, M. and Alejandro, G. (2010). High Precision Solar Tracking System. *Proceedings of the World Congress on Engineering, London, U.K.*, vol. 2.
Available at: http://www.iaeng.org/publication/WCE2010/WCE2010_pp844-846.pdf

Bendt, P., Gaul, H. and Rabl, A. (1980). Determining the Optical Quality of Focusing Collector Without Ray Tracing. Tech. Rep., Solar Energy Research Institute, Colorado.
Available at: http://www.nrel.gov/docs/legosti/old/359.pdf

Bisenius, W. (2012). Degrees of Protection Provided by Enclosures (IP Code), Association of Electrical Equipment and Medical Imaging, Virginia, USA.
Available at: http://www.nema.org/Standards/Pages/A-Brief-Comparison-of-NEMA-250-and-IEC-60529.aspx

Blain, L. (2010). South Korea's Autonomous Robot Gun Turrets.
Available at: http://www.gizmag.com/korea-dodamm-super-aegis-autonomos-robot-gun-turret/17198/

Blanco-muriel, M., Alarcon-padilla, D.C., Lopez, T. and Lara-Coira, M. (2001). Computing the Solar Vector. *Elsevier Solar Energy*, vol. 70, no. 5, pp. 431–441.

Cleeve, E. and Ndhlovu, T. (2004). Introduction: Strategies for Meeting the Millennium Development Goals in Africa. *International Journal of Social Economics*, vol. 31, no. 1/2, pp. 9–11. ISSN 0306-8293.
Available at: http://www.emeraldinsight.com/10.1108/03068290410515385

Collier, P., Conway, G. and Venables, T. (2008). Climate Change and Africa. *Oxford Review of Economic Policy, Oxford University Press*, vol. 24, Issue, no. 2, pp. 337–353.
Available at: http://oxrep.oxfordjournals.org/content/24/2/337.abstract

Department of Energy South Africa (2011). Integrated Resource Plan for Electricity 2010 - 2030 Revision 2. Tech. Rep. March, Department of Energy.

Stellenbosch University http://scholar.sun.ac.za

Available at: http://www.energy.gov.za/IRP/irpfiles/IRP2010_2030_Final_Report_20110325.pdf

Dietrich, J.J., Steinmeyer, D.A. and Hartmann, D.T. (1986). Balanced Solar Concentrator, US Patent US4583520.
Available at: http://www.google.com/patents/US4583520

DoDaam (2013). South Korea Robot Machine Gun Turret, DoDaam Systems, South Korea.
Available at: http://www.military.com/video/guns/machine-guns/new-machine-gun-kills-from-3-miles/2207410055001/

Duffie, J. and Beckman, W. (2006). *Solar Engineering of Thermal Processes*. 3rd edn. Wiley. ISBN 0471698679.

Environmental Protection Agency (2012). eGRID2012. Tech. Rep., USA Environmental Protectection Agency, Washington DC.
Available at: http://www.epa.gov/cleanenergy/energy-resources/egrid/index.html

Esmond, G., Tao, Z. and Yen, C. (2011). Array Module of Parabolic Solar Energy Receivers, US Patent US20110174359.
Available at: http://www.google.com/patents/US20110174359

Excide (2013). Industrial Batteries Powerfit S500 High Energy Density for Maximum Security, Exide Technologies Catalog.
Available at: http://elektropower.hu/Exideakkumulator/Powerfit.pdf

Fang, H. (2013). Slewing Drive Manual, Jiangyin Huafang New Energy Hi-Tech Equipment Co. Ltd, China.
Available at: https://www.acosolar.com/media/productfile/s/l/slewingdrivemanual.pdf

Gary, J., Turchi, C. and Siegel, N. (2011). CSP and the DOE Sunshot Initiative. In: *SolarPACES Conference*, vol. 1. Granada, Spain.

Grena, R. (2008). An Algorithm for the Computation of the Solar Position. *Solar Energy*, vol. 82, pp. 462–470.
Available at: http://www.scribd.com/doc/94455998/Grena-2008-An-Algorithm-for-the-Computation-of-the-Solar-Position

Greyvenstein, G.e. (2011). Introduction To Dish Stirling - Main CSP Technologies. In: *Solar South Africa Conference*, vol. 2011, pp. 1–11.
Available at: http://www.ennex.co.za/downloads/DishStirlingSolarSouthAfricaConference21June2011.pdf

Hughes, R.O. (1980). Effects of Tracking Errors on the Performance of Point Focusing Solar Collectors. *Solar Energy*, vol. 24, pp. 83–92.
Available at: http://www.sciencedirect.com/science/article/pii/0038092X80900237

Stellenbosch University http://scholar.sun.ac.za

IMO (Ingo Müller Oberflächentechnik) (2013). IMO Slew Drives Product Catalog. Available at: http://www.imo.de/uploads/media/Slew_Drive_Catalog_02.pdf

Infinia (2012). Powerdish IV, Solar Energy Solution, The Infinia Corportation USA. Available at: http://www.infiniacorp.dreamhosters.com/project/powerdish-iv/

Innova (2013). Trinum Thermodynamic Solar Cogenerating System, Innova Solar Energy, Italy.
Available at: http://www.innova.co.it/files/pdf-prodotti/datasheet_trinum_eng_25032.pdf

Juhuang (2013). Dual-axis Solar Tracker, Shandong Juhuang Photoelectric Technology Co. Ltd., China.
Available at: http://en.pv001.net/web.php?uid=24&wid=1&cid=2083

Kalogirou, S.A. (1996). Design and Construction of a One-axis Sun-tracking System. *Elsevier, Solar Energy*, vol. 57, no. 6, pp. 465–469.
Available at: http://www.researchgate.net/publication/30499755_Design_and_construction_of_a_one-axis_sun-tracking_system

Khalsa, S.S.S., Ho, C.K. and Andraka, C.E. (2011). An Automated Method to Correct Heliostat Tracking Errors. In: *SolarPACES Conference*. SolarPaces2011, Granada, Spain.

Kinoshita, G.S. (1985). The Shenandoah Parabolic Dish Solar Collector. Tech. Rep. January, Sandia National Laboratories.
Available at: http://prod.sandia.gov/techlib/access-control.cgi/1983/830583.pdf

Kiszynski, K. and Al-Hallaj, S. (2011). Renewable Energy Sources and Energy Conversion Devices. In: *Hybrid Hydrogen Systems*, vol. 2, chap. 2. Springer. ISBN 9781846284670.

Le Roux, W., Bello-Ochende, T. and Meyer, J. (2012). Solar Tracking for a Parabolic Dish Used in a Solar Thermal Brayton Cycle. *CRSES Annual Student Symposium*.
Available at: http://www.crses.sun.ac.za/files/services/conferences/annual-student-symposium-2012/22_November/7_LeRoux.pdf

Lopez, C.W. and Stone, K.W. (1993). Performance of the Southern California Edison Company Stirling Dish, Southern California Edison Co., Rosemead and Mako Enterprises, Huntington, CA., USA. Tech. Rep. October.

Makundi and Rajan (1999). United Nations Framework on Climate Change: Mitigation Options, UNFCCC CGE Global Training Workshop on Mitigation Assessment.
Available at: http://unfccc.int/resource/cd_roms/na1/mitigation/Module_3/Module3.ppt

Stellenbosch University http://scholar.sun.ac.za

Mancini, T.R. (1997). Solar-Electric Dish Stirling System Development. Tech. Rep., Sandia National Laboratories.
Available at: `http://mac6.ma.psu.edu/stirling/reports/DE98001305.pdf`

Manfred, R. (2012). Installationsanleitung für Solarview, Datenlogger und Webvisualisierungstool, RichterData, Germany. pp. 1–32.

Prinsloo, G., Dobson, R. and Schreve, K. (2013*a*). Carbon Impact Optimization as PLC control Strategy in Solar Power System Automation. In: *SolarPACES Conference*, vol. 00. Las Vegas, Nevada, USA.

Prinsloo, G., Dobson, R. and Schreve, K. (2013*b*). Mechatronic Platform with 12sqm Solar Thermal Concentrator for Rural Power Generation in Africa. In: *SolarPACES Conference*, vol. 00. Las Vegas, Nevada, USA.

Reda, I. and Andreas, A. (2008). Solar Position Algorithm for Solar Radiation Applications. *Solar Energy*, vol. 76, no. 5, pp. 577–589.

Reddy, K. and Veershetty, G. (2013). Viability Analysis of Solar Parabolic Sish Stand-alone Power Plant for Indian Conditions. *Applied Energy Elsevier*, pp. 908–922.

Rockwell Automation (2012). A Rockwell Automation White Paper on Solar Tracking Application, Rockwell Automation, USA.
Available at: `http://literature.rockwellautomation.com/idc/groups/literature/documents/wp/oem-wp009_-en-p.pdf`

Shelef, B. and Erez, S. (2011). Solar Receiver on Lightweight Solar Reflector, US Patent US20110247679.
Available at: `http://www.google.com/patents/US20110247679`

Siemens (2011). Control of CPV Solar Trackers: Applications & Tools, Siemens AG, Germany.
Available at: `http://www.industry.usa.siemens.com/topics/us/en/solar/solar-north-america-events/IntersolarNorthAmerica2012/Documents/Siemens_solar_tracking_control.pdf`

Siemens (2013). How to Exploit Sunlight Toward Maximum Energy Yield. The Universal Solution for Solar Tracking Applications, Siemens AG, Germany.

Smith, R. and Cohn, L. (2010). Solar Support, Products and Solutions in the Solar Technology and Machine & Plant Manufacturing, IMO Anlagenbau GmbH, Germany. pp. 131–133.
Available at: `http://www.energysmith.net/articles/heliofocus.pdf`

SolarGIS (2013). SolarGIS-Solar-map-DNI-South-Africa, Download of Solar Radiation Maps: Global Horizontal Irradiation, GeoModel Solar s.r.o., Bratislava, Slovakia.
Available at: `http://solargis.info/doc/_pics/freemaps/1000px/dni/SolarGIS-Solar-map-DNI-South-Africa-en.png`

Stellenbosch University http://scholar.sun.ac.za

SolarMEMS (2013). Sun Sensor ISS-AX Technical Specifications, Solar MEMS Technologies S.L., Sevilla, Spain.

Solartron (2013). SolarBeam 7M Parabolic Concentrator, Solartron Energy Systems Inc., Nova Scotia, Canada.
Available at: `http://www.solartronenergy.com/solar-concentrator/specifications/`

Southwest Solar Technologies (2013). SolarCAT Turbo Generator Solution, Brayton Energy, Hampton, USA.
Available at: `http://www.braytonenergy.net/hybrid-solar/#solarcat`

Stellenbosch University (2013). The Hope Project, Matie Community Service, University of Stellenbosch, Stellenbosch, South Africa.
Available at: `http://thehopeproject.co.za/hope/projects/academic/EnergyAndTheEnvironment/Pages/default.aspx`

Stine, W.B. and Geyer, M. (2001). *Power from the Sun, Published online by William B. Stine and Michael Geyer.*
Available at: `http://www.powerfromthesun.net/book.html`

TitanTracker (2013). Titan Tracker, Solar Parabolic Dish Concentrator Stirling, Cabanillas Ingenieros, Castilla-La Mancha, Spain.
Available at: `http://www.titantracker.es/v_portal/informacion/informacionver.asp?cod=1229&te=720&idage=1491&vap=0`

Treasury (2010). Reducing Greenhouse Gas Emissions: The Carbon Tax Option, Discussion Paper, Department of National Treasury, South Africa.
Available at: `http://www.treasury.gov.za/publiccomments/DiscussionPaperCarbonTaxes81210.pdf`

Tsadka, S., Segev, R., Migalovich, P., Levin, O., Tarazi, E. and Whelan, R. (2008). Solar Electricity Generation System, PCT Patent WO2009034573 A3.

Tsoutsos, T., Gekas, V. and Marketaki, K. (2003). Technical and Economical Evaluation of Solar Thermal Power Generation. *Renewable Energy*, vol. 28, no. 6, pp. 873–886.
Available at: `https://www.etde.org/etdeweb/details_open.jsp?osti_id=20327746`

VariZoom (2013). Camera Crane Boom, Varizoom Texas, USA.
Available at: `http://www.cameracraneboom.com/`

WGAssociates (2001). Solar Dish Stirling Power Systems, WGAssociates Texas, USA.

Wood, T. (2010). Climate Analysis Using Autodesk Ecotect Weather Tool and Solar Tool, Integrated Design Lab, Montana State University, USA. Montana.
Available at: `http://www.idlbozeman.com/storage/pdfs/Part3WeatherSolarCompatibilityMode.pdf`

Stellenbosch University http://scholar.sun.ac.za

Yedamale, P. (2003). Brushless DC motor Fundamentals, Microchip Technology Application Note-AN885.
Available at: `http://ww1.microchip.com/downloads/en/AppNotes/00885a.pdf`